JUAN CARLOS QUINTÃO

SISTEMA AQUOSO BIFÁSICO: OBTENÇÃO DE NOVOS SISTEMAS, PARTIÇÃO E DETERMINAÇÃO DE CLORANFENICOL

Tese apresentada à Universidade Federal de Viçosa, como parte das exigências do Programa de Pós-Graduação em Agroquímica, para a obtenção do título de *Doctor Scientiae*.

VIÇOSA
MINAS GERAIS - BRASIL
2018

Ficha catalográfica preparada pela Biblioteca Central da Universidade Federal de Viçosa - Câmpus Viçosa

T
Q7s
2018

Quintão, Juan Carlos, 1985-
Sistema aquoso bifásico : obtenção de novos sistemas, partição e determinação de cloranfenicol / Juan Carlos Quintão. – Viçosa, MG, 2018.
xix, 103f. : il. (algumas color.) ; 29 cm.

Inclui apêndice.
Orientador: Maria do Carmo Hespanhol.
Tese (doutorado) - Universidade Federal de Viçosa.
Inclui bibliografia.

1. Cloranfenicol. 2. Sistemas aquosos bifásicos. 3. Química verde. 4. Extração (Química). 5. Partição de fases. I. Universidade Federal de Viçosa. Departamento de Química. Programa de Pós-Graduação em Agroquímica. II. Título.

CDD 22. ed. 541.3

JUAN CARLOS QUINTÃO

SISTEMA AQUOSO BIFÁSICO: OBTENÇÃO DE NOVOS SISTEMAS, PARTIÇÃO E DETERMINAÇÃO DE CLORANFENICOL

Tese apresentada à Universidade Federal de Viçosa, como parte das exigências do Programa de Pós-Graduação em Agroquímica, para a obtenção do título de *Doctor Scientiae*.

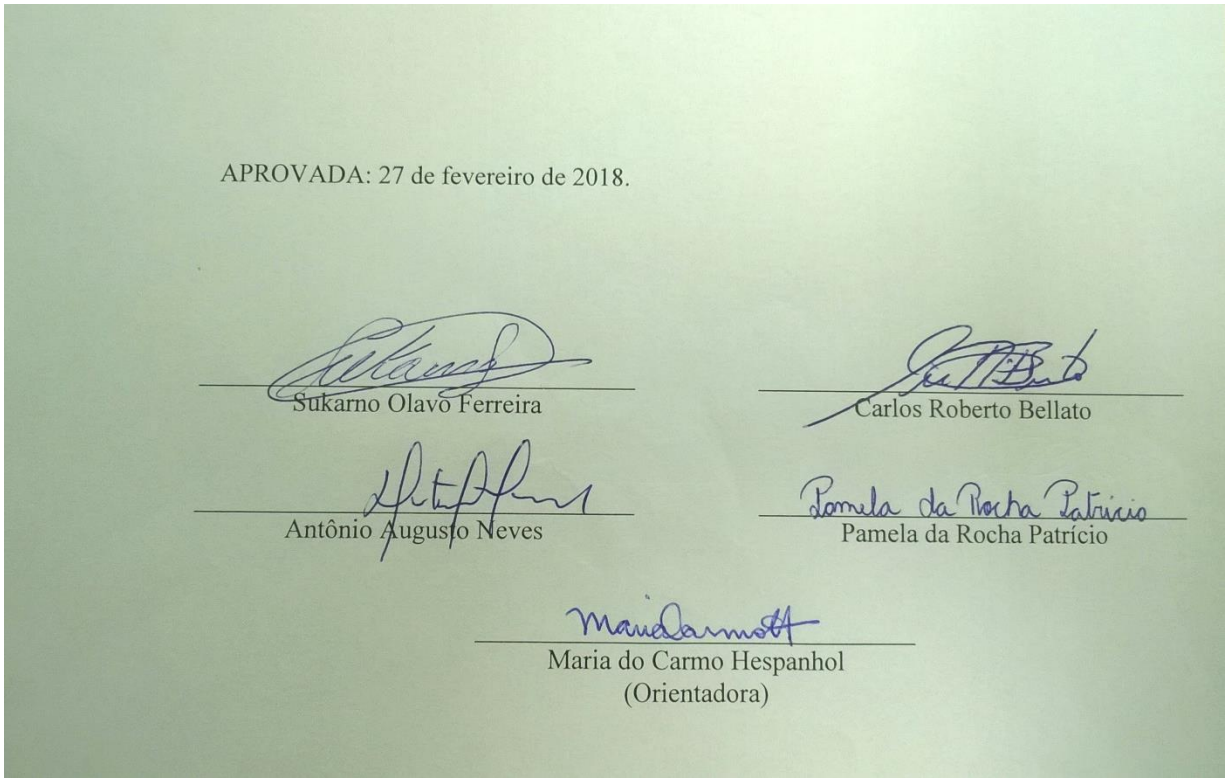

APROVADA: 27 de fevereiro de 2018.

Sukarno Olavo Ferreira

Carlos Roberto Bellato

Antônio Augusto Neves

Pamela da Rocha Patrício

Maria do Carmo Hespanhol
(Orientadora)

À minha mãe e meus irmãos.

Abriga-te na humildade, não busque mundana estima.
O ouro afunda no mar, a palha fica por cima.

Chico Xavier

AGRADECIMENTOS

Primeiramente a Deus, pelas oportunidades, pela vida e por sempre estar ao meu lado guiando minhas escolhas.

À minha mãe Nélia, meus irmãos e Danri por toda força, apoio e orações.

À Pamela e Anne pela parceria nos projetos, amizade, churrascos, comida japonesa e contribuições profissionais e pessoais que me proporcionaram. Valeu demais, meninas!

Ao Dario e Ruben, grandes amigos estrangeiros pelos bons momentos e convivência ao longo desta caminhada.

À Natalia, que mesmo de longe esteve ao meu lado me apoiando, dividindo comigo todos os momentos e dispondo de todo amor, carinho, paciência, dedicação e companheirismo durante esse tempo de Doutoramento.

À Teresa, Fran e Bia pela amizade, momentos de descontração e trabalho nas leituras de FAAS.

Ao Hauster e Alan por toda amizade, trabalho e empenho na realização das medidas calorimétricas. Muito obrigado, meninos!

Ao Grupo QUIVECOM por todo suporte e contribuições para minha formação.

À Universidade Federal de Viçosa, Departamento de Química e ao Programa de Pós-graduação em Agroquímica por todo suporte oferecido na realização deste trabalho, além da contribuição para minha evolução como pessoa e profissional.

À Coordenação de Aperfeiçoamento de Pessoal de Nível Superior (CAPES) pela concessão da bolsa de Doutorado. Ao Instituto Nacional de Ciências e Tecnologias Analíticas Avançadas (INCTAA), Conselho Nacional de Desenvolvimento Científico e Tecnológico (CNPq) e Fundação de Amparo à Pesquisa do Estado de Minas Gerais (FAPEMIG) pelo apoio financeiro.

Ao professor Fábio e equipe do CENA por todo apoio no desenvolvimento do trabalho em fluxo. Muito obrigado!

Aos meus orientadores Carminha e Luis Henrique por todo longo percurso de ensinamentos e pelas oportunidades de aprendizado e conquista ao longo destes anos. Muito obrigado!

Aos professores, Pamela (UEMG), Sukarno (DPF-UFV), Carlos Bellato (DEQ-UFV) e Antônio Augusto (DEQ-UFV), por gentilmente aceitarem fazer parte desta defesa e contribuírem com este trabalho.

BIOGRAFIA

Juan Carlos Quintão, filho de Reinaldo Moreira Quintão e Maria Nélia Pinto, nasceu em 28 de setembro de 1985, na cidade de Marliéria, Minas Gerais.

Em fevereiro de 2005 ingressou no curso Técnico em Química Industrial do Centro Federal de Educação Tecnológica de Minas Gerais, CEFET-MG, diplomando-se como Técnico em fevereiro de 2007.

Em fevereiro de 2007 ingressou no curso de Engenharia Ambiental e Sanitária da Universidade Presidente Antônio Carlos, UNIPAC, diplomando-se com o título de Bacharel em julho de 2011.

Trabalhou em laboratórios de empresas da área de materiais cerâmicos e siderurgia, no período compreendido entre agosto de 2006 e março de 2012.

Em março de 2012, iniciou o curso de Mestrado no Programa de Pós-graduação em Agroquímica da Universidade Federal de Viçosa, obtendo o título de *Magister Scientiae* em fevereiro de 2014.

Em março de 2014, iniciou o curso de Doutorado no Programa de Pós-graduação em Agroquímica da Universidade Federal de Viçosa, submetendo-se à defesa de tese em fevereiro de 2018.

SUMÁRIO

LISTA DE SÍMBOLOS E ABREVIATURAS x
LISTA DE FIGURAS xii
LISTA DE TABELAS xv
RESUMO xvii
ABSTRACT xix
CAPÍTULO 1 1
Revisão de Literatura 1
1. Contaminantes emergentes 1
1.1 Fármacos no meio ambiente 2
1.1.1 Antibióticos 3
2. Sistema aquoso bifásico 5
2.1 Uma abordagem geral 5
2.2 Princípios e propriedades 6
2.3 Obtenção de sistema aquoso bifásico 10
3. Partição de soluto em sistema aquoso bifásico 10
OBJETIVOS 13
Objetivo geral 13
Objetivos específicos 13
REFERÊNCIAS 14
CAPÍTULO 2 23
Liquid-liquid equilibrium of the ternary ammonium salt + poly(propylene glycol) + water system 23
Abstract 23
1.Introduction 23
2.Materials and Methods 25
2.1. Materials 25
2.2. Preparation of the aqueous two-phase systems 25
2.3. Determination of equilibrium composition 25
2.4. Nonrandom two-liquid (NRTL) model and Parameter Estimation 26
3.Results and Discussion 26
3.1. Aqueous two-phase system compositions 26

3.2. Effect of the nature of anion on the phase separation process 30
3.3. Effect of temperature on ATPS composition 32
3.4. Effect of the polymer hydrophobicity on the binodal position 35
3.5. Thermodynamic modeling and Estimation Procedure 36
4. Conclusion 40
5. References 41
CAPÍTULO 3 47
Chloramphenicol partitioning in ATPS: a driving-force determination approach 47
Abstract 47
1. Introduction 48
2. Experimental section 50
2.1. Materials 50
2.2. ATPS preparation and measurements of the CAP partition coefficient 50
2.3. Thermodynamic parameters of CAP transfer 51
2.3.1. CAP transfer standard Gibbs free energy change ($\Delta_{tr}G^{\theta}$) 51
2.3.2. CAP transfer standard enthalpy change ($\Delta_{tr}H^{\theta}$) 52
2.3.3. CAP transfer standard entropy change ($T\Delta_{tr}S^{\theta}$) 53
3. Results and discussion 53
3.1. Influence of CAP concentration in the partition coefficient 53
3.2. The effect of tie-line length of aqueous two-phase systems on the partitioning of CAP 54
3.3. Effect of cation on the CAP partitioning 61
3.4. Effect of polymer molar mass on the CAP partitioning 64
3.5. Effect of anion on the CAP partitioning 66
3.6. Effect of hydrophobicity on the CAP partitioning 69
4. Conclusion 71
5. References 71
CAPÍTULO 4 79
In-syringe liquid-liquid microextraction using aqueous two-phase system coupled with UV-Vis spectrophotometry: a simple approach for preconcentration and determination of chloramphenicol in aqueous samples 79
Abstract 79
1. Introduction 79

2. Experimental 82
2.1. Reagents 82
2.2. Apparatus 82
2.3. ATPS preparation 83
2.4. ATPS preparation in-syringe 83
2.5. In-syringe flow procedure 84
3. Results and discussion 84
3.1. Evaluation of In-syringe method performance 84
4. Conclusion 90
5. References 90
CONSIDERAÇÕES FINAIS 97
APÊNDICE 98

LISTA DE SÍMBOLOS E ABREVIATURAS

$\%$(m/m): Porcentagem massa/massa

$\%$: Porcentagem

ΔH_{dil}^{θ}: Variação de entalpia padrão de diluição

$\Delta H_{dil}^{\theta,\infty}$: Variação de entalpia padrão de diluição em condição de diluição infinita

$\Delta_{mix}G$: Variação de energia livre de Gibbs de mistura

$\Delta_{mix}H$: Variação de entalpia de mistura

$\Delta_{mix}S$: Variação de entropia de mistura

$\Delta_{tr}G^{\theta}$: Variação de energia livre de Gibbs padrão de transferência

$\Delta_{tr}H^{\theta}$: Variação de entalpia padrão de transferência

$\Delta_{tr}S^{\theta}$: Variação de entropia padrão de transferência

μ_i^{FI}: Potencial químico do soluto i na fase inferior

μ_i^{FS}: Potencial químico do soluto i na fase superior

μ_i^{0}: Potencial químico padrão do soluto i

$ABS_{276\,nm}^{ERP}$: Absorbância do soluto obtida em 276 nm na fase rica em eletrólito

$ABS_{276\,nm}^{PRP}$: Absorbância do soluto obtida em 276 nm na fase rica em polímero

C_E^{FRE} ou C_E^{ERP}: Concentração de eletrólito na fase rica em eletrólito

C_E^{FRP} ou C_E^{PRP}: Concentração de eletrólito na fase rica em polímero

C_P^{FRE} ou C_P^{ERP}: Concentração de polímero na fase rica em eletrólito

C_P^{FRP} ou C_P^{PRP}: Concentração de polímero na fase rica em polímero

C_i^{FI}: Concentração do soluto i na fase inferior

C_i^{FS}: Concentração do soluto i na fase superior

X_E^{ERP}: Fração molar de eletrólito na fase rica em eletrólito

X_E^{PRP}: Fração molar de eletrólito na fase rica em polímero

X_P^{ERP}: Fração molar de polímero na fase rica em eletrólito

X_P^{PRP}: Fração molar de polímero na fase rica em polímero

a_i^{FI}: Atividade do soluto i na fase inferior

a_i^{FS}: Atividade do soluto i na fase superior

fd^{ERP}: Fator de diluição da fase rica em eletrólito

fd^{PRP}: Fator de diluição da fase rica em polímero

ABS: Absorbância

CAP: Cloranfenicol

CG: Composição global

CLA ou TLL: Comprimento da linha de amarração

FI: Fase Inferior

FRE ou ERP: Fase rica em eletrólito

FRP ou PRP: Fase rica em polímero

FS: Fase superior

ITC: Calorimetria de titulação isotérmica

K: Coeficiente de partição

LLE: Extração líquido-líquido

LLME: Micro extração líquido-líquido

ln: Logaritmo natural

M: Massa molar

n: número de moléculas

nm: Nanômetro

P: Pressão

PEG: Poli(etileno glicol)

PEO: Poli(óxido de etileno)

pH: Potencial hidrogênio iônico

PPG: Poli(propileno glicol)

PPO: Poli(óxido de propileno)

R: Constante real dos gases

SAB ou ATPS: Sistema Aquoso Bifásico

STL: Inclinação da linha de amarração

T: Temperatura

t: Tempo

u: Incerteza padrão

UV-Vis: Ultravioleta-visível

V: Volume

LISTA DE FIGURAS

CAPÍTULO 1

Fig. 1. Possíveis rotas de antibióticos no meio ambiente. 4

Fig. 2. Estrutura química do cloranfenicol**.** 5

Fig. 3. Estrutura química do poli(óxido de etileno). 7

Fig. 4. Composições químicas para um ponto de mistura do SAB formado por PEO1500 + sulfato de lítio + água na temperatura de 25 ºC. 8

Fig. 5. Diagrama de fase expresso em coordenadas retangulares de um SAB formado por um polímero e um eletrólito. 8

Fig. 6. Variação das propriedades termodinâmicas extensivas e conservação das intensivas em função das diferentes composições globais do SAB. 9

Fig. 7. Estrutura química do poli(óxido de propileno)..... 10

CAPÍTULO 2

Fig. 1. Influence of the anion on the phase diagram of the PPG425 + ammonium electrolyte + H_2O systems at 298.2 K. (■) $(NH_4)_2C_4H_4O_6$, (Δ) $(NH_4)_2C_6H_6O_7$, (●) $NH_4C_2H_3O_2$ and (○) NH_4CHO_2. 31

Fig. 2. The effect of temperature on the phase diagram of the PPG425 + electrolyte + H_2O ATPS. a) $NH_4C_2H_3O_2$: (▲) 283.2 K and (○) 298.2 K; b) NH_4CHO_2: (▲) 283.2 K and (□) 313.2 K. 33

Fig. 3. Influence of the polymer hydrophobicity on the phase diagram of the polymer + $(NH_4)_2C_6H_6O_7$ + H_2O systems at 298.2 K for (○) PPG425 and (●) PEG900. 36

CAPÍTULO 3

Fig. 1. Chemical structure of chloramphenicol. 50

Fig. 2. Partition coefficient values of CAP as a function of its concentration in ATPS formed by PEG1500 + Li_2SO_4 + H_2O in the TLL of (≅ 29 %(m/m)) at 298.2 K. 53

Fig. 3. Partition coefficient of CAP as a function of TLL in ATPS formed by PEG1500 + Li_2SO_4 + H_2O at 298.2 K. 55

Fig. 4. $\Delta_{tr}G^{\theta}$ of CAP as a function of the TLL for the ATPS composed by PEO1500 + Li_2SO_4 + H_2O at 298.2 K. 56

Fig. 5. CAP $\Delta_{dil}H$ value in polymer-rich phase (a) and electrolyte-rich phase (b) for PEO1500 + Li_2SO_4 + H_2O ATPS: (■/□) (≅ 29 %(m/m)) TLL, (●/○) (≅ 35 %(m/m))

TLL, (▲/△) (≅ 42 %(m/m)) TLL, (▼/▽) (≅ 46 %(m/m)) TLL and (◀/◁) (≅ 52 %(m/m)) TLL at 298.15 K. 57

Fig. 6. $\Delta_{tr}H^{\theta}$ of CAP as a function of the TLL for the ATPS composed by PEO1500 + Li_2SO_4 + H_2O at 298.2 K. 59

Fig. 7. $T\Delta_{tr}S^{\theta}$ of CAP as a function of the TLL for the ATPS composed by PEO1500 + Li_2SO_4 + H_2O at 298.2 K. 60

Fig. 8. CAP partition coefficient (a) and $\Delta_{tr}G^{\theta}$ (b) as a function of the tie-line length (TLL), at 298.2 K. ATPS: (●) PEO1500 + Li_2SO_4 + H_2O; (△) PEO1500 + Na_2SO_4 + H_2O; (□) PEO1500 + $MgSO_4$ + H_2O. 61

Fig. 9. $\Delta_{tr}H^{\theta}$(a) and $T\Delta_{tr}S^{\theta}$(b) as a function of the tie-line length (TLL), at 298.2 K. ATPS: (●) PEO1500 + Li_2SO_4 + H_2O; (△) PEO1500 + Na_2SO_4 + H_2O; (□) PEO1500 + $MgSO_4$ + H_2O. 63

Fig. 10. CAP partition coefficient (a) and $\Delta_{tr}G^{\theta}$(b) as a function of the tie-line length (TLL), at 298.2 K. ATPS: (●) PEO1500 + Li_2SO_4 + H_2O; (○) PEO10000 + Li_2SO_4 + H_2O; (▽) PEO35000 + Li_2SO_4 + H_2O. 64

Fig. 11. $\Delta_{tr}H^{\theta}$(a) and $T\Delta_{tr}S^{\theta}$(b) as a function of the tie-line length (TLL), at 298.2 K. ATPS: (●) PEO1500 + Li_2SO_4 + H_2O; (○) PEO10000 + Li_2SO_4 + H_2O. 65

Fig. 12. CAP partition coeficiente (a) and $\Delta_{tr}G^{\theta}$(b) as a function of the tie-line length (TLL), at 298.2 K. ATPS: (△) PEO1500 + Na_2SO_4 + H_2O; (▶) PEO1500 + $Na_3C_6H_5O_7$ + H_2O; (◁) PEO1500 + $Na_2C_4H_4O_6$ + H_2O. 66

Fig. 13. $\Delta_{tr}H^{\theta}$(a) and $T\Delta_{tr}S^{\theta}$(b) as a function of the tie-line length (TLL), at 298.2 K. ATPS: (△) PEO1500 + Na_2SO_4 + H_2O; (▶) PEO1500 + $Na_3C_6H_5O_7$ + H_2O. 68

Fig. 14. CAP partition coefficient (a) and $\Delta_{tr}G^{\theta}$ (b) as a function of the tie-line length (TLL), at 298.2 K. ATPS: (■) PEO400 + Na_2SO_4 + H_2O; (▷) PPO425 + Na_2SO_4 + H_2O. 69

Fig. 15. $\Delta_{tr}H^{\theta}$(a) and $T\Delta_{tr}S^{\theta}$(b) as a function of the tie-line length (TLL), at 298.2 K. ATPS: (■) PEO400 + Na_2SO_4 + H_2O; (▷) PPO425 + Na_2SO_4 + H_2O. 70

CAPÍTULO 4

Fig. 1. Experimental scheme of LLME in-syringe using ATPS coupled with in-flow UV-Vis detection. 83

Fig. 2. In-flow analytical signal of standards. 85

Fig. 3. Spectrum of standards. 86

Fig. 4. Determination of CAP: a) In flow analytical signal of samples, b) Spectrum of samples. 87

APÊNDICE

Fig. F1. CAP $\Delta_{dil}H$ value in polymer-rich phase (a) and electrolyte-rich phase (b) for PEO1500 + $MgSO_4$ + H_2O ATPS: (■/□) (≅ 34 %(m/m)) TLL, (●/○) (≅ 40 %(m/m)) TLL, (▲/△) (≅ 44 %(m/m)) TLL, (▼/▽) (≅ 47 %(m/m)) TLL and (◀/◁) (≅ 52 %(m/m)) TLL at 298.15 K. 98

Fig. F2. CAP $\Delta_{dil}H$ value in polymer-rich phase (a) and electrolyte-rich phase (b) for PEO1500 + Na_2SO_4 + H_2O ATPS: (■/□) (≅ 33 %(m/m)) TLL, (●/○) (≅ 36 %(m/m)) TLL, (▲/△) (≅ 40 %(m/m)) TLL, and (▼/▽) (≅ 47 %(m/m)) TLL at 298.15 K..... 99

Fig. F3. CAP $\Delta_{dil}H$ value in polymer-rich phase (a) and electrolyte-rich phase (b) for PEO10000 + Li_2SO_4 + H_2O ATPS: (■/□) (≅ 22 %(m/m)) TLL, (●/○) (≅ 26 %(m/m)) TLL, (▲/△) (≅ 31 %(m/m)) TLL, (▼/▽) (≅ 34 %(m/m)) TLL and (◀/◁) (≅ 37 %(m/m)) TLL at 298.15 K. 100

Fig. F4. CAP $\Delta_{dil}H$ value in polymer-rich phase (a) and electrolyte-rich phase (b) for PPO425 + Na_2SO_4 + H_2O ATPS: (■/□) (≅ 31 %(m/m)) TLL, (●/○) (≅ 48 %(m/m)) TLL, (▲/△) (≅ 59 %(m/m)) TLL, and (▼/▽) (≅ 69 %(m/m)) TLL at 298.15 K..... 101

Fig. F5. CAP $\Delta_{dil}H$ value in polymer-rich phase (a) and electrolyte-rich phase (b) for PEO400 + Na_2SO_4 + H_2O ATPS: (■/□) (≅ 38 %(m/m)) TLL, (●/○) (≅ 41 %(m/m)) TLL, (▲/△) (≅ 46 %(m/m)) TLL, and (▼/▽) (≅ 51 %(m/m)) TLL at 298.15 K..... 102

Fig. F6. CAP $\Delta_{dil}H$ value in polymer-rich phase (a) and electrolyte-rich phase (b) for PEO1500 + $Na_3C_6H_5O_7$ + H_2O ATPS: (■/□) (≅ 28 %(m/m)) TLL, (●/○) (≅ 38 %(m/m)) TLL, (▲/△) (≅ 45 %(m/m)) TLL, (▼/▽) (≅ 52 %(m/m)) TLL and (◀/◁) (≅ 56 %(m/m)) TLL at 298.15 K. 103

LISTA DE TABELAS

CAPÍTULO 2

Table 1. Specification of chemical samples. 25

Table 2. Experimental (liquid + liquid) equilibrium data for the system PPG425 (1) + $NH_4C_2H_3O_2$ (electrolyte) (2) + water (3) for mole fractions x at the temperature 283.2 to 313.2 K and pressure p = 0.09341 MPa. [a] 27

Table 3. Experimental (liquid + liquid) equilibrium data for the system PPG425 (1) + $(NH_4)_2C_4H_4O_6$ (electrolyte) (2) + water (3) for mole fractions x at the temperature 283.2 K, 298.2 K and pressure p = 0.09341 MPa.[a] 28

Table 4. Experimental (liquid + liquid) equilibrium data for the system PPG425 (1) + $(NH_4)_2C_6H_6O_7$ (electrolyte) (2) + water (3) for mole fractions x at the temperature 298.2 K, 313.2 K and pressure p = 0.09341 MPa.[a] 28

Table 5. Experimental (liquid + liquid) equilibrium data for the system PPG425 (1) + NH_4CHO_2 (electrolyte) (2) + water (3) for mole fractions x at the temperature 283.2 to 313.2 K and pressure p = 0.09341 MPa.[a] 29

Table 6. Experimental (liquid + liquid) equilibrium data for the system PEO900 (1) + $(NH_4)_2C_6H_6O_7$ (electrolyte) (2) + water (3) for mole fractions x at the temperature 298.2 K and pressure p = 0.09341 MPa.[a] 29

Table 7. STL systems values at 283.2, 298.2, and 313.2 K. 35

Table 8. Estimated NRTL parameters. 39

Table 9. Root mean square deviations in ternary systems. 40

CAPÍTULO 3

Table 1. CAP $\Delta_{dil}H^{\theta,\infty}$ values in polymer-rich phase and electrolyte-rich phase, for different TLL of system PEO1500 + Li_2SO_4 + H_2O at 298.15 K. 57

Table 2. $\Delta_{tr}H^{\theta}$ and $T\Delta_{tr}S^{\theta}$ obtained CAP transfer process in ATPS formed by different cations 63

CAPÍTULO 4

Table 1. Analytical figures of merit of In-syringe method for CAP determination 87

Table 2. Results of chloramphenicol determination in spiked deionized water sample. 87

Table 3. Comparison of some methods for CAP determination. 89

APÊNDICE

Table T1. CAP $\Delta_{dil}H^{\theta,\infty}$ values in polymer-rich phase and electrolyte-rich phase, for different TLL of system PEO1500 + $MgSO_4$ + H_2O at 298.15 K. 98
Table T2. CAP $\Delta_{dil}H^{\theta,\infty}$ values in polymer-rich phase and electrolyte-rich phase, for different TLL of system PEO1500 + Na_2SO_4 + H_2O at 298.15 K. 99
Table T3. CAP $\Delta_{dil}H^{\theta,\infty}$ values in polymer-rich phase and electrolyte-rich phase, for different TLL of system PEO10000 + Li_2SO_4 + H_2O at 298.15 K. 100
Table T4. CAP $\Delta_{dil}H^{\theta,\infty}$ values in polymer-rich phase and electrolyte-rich phase, for different TLL of system PPO425 + Na_2SO_4 + H_2O at 298.15 K 101
Table T5. CAP $\Delta_{dil}H^{\theta,\infty}$ values in polymer-rich phase and electrolyte-rich phase, for different TLL of system PEO400 + Na_2SO_4 + H_2O at 298.15 K 102
Table T6. CAP $\Delta_{dil}H^{\theta,\infty}$ values in polymer-rich phase and electrolyte-rich phase, for different TLL of system PEO1500 + $Na_3C_6H_5O_7$ + H_2O at 298.15 K. 103

RESUMO

QUINTÃO, Juan Carlos, D.Sc., Universidade Federal de Viçosa, fevereiro de 2018. **Sistema aquoso bifásico: obtenção de novos sistemas, partição e determinação de Cloranfenicol**. Orientadora: Maria do Carmo Hespanhol. Coorientadores: Luis Henrique Mendes da Silva e Fábio Rodrigo Piovezani Rocha.

Contaminantes emergentes têm sido mencionados frequentemente como ameaças potenciais ao meio ambiente. Os produtos farmacêuticos são uma classe representativa desses contaminantes, com destaque para os antibióticos. Sistemas Aquosos Bifásicos (SAB) são uma alternativa potencial para partição/extração de antibióticos. Para isso é de grande importância o desenvolvimento de dados de equilíbrio líquido-líquido para esses sistemas, ampliando sua faixa de aplicação. Assim, dados de equilíbrio líquido-líquido para SAB compostos pelos polímeros poli(óxido de propileno) (PPO425) e poli(óxido de etileno) (PEO900) e diferentes eletrólitos de amônio ($NH_4C_2H_3O_2$, $(NH_4)_2C_4H_4O_6$, $(NH_4)_2C_6H_6O_7$ e NH_4CHO_2) foram determinados em diferentes temperaturas. Os parâmetros energéticos para estes sistemas foram estudados através do modelo nonrandom two-liquid (NRTL) como também os fatores que influenciam sua formação (ânion, hidrofobicidade e temperatura). Foi verificado que o aumento da temperatura aumenta a área bifásica em todos os sistemas e que o ânion tartarato apresentou maior capacidade em formar SAB com PPO425. O modelo NRTL apresentou resultados satisfatórios com desvios de 1,82 %. Em outro trabalho, realizou-se o estudo termodinâmico das forças motrizes envolvidas no processo de partição do antibiótico cloranfenicol em diferentes SAB formados por polímero e eletrólito. Os parâmetros termodinâmicos variação da energia livre de Gibbs de transferência ($\Delta_{tr}G^{\theta}$), variação de entalpia padrão de transferência ($\Delta_{tr}H^{\theta}$) e variação de entropia padrão de transferência $\Delta_{tr}S^{\theta}$ foram determinados, variando de (-15.45±0.02) kJ mol^{-1} < $\Delta_{tr}G^{\theta}$ < (-2.64±0.02) kJ mol^{-1}, (-80.88±1.30) kJ mol^{-1} < $\Delta_{tr}H^{\theta}$ < (-8.33±0.04) kJ e (-64.09±0.85) kJ mol^{-1} < T$\Delta_{tr}S^{\theta}$ < (1.26±0.12) kJ mol^{-1}, mostrando que o processo de transferência de cloranfenicol da fase rica em eletrólito para a fase rica em polímero é entalpicamente dirigido e ocorre espontaneamente. Os efeitos da natureza do cátion, ânion, massa molar e hidrofobicidade do polímero foram investigados, mostrando a influência dessas propriedades nos parâmetros termodinâmicos. No último capítulo é apresentada a proposta de um método em fluxo para extração, pré-concentração e

determinação de cloranfenicol em amostra aquosa usando SAB com detecção UV-Vis.

ABSTRACT

QUINTÃO, Juan Carlos, D.Sc., Universidade Federal de Viçosa, February, 2018. **Aqueous two-phase system: obtaining new systems, partitioning and determination of Chloramphenicol.** Adviser: Maria do Carmo Hespanhol. Co-Advisers: Luis Henrique Mendes da Silva and Fábio Rodrigo Piovezani Rocha.

Emerging pollutants have often been mentioned as potential threats to the environment. Pharmaceuticals are a representative class of these contaminants, especially antibiotics. Aqueous Two Phase Systems (ATPS) are a potential alternative for antibiotic partition/extraction. For this, the development of liquid-liquid equilibrium data for these systems is highly important, expanding its range of application. Thus, liquid-liquid equilibrium data for ATPS composed of poly(polypropylene oxide) (PPO425) and poly(ethylene oxide) (PEO900) and different ammonium electrolytes ($NH_4C_2H_3O_2$, $(NH_4)_2C_4H_4O_6$, $(NH_4)_2C_6H_6O_7$ and NH_4CHO_2) were determinated at different temperatures. The energetic parameters for these systems were assessed with the nonrandom two-liquid (NRTL) model as well as the factors that influence its formation (anion, hydrophobicity and temperature). It was verified that temperature increases enlarge the biphasic area in all systems and that the tartrate anion presented greater capacity to form ATPS with PPO425. The NRTL model presented satisfactory results with deviations of 1.82 %. In another work, the thermodynamic study of the driving forces involved in the process of partitioning the antibiotic chloramphenicol was carried out in different ATPS formed by polymer and electrolyte. The thermodynamic parameters transfer standard Gibbs free energy change ($\Delta_{tr}G^{\theta}$), transfer standard enthalpy change ($\Delta_{tr}H^{\theta}$), and transfer standard entropy change ($\Delta_{tr}S^{\theta}$) were determined, ranging from (-15.45±0.02) kJ mol^{-1} < $\Delta_{tr}G^{\theta}$ < -(2.64±0.02) kJ mol^{-1}, (-80.88±1.30) kJ mol^{-1} < $\Delta_{tr}H^{\theta}$ < (-8.33±0.04) kJ and (-64.09±0.85) kJ mol^{-1} < T$\Delta_{tr}S^{\theta}$ < (1.26±0.12) kJ mol^{-1}, showing that the chloramphenicol transfer process from the electrolyte-rich phase to the polymer-rich phase is enthalphically driven and occurs spontaneously. The effects of the cation nature, anion, molar mass and hydrophobicity of the polymer were investigated, showing the influence of these properties on the thermodynamic parameters. In the last chapter a method in flow for extraction, preconcentration and determination of chloramphenicol in aqueous sample using ATPS with UV-Vis detection is proposed.

CAPÍTULO 1

Revisão de Literatura

1. Contaminantes emergentes

Em razão das mudanças ocorridas em todo mundo, no que diz respeito aos aspectos econômicos, sociais e demográficos, tem-se observado o surgimento de novas ameaças químicas ao meio ambiente devido à presença dos denominados contaminantes emergentes. Estes contaminantes, encontrados em ambientes aquáticos e terrestres [1], pertencem a diferentes classes de produtos químicos que são definidos como poluentes previamente não reconhecidos ou que foram introduzidos e/ou identificados recentemente [2].

Os contaminantes emergentes são oriundos de fármacos e seus metabólitos (humanos e veterinários), produtos de higiene pessoal, surfactantes, resíduos de surfactantes, aditivos de gasolina, produtos e subprodutos de desinfecção, nitrosaminas, drogas ilegais e seus metabólitos, hormônios, compostos disruptores endócrinos, retardadores de chamas, plásticos organofosfatados, nanomateriais, edulcorantes artificiais, compostos perfluorados, pesticidas polares (e seus produtos de degradação), toxinas de algas, siloxanos, perclorato, benzotriazóis, genes resistentes a antibióticos, dentre outros [1-3]. Além dessa diversidade de contaminantes, outro problema que se soma são as possíveis transformações que eles podem sofrer no meio ambiente ou durante o tratamento de águas de despejo urbanas e industriais. Isto resulta em um grande número de derivados desconhecidos ou produtos de transformação [4]. Os processos de transformação no ambiente incluem biodegradação, oxidação e redução química, hidrólise e fotólise. Embora esses processos possam reduzir as cargas de contaminantes, alguns dos produtos de transformação são considerados mais tóxicos do que o composto original, gerando preocupações em relação aos riscos ao meio ambiente tanto quanto seus compostos de origem [5, 6].

Um agravante dos contaminantes emergentes é que, muitas vezes, é encontrada no ambiente uma mistura complexa desses contaminantes, o que pode levar a efeitos sinérgicos indesejados. A ubiquidade de um elevado número de contaminantes potencialmente tóxicos no meio ambiente é decorrente da combinação

de baixas taxas de remoção e liberação contínua, porém ainda existe a necessidade de entender melhor sua ocorrência, destino e impacto ambiental [7]. Além disso, ainda não existe uma legislação específica que rege sobre a descarga de contaminantes emergentes e a necessidade de monitorá-los no meio ambiente [8]. Existem apenas algumas regulamentações divulgadas nos últimos anos [9]em decorrência dos possíveis efeitos adversos que estes poluentes podem causar no ambiente, mesmo em baixos níveis.

A contaminação ambiental ocorre principalmente pela descarga de águas residuais “in natura” e tratadas, cujo tratamento não foi projetado para remover contaminantes emergentes, resultando na contaminação das águas superficiais [7]. O descarte de produtos químicos responsáveis pela origem dos contaminantes emergentes no solo também pode levar à contaminação de mananciais por escoamento superficial e de aquíferos por infiltração. A agricultura animal e a aquicultura, também provocam contaminação ambiental, especialmente devido ao uso de antibióticos e hormônios [1]. Assim, os contaminantes emergentes vêm sendo encontrados em todo mundo em efluentes de estação de tratamento de águas residuais [10-12] e em águas de superfície [13-15], para consumo humano [16, 17] e subterrâneas [18]. Esses contaminantes estão concomitantemente presentes em níveis de concentração de ng L^{-1} a μg L^{-1} [8].

1.1 Fármacos no meio ambiente

Novos fármacos têm sido cada vez mais usados pela sociedade e isto tem acarretado no aumento da quantidade e do número de contaminantes emergentes no ambiente. Dentre os fármacos mais usados podem-se destacar os antibióticos [19, 20]. Essa classe é cada vez mais notada devido aos seus impactos negativos conhecidos sobre espécies aquáticas [21, 22] e ecossistemas [6], além de potenciais impactos na saúde humana [23-25].

Embora nem todos os fármacos sejam persistentes, seu uso contínuo e liberação para o meio ambiente os tornam "pseudo-persistentes" [26]. Estes produtos possuem maior potencial para a persistência ambiental em relação a outros contaminantes porque sua fonte se reabastece continuamente [26].

A maior preocupação com as implicações tóxicas dos fármacos é que eles foram criados especificamente para maximizar a atividade biológica em baixas doses e atingir certos mecanismos metabólicos e enzimáticos. Esse modo de ação pode ser

aplicado a toda biota aquática, que é involuntariamente exposta a fármacos em seu ambiente natural, aumentando assim o risco de efeitos ecotoxicológicos [27].

1.1.1 Antibióticos

Desde a descoberta da penicilina no início do século 20 pelo bacteriologista escocês Alexander Fleming, os antibióticos tornaram-se indispensáveis para a saúde humana e animal [28] devido a sua eficácia no tratamento de várias doenças. De acordo com a definição clássica, antibiótico é um composto produzido por um microorganismo que inibe o crescimento de outro microorganismo [29]. Ao longo dos anos, esta definição foi expandida, referindo-se a substâncias com atividades antibacteriana, antifúngica, ou antiparasitária, incluindo produtos sintéticos e semi-sintéticos [29].

Dentre os fármacos, os antibióticos são considerados uma das drogas mais utilizadas [28]. Os valores que comprovam essa afirmativa são bastante expressivos em países, por exemplo, como a China, que é um dos maiores produtores e consumidores de antibióticos do mundo [30], apresentando no ano de 2013, uma produção de 248000 e um consumo de 162000 toneladas, sendo 48% deste valor destinado ao uso humano e o restante ao uso animal [30, 31]. Estima-se ainda que China e países como Estados Unidos, Brasil, Índia e México deverão estar entre os cinco maiores países consumidores de antibióticos para criação animal em 2030 [32].

Uma grande preocupação em relação à liberação de antibióticos, seus metabólitos e produtos de transformação no meio ambiente é porque eles podem afetar as funções ecológicas e a estrutura da comunidade microbiana [33], além de promover a resistência dos microrganismos [34]. Estes poluentes podem ser encontrados no ambiente em baixas concentrações (ng kg^{-1} a μg kg^{-1}) [35-37], podendo em algumas situações, alcançar valores de concentrações superiores a 1 mg kg^{-1} [38].

As possíveis rotas de antibióticos, usados em medicina humana e veterinária, no meio ambiente são mostradas na Fig. 1. Nota-se que após o consumo dos antibióticos por seres humanos ou animais, estes podem ser transportados para o meio ambiente através de águas residuais agrícolas e municipais, e de resíduos animais [39]. Os contaminantes excretados através de urina e fezes podem estar na sua forma originalmente consumida [29], já que 30 a 90 % dos antibióticos permanecem inalterados quando excretados, assim como na forma de metabólitos

e/ou produtos de transformação [40-42]. O resíduo líquido oriundo dos processos de tratamento é descarregado diretamente no ambiente aquático, enquanto o resíduo sólido gerado é depositado no solo como fertilizante. Assim, os contaminantes emergentes podem alcançar as águas subterrâneas através da lixiviação no solo, bem como atingir águas superficiais devido ao escoamento superficial [43].

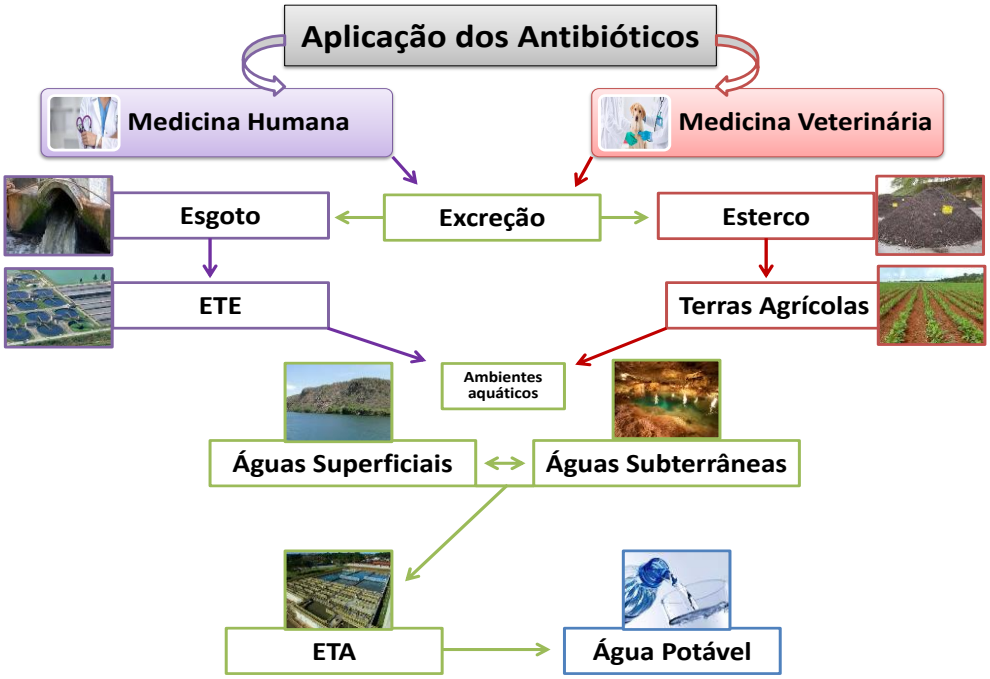

Fig. 1. Possíveis rotas de antibióticos no meio ambiente.

Os antibióticos podem ser divididos em diversas classes, tais como ß-lactâmicos, quinolonas, tetraciclinas, macrolídeos, sulfonamidas, aminoglicosídeos, nitrofuranos, anfenicóis, dentre outros, destacando sua atividade antimicrobiana, usos comuns e características químicas [29, 44]. Dentre eles, os anfenicóis são uma classe de amplo espectro, altamente eficiente contra bactérias gram-positivas e gram-negativas, além de serem eficazes contra microrganismos anaeróbios. Essa classe inclui cloranfenicol, tianfenicol e florfenicol que, embora de origem natural, têm sido sintetizados [45].

O cloranfenicol (Fig. 2) foi o primeiro anfenicol disponível, sendo amplamente utilizado na década de 1950 pelas medicinas humana e veterinária [46]. Embora seja muito eficiente, foi banido da produção de alimentos animais em vários países devido aos graves efeitos adversos à saúde humana [47]. Hoje, seu uso na medicina humana é restrito a infecções oftálmicas e algumas graves infecções,

enquanto o uso veterinário inclui os tratamentos entérico, pulmonares, de pele, abscessos de órgãos e mastite [45].

O cloranfenicol pode ser eliminado intacto ou biotransformado no seu metabólito cloranfenicol glucuronido [47]. Seu uso indiscriminado está associado a vários efeitos colaterais, como resistência bacteriana, reações alérgicas, anemia aplástica, depressão da medula óssea e "síndrome do bebê cinza"[45]. Há também indícios de que o cloranfenicol pode causar câncer [45].

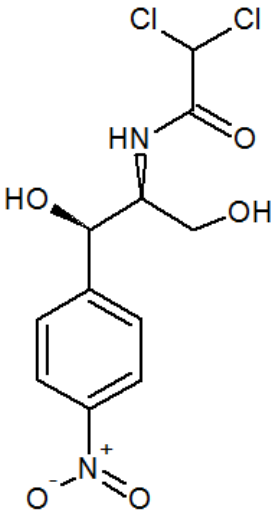

Fig. 2. Estrutura química do cloranfenicol**.**

Diante do potencial risco que o cloranfenicol pode causar aos seres humanos e também a determinados organismos no meio ambiente, é de fundamental importância o desenvolvimento de metodologias capazes de extrair e também quantificar este antibiótico em diferentes matrizes. Uma alternativa simples, de baixo custo e ambientalmente segura que pode contribuir para o avanço científico nesta área seria o uso de sistema aquoso bifásico (SAB).

2. Sistema aquoso bifásico

2.1 Uma abordagem geral

O SAB é considerado uma alternativa eficiente, versátil e ambientalmente segura para a purificação e separação de diferentes solutos [48-52]. Ele foi descoberto

por Martinus Willem Beijerinck em 1896, porém somente na década de 1950 o SAB foi aplicado para partição/purificação pelo cientista Per-Åke Albertsson [52].

O SAB pode ser usado para realizar a extração líquido-líquido devido a partição preferencial de determinado soluto para uma das fases do sistema. Os métodos de extração líquido-líquido que empregam SAB oferecem várias vantagens comparadas aos métodos convencionais de extração, pois não se utiliza solvente orgânico, a separação de fases é rápida, os materiais utilizados são de baixo custo e não tóxicos [49, 53]. Devido às suas vantagens, o SAB tornou-se uma técnica emergente importante para a separação [54] e que futuramente poderá ser aplicada industrialmente para separar e purificar produtos químicos, farmacêuticos e alimentícios em grande escala [55].

2.2 Princípios e propriedades

O SAB é formado pela mistura de duas espécies químicas e água. As duas fases do SAB se formam quando as duas espécies químicas e a água são misturadas em determinadas condições termodinâmicas específicas tais como composição, temperatura e pressão [54]. Essas espécies podem ser dois polímeros quimicamente distintos [56], um polímero e um eletrólito [57], dois eletrólitos [58], e ainda dois surfactantes [59].

O processo de formação das duas fases em um sistema composto por polímero-polímero ou polímero-eletrólito ocorrerá em função das interações intermoleculares, expressas em termos de energia livre de Gibbs, entre os constituintes formadores do SAB [60]. Desta forma, a energia livre de Gibbs de mistura ($\Delta_{mix}G$), relacionada à formação de uma solução, será função das interações e distribuições das moléculas na solução [60]. De acordo com a clássica equação tem-se:

$$\Delta_{mix}G = \Delta_{mix}H - T\Delta_{mix}S \quad (1)$$

onde $\Delta_{mix}H$ corresponde a variação de entalpia de mistura, $\Delta_{mix}S$ a variação de entropia de mistura e T a temperatura.

Quando $\Delta_{mix}G < 0$ a mistura formará espontaneamente um sistema homogêneo e, caso contrário, o sistema buscará uma nova configuração, como por exemplo, a separação em duas fases, para alcançar uma menor energia livre [60].

O SAB tem como principal característica seu elevado conteúdo de água, que é o componente majoritário em ambas as fases, fornecendo assim um ambiente mais ameno e de baixa tensão interfacial para a purificação e separação de solutos, principalmente biomoléculas [61, 62]. Além da água, cada uma das fases é rica em um dos demais componentes formadores do sistema; por exemplo, uma fase é rica em polímero e a outra em eletrólito [63]. O SAB formado por polímero-eletrólito é o mais utilizado na extração líquido-líquido [52, 64]. Comparado ao SAB constituído por polímero-polímero, o SAB formado por polímero-eletrólito tem a vantagem de apresentar maior diferença de densidade entre as fases, menor viscosidade e maior seletividade [54]. Ainda em relação ao SAB composto por polímero-eletrólito, o poli(óxido de etileno), PEO (Fig. 3), tem sido predominantemente empregado em combinação com diferentes eletrólitos. Isto porque o PEO apresenta baixo custo e baixa viscosidade, é biocompatível, não é tóxico, e é solúvel em água [48, 65].

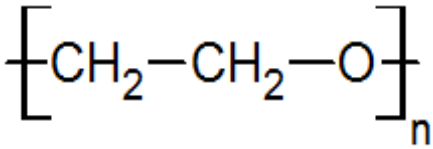

Fig. 3. Estrutura química do poli(óxido de etileno).

A Fig. 4 mostra um exemplo de SAB constituído por polímero + eletrólito + água com as respectivas composições da fase rica em polímero, fase rica em eletrólito e composição global dos componentes obtidas a 25 ^{o}C [55].

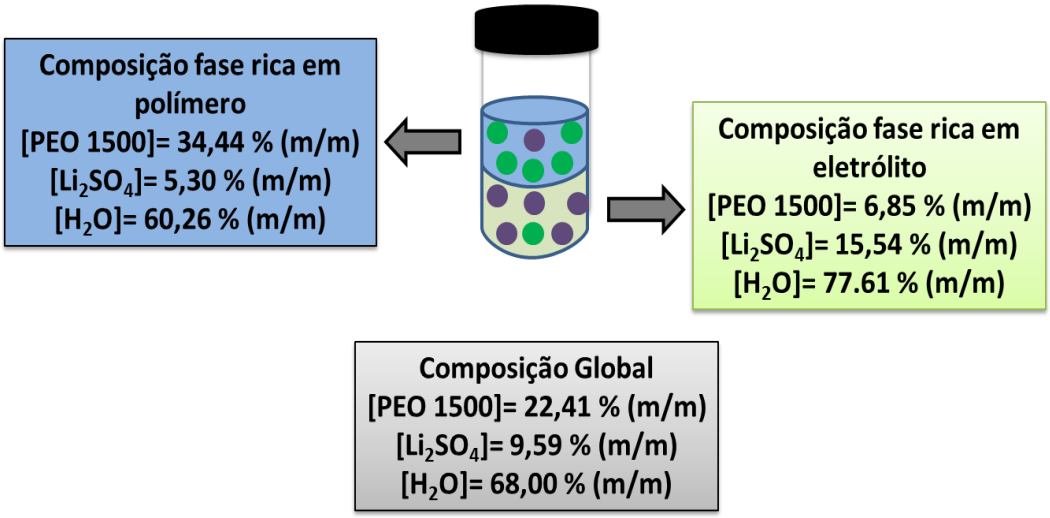

Fig. 4. Composições químicas para um ponto de mistura do SAB formado por PEO1500 + sulfato de lítio + água na temperatura de 25 ºC.

Os dados de composição química referente às duas fases que estão em equilíbrio termodinâmico podem ser representados através de um diagrama de fase retangular como mostrado na Fig. 5 [66].

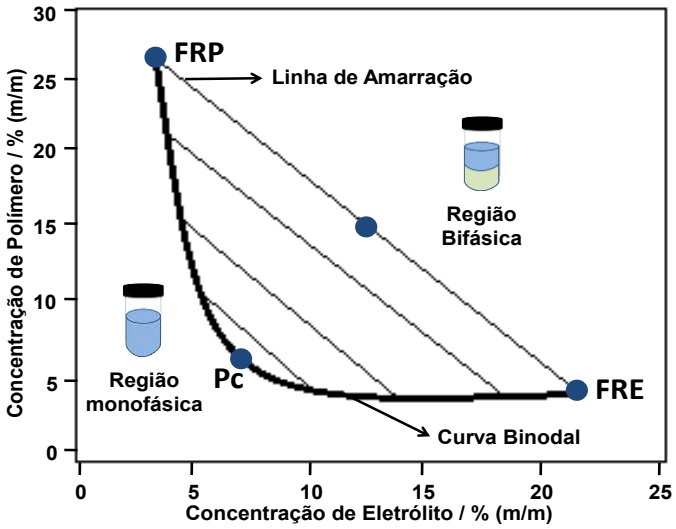

Fig. 5. Diagrama de fase expresso em coordenadas retangulares de um SAB formado por um polímero e um eletrólito.

No diagrama, o eixo das abscissas expressa a concentração do componente 1 (por exemplo, um eletrólito), enquanto o eixo das ordenadas expressa a concentração do componente 2 (por exemplo, polímero), ambas em porcentagem massa-massa, %(m/m). A curva binodal delimita a região onde o sistema é monofásico e bifásico

[60, 66]. As linhas de amarração (LA), também chamadas *"tie-lines"*, ligam os pontos que representam a composição da fase rica em polímero (FRP) com a da fase rica em eletrólito (FRE) [60, 66], sendo que quando o comprimento dessas linhas aproxima-se de zero, atinge-se o ponto crítico (Pc).

As diferentes composições globais pertencentes a uma mesma LA apresentam propriedades termodinâmicas intensivas (por exemplo, concentração e densidade) das fases idênticas, enquanto as propriedades termodinâmicas extensivas (por exemplo, volume e massa) são diferentes, como mostrado na Fig. 6.

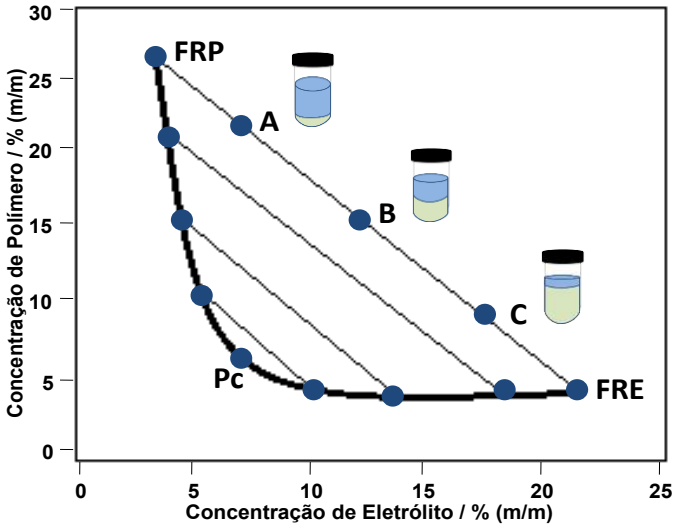

Fig. 6. Variação das propriedades termodinâmicas extensivas e conservação das intensivas em função das diferentes composições globais do SAB.

Diferentes composições globais (A, B e C), apresentam composições idênticas tanto na FRP quanto na FRE. Entretanto, os volumes de fase são diferentes. O comprimento da linha de amarração (CLA) é uma propriedade importante a ser estudada quando se trabalha com SAB, pois ele expressa a diferença das propriedades termodinâmicas intensivas entre as fases em equilíbrio, sendo uma variável determinante na partição de solutos [60, 66]. O CLA pode ser calculado de acordo com a Equação 2:

$$CLA = [(C_P^{FRP} - C_P^{FRE})^2 + (C_E^{FRP} - C_E^{FRE})^2]^{1/2} \quad (2)$$

onde C_P^{FRP} e C_P^{FRE} são as concentrações de polímero na fase rica em polímero e em eletrólito, respectivamente; C_E^{FRP} e C_E^{FRE} são as concentrações de eletrólito na fase

rica em polímero e em eletrólito, respectivamente. As concentrações são dadas em %(m/m). À medida que o CLA aumenta, as fases ricas em polímero e em eletrólito tornam-se mais diferentes em relação às suas propriedades termodinâmicas intensivas, e normalmente isto favorece a eficiência na extração/partição de solutos [60, 66].

2.3 Obtenção de sistema aquoso bifásico

A obtenção de novos SAB é de grande importância uma vez que, com esses novos diagramas, aumentam-se as possibilidades de aplicação desses sistemas na partição/extração de um número cada vez maior de solutos. Com a modulação das propriedades dos componentes formadores do SAB (tipo de eletrólito e massa molar/hidrofobicidade da macromolécula) pode-se aumentar a diferença das propriedades termodinâmicas entre as fases do sistema. Isto favorece a interação do analito com o componente majoritário da fase com a qual ele tem maior afinidade.

A obtenção de novos diagramas contribui também para ampliar o entendimento a respeito da formação destes sistemas, o que é de fundamental importância para pesquisadores que trabalham com SAB. Baseado nisso, uma boa alternativa seria a obtenção de SAB tendo como polímero formador do sistema o poli(propileno glicol), (PPG) (Fig. 7), uma vez que diagramas contendo esse tipo de polímero são escassos [57]. Essa macromolécula possui um grupo metil que confere à mesma característica mais hidrofóbica, favorecendo assim a partição/extração de solutos desta natureza [67].

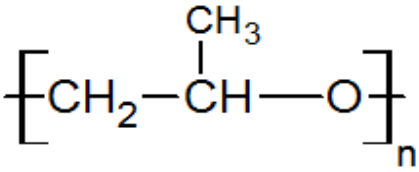

Fig. 7. Estrutura química do poli(óxido de propileno).

3. Partição de soluto em sistema aquoso bifásico

Quando dois líquidos imiscíveis são colocados em contato um com o outro e separam-se em duas fases, as moléculas de soluto tendem a se distribuir de forma desigual entre elas [68]. Isso ocorre devido a um intrincado e delicado balanço de interações entre o soluto e os constituintes presentes em cada fase [60]. Essa

distribuição do soluto entre as fases superior e inferior do SAB estabelece uma relação de equilíbrio, a partir da qual se pode obter o parâmetro termodinâmico "coeficiente de partição" (K). Para a determinação de K é necessário estimar o potencial químico do soluto em cada fase do SAB [60].

No processo de partição, considerando que o sistema está em equilíbrio termodinâmico, o potencial químico de uma determinada espécie *i* em ambas as fases constituintes do sistema devem ser iguais.

$$\mu_i^{FS} = \mu_i^{FI} \tag{3}$$

O potencial químico da espécie *i* nas fases superior e inferior do sistema pode ser expresso de acordo com as equações 4 e 5.

$$\mu_i^{FS} = \mu_i^o(FS) + R\ T\ ln\ a_i^{FS} \tag{4}$$

$$\mu_i^{FI} = \mu_i^o(FI) + R\ T\ ln\ a_i^{FI} \tag{5}$$

onde $\mu_i^o(FS)$ e $\mu_i^o(FI)$ são os potenciais químicos no estado padrão da espécie *i* na fase superior e inferior, respectivamente; R é a constante universal dos gases; T é a temperatura absoluta do sistema; a_i^{FS} e a_i^{FI} são, respectivamente, a atividade do soluto *i* na fase superior e inferior do sistema.

Substituindo as equações 4 e 5, na equação 3 obtém-se a equação 6:

$$\mu_i^o(FS) + R\ T\ ln\ a_i^{FS} = \mu_i^o(FI) + R\ T\ ln\ a_i^{FI} \tag{6}$$

Reorganizando a equação 6, obtém-se a equação 7:

$$\mu_i^o(FS) - \mu_i^o(FI) + R\ T\ ln\ a_i^{FS} - R\ T\ ln\ a_i^{FI} = 0 \tag{7}$$

Rearranjando a equação 7, obtém-se a equação 8:

$$\mu_i^o(FS) - \mu_i^o(FI) = -R\ T\ ln\frac{a_i^{FS}}{a_i^{FI}} \tag{8}$$

A diferença $\mu_i^o(FS) - \mu_i^o(FI)$ equivale à variação de energia livre de Gibbs do sistema quando um mol do soluto *i*, no estado padrão, transfere-se da fase inferior para fase superior do sistema. A variação de energia livre de Gibbs padrão de transferência ($\Delta_{tr}G^o$) é o nome dado à diferença entre os potenciais da FS e FI.

A razão $\frac{a_i^{FS}}{a_i^{FI}}$ é o parâmetro termodinâmico denominado "coeficiente de partição". Assim, a equação 8 pode ser reescrita da seguinte forma:

$$\Delta_{tr}G^o = -R\ T\ ln\ K \tag{9}$$

Em condições de diluição infinita o "coeficiente de partição" (K) pode ser dado por:

$$K = \frac{C_i^{FS}}{C_i^{FI}} \tag{10}$$

onde C_i^{FS}e C_i^{FI}são as concentrações do soluto i em condições de diluição infinita, o que não altera o estado termodinâmico do SAB.

Dessa forma, é possível relacionar o parâmetro K, obtido experimentalmente, com $\Delta_{tr}G^o$, envolvendo todas as interações ocorridas no SAB [60]. Ainda em relação ao processo de partição, a alteração das propriedades das fases também contribui para a distribuição do soluto, como, por exemplo, composição do SAB (CLA), temperatura, pH, tipo e massa molar da macromolécula, hidrofobicidade da macromolécula, tipo de eletrólito, etc [68]. Essa modulação de propriedades contribui para aumentar a eficiência da separação e consequentemente maximizar a recuperação do soluto [68, 69].

O crescente interesse a respeito dos SAB tem proporcionado sua utilização como ferramenta analítica e de processos, incluindo purificação e concentração de solutos [52, 70].

O conhecimento a respeito dos mecanismos de partição em SAB, juntamente com a integração dos mesmos a outras ferramentas, aumenta as possibilidades na ciência da separação, resultando em inúmeros avanços nas aplicações [52].

OBJETIVOS

Objetivo geral

O trabalho proposto apresenta como objetivo obter novos sistemas aquosos bifásicos hidrofóbicos, realizar um estudo termodinâmico da partição de soluto emergente em sistema aquoso bifásico e desenvolver um método para extração/quantificação de contaminante emergente utilizando sistema aquoso bifásico.

Objetivos específicos

1. Obter diagramas de fase formados pelos polímeros poli(propileno glicol) de massa molar 425 g mol^{-1} e poli(etileno glicol) de massa molar 900 g mol^{-1} e eletrólitos compostos pelo cátion amônio nas temperaturas de 283,2, 298,2 e 313,2 K.

2. Avaliar os efeitos do ânion formador do sistema aquoso bifásico (SAB) no processo de separação de fase, o efeito da temperatura na composição do SAB e o efeito da hidrofobicidade na posição da curva binodal.

3. Realizar um estudo termodinâmico para compreensão do processo de transferência de cloranfenicol, através da determinação dos parâmetros variação da energia livre de Gibbs padrão de transferência ($\Delta_{tr}G^{\theta}$), variação da entalpia padrão de transferência ($\Delta_{tr}H^{\theta}$) e variação da entropia padrão de transferência ($\Delta_{tr}S^{\theta}$).

4. Avaliar os efeitos causados na partição do soluto pelas variações das propriedades do SAB como massa molar e hidrofobicidade do polímero, tipo de cátion e tipo de ânion.

5. Propor um método por análise em fluxo para extração/determinação de cloranfenicol em matrizes aquosas usando sistema aquoso bifásico com detecção UV-Vis.

REFERÊNCIAS

[1] K. Noguera-Oviedo, D.S. Aga, Lessons learned from more than two decades of research on emerging contaminants in the environment, J. Hazard. Mater., 316 (2016) 242-251.

[2] A. Aguera, M.J.M. Bueno, A.R. Fernandez-Alba, New trends in the analytical determination of emerging contaminants and their transformation products in environmental waters, Environ Sci Pollut Res Int, 20 (2013) 3496-3515.

[3] S.D. Richardson, S.Y. Kimura, Water Analysis: Emerging Contaminants and Current Issues, Anal. Chem, 88 (2016) 546-582.

[4] D. Fatta-Kassinos, M.I. Vasquez, K. Kümmerer, Transformation products of pharmaceuticals in surface waters and wastewater formed during photolysis and advanced oxidation processes – Degradation, elucidation of byproducts and assessment of their biological potency, Chemosphere, 85 (2011) 693-709.

[5] B.I. Escher, K. Fenner, Recent Advances in Environmental Risk Assessment of Transformation Products, Environ. Sci. Technol, 45 (2011) 3835-3847.

[6] M.D. Celiz, J. Tso, D.S. Aga, Pharmaceutical metabolites in the environment: Analytical challenges and ecological risks, Environ. Toxicol. Chem., 28 (2009) 2473-2484.

[7] B. Petrie, R. Barden, B. Kasprzyk-Hordern, A review on emerging contaminants in wastewaters and the environment: current knowledge, understudied areas and recommendations for future monitoring, Water Res., 72 (2015) 3-27.

[8] E.J. Tiedeken, A. Tahar, B. McHugh, N.J. Rowan, Monitoring, sources, receptors, and control measures for three European Union watch list substances of emerging concern in receiving waters - A 20 year systematic review, Sci. Total Environ., 574 (2017) 1140-1163.

[9] M.O. Barbosa, N.F.F. Moreira, A.R. Robeiro, M.F.R. Pereira, A.M.T. Silva, Occurrence and removal of organic micropollutants: An overview of the watch list of EU Decision 2015/495, Water Res., (2016).

[10] V.G. Samaras, A.S. Stasinakis, D. Mamais, N.S. Thomaidis, T.D. Lekkas, Fate of selected pharmaceuticals and synthetic endocrine disrupting compounds during wastewater treatment and sludge anaerobic digestion, J. Hazard. Mater., 244-245 (2013) 259-267.

[11] Q. Sun, M. Lv, A. Hu, X. Yang, C.-P. Yu, Seasonal variation in the occurrence and removal of pharmaceuticals and personal care products in a wastewater treatment plant in Xiamen, China, J. Hazard. Mater., 277 (2014) 69-75.

[12] J. Martín, D. Camacho-Muñoz, J.L. Santos, I. Aparicio, E. Alonso, Occurrence of pharmaceutical compounds in wastewater and sludge from wastewater treatment plants: Removal and ecotoxicological impact of wastewater discharges and sludge disposal, J. Hazard. Mater., 239-240 (2012) 40-47.

[13] L. Kong, K. Kadokami, S. Wang, H.T. Duong, H.T.C. Chau, Monitoring of 1300 organic micro-pollutants in surface waters from Tianjin, North China, Chemosphere, 122 (2015) 125-130.

[14] S. Bayen, H. Zhang, M.M. Desai, S.K. Ooi, B.C. Kelly, Occurrence and distribution of pharmaceutically active and endocrine disrupting compounds in Singapore's marine environment: Influence of hydrodynamics and physical-chemical properties, Environ. Pollut, 182 (2013) 1-8.

[15] A.L. Batt, T.M. Kincaid, M.S. Kostich, J.M. Lazorchak, A.R. Olsen, Evaluating the extent of pharmaceuticals in surface waters of the United States using a National-scale Rivers and Streams Assessment survey, Environ. Toxicol. Chem., 35 (2016) 874-881.

[16] L.P. Padhye, H. Yao, F.T. Kung'u, C.-H. Huang, Year-long evaluation on the occurrence and fate of pharmaceuticals, personal care products, and endocrine

disrupting chemicals in an urban drinking water treatment plant, Water Res., 51 (2014) 266-276.

[17] G.C.C. Yang, C.-H. Yen, C.-L. Wang, Monitoring and removal of residual phthalate esters and pharmaceuticals in the drinking water of Kaohsiung City, Taiwan, J. Hazard. Mater., 277 (2014) 53-61.

[18] Y. Cabeza, L. Candela, D. Ronen, G. Teijon, Monitoring the occurrence of emerging contaminants in treated wastewater and groundwater between 2008 and 2010. The Baix Llobregat (Barcelona, Spain), J. Hazard. Mater., 239-240 (2012) 32-39.

[19] B. Tiwari, B. Sellamuthu, Y. Ouarda, P. Drogui, R.D. Tyagi, G. Buelna, Review on fate and mechanism of removal of pharmaceutical pollutants from wastewater using biological approach, Bioresour. Technol., 224 (2017) 1-12.

[20] T. Heberer, Occurrence, fate, and removal of pharmaceutical residues in the aquatic environment: a review of recent research data, Toxicol. Lett., 131 (2002) 5-17.

[21] B.W. Brooks, Fish on Prozac (and Zoloft): Ten years later, Aquat. Toxicol., 151 (2014) 61-67.

[22] M. Crane, C. Watts, T. Boucard, Chronic aquatic environmental risks from exposure to human pharmaceuticals, Sci. Total Environ., 367 (2006) 23-41.

[23] G.M. Bruce, R.C. Pleus, S.A. Snyder, Toxicological Relevance of Pharmaceuticals in Drinking Water, Environ. Sci.Technol., 44 (2010) 5619-5626.

[24] V.L. Cunningham, S.P. Binks, M.J. Olson, Human health risk assessment from the presence of human pharmaceuticals in the aquatic environment, Regul. Toxicol. Pharmacol., 53 (2009) 39-45.

[25] A. Kumar, B. Chang, I. Xagoraraki, Human Health Risk Assessment of Pharmaceuticals in Water: Issues and Challenges Ahead, Int. J. Environ. Res. Public Health, 7 (2010) 3929-3953.

[26] A.J. Ebele, M. Abou-Elwafa Abdallah, S. Harrad, Pharmaceuticals and personal care products (PPCPs) in the freshwater aquatic environment, Emerging Contaminants, 3 (2017) 1-16.

[27] E. Fabbri, S. Franzellitti, Human pharmaceuticals in the marine environment: Focus on exposure and biological effects in animal species, Environ. Toxicol. Chem., 35 (2016) 799-812.

[28] S. Klatte, H.-C. Schaefer, M. Hempel, Pharmaceuticals in the environment - A short review on options to minimize the exposure of humans, animals and ecosystems, Sustainable Chemistry and Pharmacy, (2016).

[29] K. Kummerer, Antibiotics in the aquatic environment-a review-part I, Chemosphere, 75 (2009) 417-434.

[30] M. Qiao, G.-G. Ying, A.C. Singer, Y.-G. Zhu, Review of antibiotic resistance in China and its environment, Environ. Int., 110 (2018) 160-172.

[31] Q.-Q. Zhang, G.-G. Ying, C.-G. Pan, Y.-S. Liu, J.-L. Zhao, Comprehensive Evaluation of Antibiotics Emission and Fate in the River Basins of China: Source Analysis, Multimedia Modeling, and Linkage to Bacterial Resistance, Environ. Sci. Technol., 49 (2015) 6772-6782.

[32] T. Boeckel, C. Brower, M. Gilbert, B. T. Grenfell, S. A. Levin, T. Robinson, A. Teillant, R. Laxminarayan, Global trends in antimicrobial use in food animals, PNAS, 112 (2015) 5649-5654.

[33] C. Ding, J. He, Effect of antibiotics in the environment on microbial populations, Appl. Microbiol. Biotechnol., 87 (2010) 925-941.

[34] R.I. Aminov, The role of antibiotics and antibiotic resistance in nature, Environ. Microbiol., 11 (2009) 2970-2988.

[35] F. Tamtam, F. Mercier, B. Le Bot, J. Eurin, Q. Tuc Dinh, M. Clément, M. Chevreuil, Occurrence and fate of antibiotics in the Seine River in various hydrological conditions, Sci. Total Environ., 393 (2008) 84-95.

[36] L. Tong, S. Huang, Y. Wang, H. Liu, M. Li, Occurrence of antibiotics in the aquatic environment of Jianghan Plain, central China, Sci. Total Environ., 497-498 (2014) 180-187.

[37] V. Homem, A. Alves, L. Santos, Development and Validation of a Fast Procedure To Analyze Amoxicillin in River Waters by Direct-Injection LC-MS/MS, J. Chem. Educ., 91 (2014) 1961-1965.

[38] H. Liu, G. Zhang, C.-Q. Liu, L. Li, M. Xiang, The occurrence of chloramphenicol and tetracyclines in municipal sewage and the Nanming River, Guiyang City, China, J. Environ. Monit., 11 (2009) 1199-1205.

[39] K. Chen, J.L. Zhou, Occurrence and behavior of antibiotics in water and sediments from the Huangpu River, Shanghai, China, Chemosphere, 95 (2014) 604-612.

[40] W.-h. Xu, G. Zhang, S.-c. Zou, X.-d. Li, Y.-c. Liu, Determination of selected antibiotics in the Victoria Harbour and the Pearl River, South China using high-performance liquid chromatography-electrospray ionization tandem mass spectrometry, Environ. Pollut., 145 (2007) 672-679.

[41] H.W. Leung, T.B. Minh, M.B. Murphy, J.C.W. Lam, M.K. So, M. Martin, P.K.S. Lam, B.J. Richardson, Distribution, fate and risk assessment of antibiotics in sewage treatment plants in Hong Kong, South China, Environ. Int., 42 (2012) 1-9.

[42] S. Rodríguez-Mozaz, S. Chamorro, E. Marti, B. Huerta, M. Gros, A. Sànchez-Melsió, C. Borrego, D. Barcelo, J. Balcazar, Occurrence of antibiotics and antibiotic

resistance genes in hospital and urban wastewaters and their impact on the receiving river, Water Res., 69 (2015) 234-242.

[43] A. Nikolaou, S. Meric, D. Fatta, Occurrence patterns of pharmaceuticals in water and wastewater environments, Anal. Bioanal. Chem., 387 (2007) 1225-1234.

[44] L. Santos, F. Ramos, Analytical strategies for the detection and quantification of antibiotic residues in aquaculture fishes: A review, Trends Food Sci. Technol., 52 (2016) 16-30.

[45] L.R. Guidi, P.A.S. Tette, C. Fernandes, L.H.M. Silva, M.B.A. Gloria, Advances on the chromatographic determination of amphenicols in food, Talanta, 162 (2017) 324-338.

[46] E. Gikas, P. Kormali, D. Tsipi, A. Tsarbopoulos, Development of a Rapid and Sensitive SPE-LC-ESI MS/MS Method for the Determination of Chloramphenicol in Seafood, J. Agric. Food Chem., 52 (2004) 1025-1030.

[47] J.C. Hanekamp, A. Bast, Antibiotics exposure and health risks: Chloramphenicol, Environ. Toxicol. Pharmacol., 39 (2015) 213-220.

[48] D.S. de Araujo, L.I. Mafra, C.I. Yamamoto, E.F. de Andrade, M.O. de Souza, M.R. Mafra, F. de Castilhos, Aqueous two-phase (polyethylene glycol+sodium sulfate) system for caffeine extraction: Equilibrium diagrams and partitioning study, J. Chem. Thermodyn., 98 (2016) 86-94.

[49] R.C. da Cunha, P.R. Patrício, S.J.R. Vargas, L.H.M.d. Silva, M.C.H. da Silva, Green recovery of mercury from domestic and industrial waste, J. Hazard. Mater., 304 (2016) 417-424.

[50] J.M. de Alvarenga, R.A. Fideles, M.V. da Silva, G.F. Murari, J.G. Taylor, L.R. de Lemos, G.D. Rodrigues, A.B. Mageste, Partition study of textile dye Remazol Yellow Gold RNL in aqueous two-phase systems, Fluid Phase Equilib., 391 (2015) 1-8.

[51] W. Zhang, G. Zhang, J. Han, Y. Yan, B. Chen, C. Sheng, Y. Liu, Phase equilibrium and chloramphenicol partitioning in aqueous two-phase system composed of 1-hydroxylhexyl-3-methylimidazolium chloride-salt, J. Mol. Liq., 193 (2014) 226-231.

[52] S. Ahmed, Aqueous two-phase system (ATPS): an overview and advances in its applications, Biol. Proced. Online, 18 (2016) 1-18.

[53] M. Yavari, G.R. Pazuki, M. Vossoughi, S.A. Mirkhani, A.A. Seifkordi, Partitioning of alkaline protease from Bacillus licheniformis (ATCC 21424) using PEG-K_2HPO_4 aqueous two-phase system, Fluid Phase Equilib., 337 (2013) 1-5.

[54] W. Zhang, Y. Hu, Y. Wang, J. Han, L. Ni, Y. Wu, Liquid-liquid equilibrium of aqueous two-phase systems containing poly(ethylene glycol) of different molecular weights and several ammonium salts at 298.15K, Thermochim. Acta, 560 (2013) 47-54.

[55] J.P. Martins, C.P. Carvalho, L.H.M. da Silva, J.S.R. Coimbra, M.C.H. da Silva, G.D. Rodrigues, L.A. Minim, Liquid-Liquid Equilibria of an Aqueous Two-Phase System Containing Poly(ethylene) Glycol 1500 and Sulfate Salts at Different Temperatures, J. Chem. Eng. Data, 53 (2008) 238-241.

[56] Z. Zhao, Q. Li, X. Ji, R. Dimova, R. Lipowsky, Y. Liu, Molar mass fractionation in aqueous two-phase polymer solutions of dextran and poly(ethylene glycol), J. Chromatogr. A, 1452 (2016) 107-115.

[57] J.C. Quintão, P.R. Patrício, A.C.G. Veloso, R.M.M. de Carvalho, L.H.M. da Silva, M.C. Hespanhol, Liquid-liquid equilibrium of the ternary ammonium salt + poly(propylene glycol) + water system, Fluid Phase Equilib., 442 (2017) 96-103.

[58] S. Malekghasemi, B. Mokhtarani, S. Hamzehzadeh, H. Hajfarajollah, A. Sharifi, M. Mirzaei, Phase diagrams of aqueous biphasic systems composed of ionic liquids

and dipotassium carbonate at different temperatures, Fluid Phase Equilib, 415 (2016) 193-202.

[59] J.X. Xiao, U. Sivars, F. Tjerneld, Phase behavior and protein partitioning in aqueous two-phase systems of cationic-anionic surfactant mixtures, J. Chromatogr. B Biomed. sci. appl., 743 (2000) 327-338.

[60] L.H.M. da Silva, W. Loh, Sistemas aquosos bifásicos: fundamentos e aplicações para partição/purificação de proteínas, Quim. Nova, 29 (2006) 1345-1351.

[61] T. Murugesan, M. Perumalsamy, Liquid-Liquid Equilibria of Poly(ethylene glycol) 2000 + Sodium Citrate + Water at (25, 30, 35, 40, and 45) °C, J. Chem. Eng. Data, 50 (2005) 1392-1395.

[62] R.M. de Oliveira, J.S.R. Coimbra, L.A. Minim, L.H.M. da Silva, M.P.F. Fontes, Liquid-Liquid Equilibria of Biphasic Systems Composed of Sodium Citrate + Polyethylene(glycol) 1500 or 4000 at Different Temperatures, J. Chem. Eng. Data, 53 (2008) 895-899.

[63] R. Govindarajan, K. Divya, M. Perumalsamy, Phase Behavior and Density for Binary and Ternary Solutions of PEG 4000 + Triammonium Citrate + Water Aqueous Two Phase Systems at Different Temperatures, J. Chem. Eng. Data, 58 (2013) 315-321.

[64] F. Ruiz-Ruiz, J. Benavides, O. Aguilar, M. Rito-Palomares, Aqueous two-phase affinity partitioning systems: Current applications and trends, J. Chromatogr. A, 1244 (2012) 1-13.

[65] R. Iyyaswami, P. Belur, B. Girish, Vishwanatha, V.H. Nagaraj, Development and Evaluation of PEG-Lithium Citrate Salt Based Aqueous Two Phase System and Its Application in Partitioning of Proteins from Fish Industry Effluent, Sep. Sci. Technol., 474 (2012) 591-598.

[66] M.C.H. da Silva, L.H.M. da Silva, F.J. Paggioli, J.S.R. Coimbra, L.A. Minim, Sistema aquoso bifásico: uma alternativa eficiente para extração de íons, Quim. Nova, 29 (2006) 1332-1339.

[67] U. Dorn, S. Enders, Heat of mixing and liquid-liquid equilibrium of water + polypropylene glycol (PPG) with different molecular weights and water + propylene glycol dimethyl ether, Fluid Phase Equilib., 424 (2016) 58-67.

[68] M. Jayapal, I. Regupathi, T. Murugesan, Liquid-Liquid Equilibrium of Poly(ethylene glycol) 2000 + Potassium Citrate + Water at (25, 35, and 45) °C, J. Chem. Eng. Data, 52 (2007) 56-59.

[69] D. Ramya, S. Arumugam, S. Saravanan, Liquid-liquid Equilibria of aqueous two-phase systems containing poly (ethylene glycol) of different molecular weight and potassium citrate, Int. J. Chem. Sci., 10 (2012) 365-376.

[70] A.L. Grilo, M.R. Aires-Barros, A.M. Azevedo, Partitioning in Aqueous Two-Phase Systems: Fundamentals, Applications and Trends, Sep. Purif. Rev., 45 (2016) 68-80.

CAPÍTULO 2

Liquid-liquid equilibrium of the ternary ammonium salt + poly(propylene glycol) + water system

Abstract

Aqueous two-phase systems (ATPS) have been investigated as alternative systems for liquid-liquid extraction. Many ATPS phase diagrams for poly(ethylene glycol) (PEG) have been reported, but little information is available regarding liquid-liquid equilibrium data for poly(propylene glycol) (PPG). In the present work, the phase diagrams for PPG425 + ammonium acetate + H_2O, PPG425 + ammonium tartrate + H_2O, PPG425 + ammonium citrate + H_2O, PPG425 + ammonium formate + H_2O, and PEG900 + ammonium citrate + H_2O were experimentally determined at 283.2, 298.2, and 313.2 K. The study of statistic treatment was introduced by the nonrandom two-liquid (NRTL) model. This model is used to estimate the energetic parameters of the studied systems. The binary interactions of the calculated parameters are very important for designing or optimizing industrial processes. The results were considered very satisfactory with global root mean square deviations of 1.82 %. Factors affecting the phase-forming capability of the polymer + electrolyte + water ATPS, such as anion structure, temperature and polymer hydrophobicity were evaluated. For all systems, the increase in temperature enlarges the area of the phase diagram, indicating the enthalpic contribution to the formation of the biphasic system. The ability of the different anions to induce ATPS formation with PPG425 followed the order: $C_4H_4O_6^{2-}$ (tartrate) > $C_6H_6O_7^{2-}$ (citrate) > $C_2H_3O_2^-$ (acetate) > CHO_2^- (formate). The ATPS involving PPG425 showed a larger two-phase area than that observed in the system formed by PEG900, which is more hydrophilic than PPG425.

Keywords: Aqueous two-phase systems, Phase diagram, Poly(propylene glycol), Poly(ethylene glycol), NRTL.

1. Introduction

Liquid-liquid extraction using aqueous two-phase systems (ATPS) has been used to extract metals [1-3], dyes [4-6], biomolecules [7-9], and phenolic compounds

[10, 11]. These systems can be formed by the mixture of aqueous solutions of incompatible polymers [12-14], by a polymer and an electrolyte [4, 15-18], or by two electrolytes [4, 19-21] at specific conditions of temperature, pressure, and composition. The resultant system is composed of two phases, a polymer-rich phase (PRP) and an electrolyte-rich phase (ERP).

The most commonly used ATPS contain hydrophilic macromolecules of poly(ethylene glycol) (PEG) [3, 9, 10, 22]. This polymer is used in partitioning studies of water soluble compounds, since the selective distribution of substances between the phases at equilibrium is a consequence of the interactions established between the solutes and the phase-forming constituents [1, 2, 5, 23]. In order to extend the applicability of the system to hydrophobic compounds, a possibility is to use poly(propylene glycol) (PPG) as the ATPS-forming component. There are several reports detailing the liquid-liquid equilibrium data for PEG, but the literature still lacks the phase diagrams for PPG. This macromolecule displays hydrophobic characteristics due to the presence of one additional methyl group per monomer when compared to PEG [24]. This remarkable property enables the handling of strategic hydrophobic compounds in ATPS [24]. Moreover, PPG is biodegradable [25], can be recovered by heating [25], and is safe [25, 26], enabling its use in the food and cosmetics industry [26].

In the present work, we report the determination of the experimental liquid-liquid equilibrium data for ATPS containing PPG with an average molar mass of 425 g mol^{-1} (PPG425) and different electrolytes: PPG425 + $NH_4C_2H_3O_2$ + H_2O, PPG425 + $(NH_4)_2C_4H_4O_6$+ H_2O, PPG425 + $(NH_4)_2C_6H_6O_7$ + H_2O, and PPG425 + NH_4CHO_2 + H_2O at 283.2, 298.2, and 313.2 K. One ATPS containing poly(ethylene glycol) with an average molar mass of 900 g mol^{-1} (PEG900) +$(NH_4)_2C_6H_6O_7$ + H_2O was also investigated at 298.2 K.

The interest in studying the ammonium salts in this work, it is because these salts are less aggressive to analytical instruments, and due to the existence of few phase diagrams formed by organic anions with the ammonium cations.

The non-random two-liquid (NRTL) [27] model was used to represent the energy parameters of the system. The temperature is the dependent variable of this model. The experimental data were correlated with the modified NRTL model for the activity coefficient, with estimation of new interaction parameters.

2. Materials and Methods

2.1. Materials

Deionized water (Millipore, Milli-Q) was used to prepare all solutions. Analytical-grade reagents were used as received without further purification as shown in Table 1.

Table 1. Specification of chemical samples.

Chemical Name	Source	Initial Mole Fraction Purity
PPG425[a]	Aldrich	0.999
PEG900[b]	Aldrich	0.999
Ammonium citrate dibasic	Fluka	0.990
Ammonium acetate	Neon	0.980
Ammonium tartrate	Vetec	0.990
Ammonium formate	Vetec	0.960

[a] Poly(propylene glycol) with an average molar mass of 425 g mol^{-1}.
[b] Poly(ethylene glycol) with an average molar mass of 900 g mol^{-1}.

2.2. Preparation of the aqueous two-phase systems

Aqueous stock solutions of PPG425 and the electrolyte were prepared using an analytical balance (AY 220, Shimadzu; uncertainty of ± 0.0001 g). Appropriate quantities of these stock solutions were weighed in glass vessels to obtain the desired global compositions. The samples were stirred in a vortex mixer (Certomat MV, B. Braun Biotech International) until the system became cloudy, and were placed in a temperature-controlled bath (MQBTC 99-20, Micro-quimica; uncertainty of ± 0.1 K) at 283.2, 298.2, or 313.2 K for at least 48 h. The thermodynamic equilibrium was characterized by the presence of two clear phases that were collected and appropriately diluted for quantification.

2.3. Determination of equilibrium composition

The electrolyte concentration (ammonium acetate, ammonium citrate, ammonium formate, and ammonium tartrate) was determined by conductivity (DM-32, Digimed) after obtaining the analytical curves ($R^2 \geq 0.999$) of the electrolyte in the dynamic range of 1.00×10^{-3} to 300×10^{-3} % (w/w). The electrolyte solutions show

the same conductivity in water and in the diluted polymer solution. A refractometer (Abbe 09-2011, Analytik Jena) was used to measure the PPG425 and PEG900 concentrations. Aqueous polymer solutions (or electrolyte aqueous solutions) were prepared and analyzed in a refractometer, and analytical curves with similar linear adjustments for PPG425 / PEG900 and electrolyte were obtained. Thus, the refractive index was considered an additive property, i.e., the refractive index value is proportional to the sum of the concentration of electrolyte and polymer for the ATPS phases. The total concentration of the phase components (polymer and electrolyte) was determined by the refractive index, and the PPG425/PEG900 concentration was obtained by subtracting the electrolyte concentration (acquired by conductivity). The water content was determined from the mass balance. All analytical measurements were performed in duplicate.

2.4. Nonrandom two-liquid (NRTL) model and Parameter Estimation

The NRTL activity coefficient model was used in this work. The experimental data were correlated with this model and new thermodynamic interaction parameters were estimated. The equations of the original NRTL model were altered for systems containing electrolytes and polymers. This model has five adjustable parameters for each binary pair.

The estimation of the new binary interaction parameters was performed using the FORTRAN code WTML-LLE (weight temperature-maximum likelihood – liquid-liquid equilibrium).

3. Results and Discussion

3.1. Aqueous two-phase system compositions

In general, ATPS containing a macromolecule, electrolyte, and water are more efficient than ATPS formed by two macromolecules and water for the extraction and purification of different solutes. Therefore, the modification of the ATPS-forming polymer or electrolyte allows modulation of the characteristics of the phases, to enable their application for different compounds. The phase compositions for new aqueous two-phase systems formed by PPG425 + $NH_4C_2H_3O_2$ + H_2O, PPG425 + $(NH_4)_2C_4H_4O_6$ + H_2O, PPG425 + $(NH_4)_2C_6H_6O_7$ + H_2O, PPG425 + NH_4CHO_2 + H_2O, and PEG900 + $(NH_4)_2C_6H_6O_7$ + H_2O at different temperatures

(283.2, 298.2, and 313.2 K) and the tie-line lengths (TLL) are shown in Tables 2 to 6. The standard uncertainties were calculated using the compositions of the polymer-rich phase and electrolyte-rich phase at 298.2 K and 313.2 K. The measurements at 283.2 K were difficult to carry out due long period necessary to splitting phase and reach the thermodynamic equilibrium, being thus less precise. The phase compositions are presented in mole fraction (x).

Table 2. Experimental (liquid + liquid) equilibrium data for the system PPG425 (1) + $NH_4C_2H_3O_2$ (electrolyte) (2) + water (3) for mole fractions x at the temperature 283.2 to 313.2 K and pressure p = 0.09341 MPa. [a]

Overall			polymer-rich phase(PRP)			electrolyte-rich phase(ERP)			
x_1	x_2	x_3	x_1	x_2	x_3	x_1	x_2	x_3	TLL
T = 283.2 K									
0.3338	0.02362	0.6425	0.6275	0.004737	0.3662	0.1318	0.03883	0.8173	0.4969
0.3440	0.02619	0.6298	0.6605	0.004714	0.3332	0.1106	0.04579	0.8295	0.5514
0.3543	0.02883	0.6168	0.6672	0.004814	0.3265	0.1054	0.04770	0.8323	0.5634
0.3651	0.03156	0.6034	0.6729	0.004527	0.3211	0.08963	0.05425	0.8397	0.5854
0.3761	0.03440	0.5895	0.6897	0.004879	0.3039	0.07230	0.06001	0.8496	0.6199
T = 298.2 K									
0.2940	0.01220	0.6938	0.4461	0.006281z	0.5476	0.1520	0.01792	0.8301	0.2943
0.3024	0.01255	0.6851	0.4608	0.005994	0.5332	0.1410	0.01961	0.8394	0.3201
0.3115	0.01291	0.6756	0.4769	0.005720	0.5174	0.1279	0.02125	0.8509	0.3493
0.3205	0.01328	0.6662	0.4984	0.005431	0.5174	0.1209	0.02290	0.8562	0.3779
0.3299	0.01366	0.6565	0.5144	0.005259	0.4804	0.1143	0.02444	0.8613	0.4006
T = 313.2 K									
0.3024	0.01255	0.6851	0.6132	0.001971	0.3848	0.05537	0.02314	0.9215	0.5582
0.3297	0.01367	0.6566	0.6845	0.001522	0.3140	0.05534	0.02439	0.9203	0.6296

[a] Standard uncertainties u are u(temperature) = 0.1 K, u(PPG_{PRP}) = 0.0091, u(PPG_{ERP}) = 0.00185, u($electrolyte_{PRP}$) = 0.000027, u($electrolyte_{ERP}$) = 0.00064, u($water_{PRP}$)= 0.0099, u($water_{ERP}$)= 0.0012 and u(p) = 0.20 kPa.

Table 3. Experimental (liquid + liquid) equilibrium data for the system PPG425 (1) + $(NH_4)_2C_4H_4O_6$ (electrolyte) (2) + water (3) for mole fractions x at the temperature 283.2 K, 298.2 K and pressure p = 0.09341 MPa.[a]

overall			polymer-rich phase(PRP)			electrolyte-rich phase(ERP)			
x_1	x_2	x_3	x_1	x_2	x_3	x_1	x_2	x_3	TLL
T = 283.2 K									
0.2678	0.01233	0.7199	0.5182	0.0005435	0.4813	0.01534	0.03018	0.9545	0.5037
0.2873	0.01303	0.6996	0.5494	0.0004443	0.4502	0.01317	0.03238	0.9545	0.5372
0.3088	0.01379	0.6774	0.5577	0.0004907	0.4419	0.01277	0.03471	0.9525	0.5460
T = 298.2 K									
0.2195	0.005090	0.7754	0.3452	0.001972	0.6528	0.08146	0.008314	0.9102	0.2638
0.2274	0.005260	0.7673	0.3600	0.001741	0.6383	0.07465	0.008949	0.9164	0.2854
0.2360	0.005500	0.7585	0.3742	0.001602	0.6242	0.06551	0.009857	0.9246	0.3088
0.2445	0.005560	0.7499	0.3943	0.001467	0.6043	0.05782	0.01101	0.9246	0.3366
0.2522	0.005740	0.7420	0.4082	0.001282	0.5905	0.05190	0.01202	0.9361	0.3565

[a] Standard uncertainties u are u(temperature) = 0.1 K, $u(PPG_{PRP})$ = 0.0018, $u(PPG_{ERP})$ = 0.00073, $u(electrolyte_{PRP})$ = 0.000012, $u(electrolyte_{ERP})$ = 0.000128, $u(water_{PRP})$= 0.0018, $u(water_{ERP})$= 0.0005 and u(p) = 0.20 kPa.

Table 4. Experimental (liquid + liquid) equilibrium data for the system PPG425 (1) + $(NH_4)_2C_6H_6O_7$ (electrolyte) (2) + water (3) for mole fractions x at the temperature 298.2 K, 313.2 K and pressure p = 0.09341 MPa.[a]

overall			polymer-rich phase(PRP)			electrolyte-rich phase(ERP)			
x_1	x_2	x_3	x_1	x_2	x_3	x_1	x_2	x_3	TLL
T = 298.2 K									
0.2406	0.005247	0.7541	0.3436	0.002684	0.6537	0.07613	0.01010	0.9138	0.2676
0.2600	0.005517	0.7345	0.3821	0.002171	0.6158	0.05399	0.01329	0.9327	0.3283
0.2805	0.005816	0.7137	0.4081	0.001774	0.5902	0.04364	0.01543	0.9409	0.3647
0.3013	0.006133	0.6926	0.4387	0.001514	0.5597	0.03304	0.01817	0.9488	0.4060
0.3235	0.006477	0.6701	0.4656	0.001274	0.5332	0.02607	0.02022	0.9537	0.4399
T = 313.2 K									
0.2410	0.005239	0.7538	0.5416	0.0004768	0.4580	0.04105	0.008862	0.9501	0.5006
0.2598	0.005523	0.7347	0.5625	0.0003731	0.4372	0.03483	0.01012	0.9551	0.5277
0.2804	0.005818	0.7138	0.5654	0.0003857	0.4342	0.03055	0.01100	0.9585	0.5350
0.3021	0.006140	0.6917	0.5967	0.0003586	0.4029	0.02532	0.01272	0.9620	0.5716

[a] Standard uncertainties u are u(temperature) = 0.1 K, $u(PPG_{PRP})$ = 0.0122, $u(PPG_{ERP})$ = 0.00144, $u(electrolyte_{PRP})$ = 0.0000162 , $u(electrolyte_{ERP})$ = 0.000341, $u(water_{PRP})$= 0.0122, $u(water_{ERP})$= 0.0009 and u(p) = 0.20 kPa.

Table 5. Experimental (liquid + liquid) equilibrium data for the system PPG425 (1) + NH_4CHO_2 (electrolyte) (2) + water (3) for mole fractions x at the temperature 283.2 to 313.2 K and pressure p = 0.09341 MPa.[a]

Overall			polymer-rich phase(PRP)			electrolyte-rich phase(ERP)			
x_1	x_2	x_3	x_1	x_2	x_3	x_1	x_2	x_3	TLL
				T = 283.2 K					
0.3278	0.02611	0.6461	0.6410	0.005622	0.3534	0.1536	0.03710	0.8093	0.4884
0.3616	0.02834	0.6101	0.6572	0.006743	0.3361	0.1445	0.04439	0.8111	0.5141
0.3799	0.02955	0.5906	0.6763	0.006954	0.3168	0.1454	0.04834	0.8063	0.5325
				T = 298.2 K					
0.2964	0.01554	0.6881	0.4832	0.007529	0.5093	0.1552	0.02269	0.8221	0.3283
0.3171	0.01616	0.6667	0.5169	0.007254	0.4758	0.1465	0.02646	0.8270	0.3709
0.3398	0.01682	0.6434	0.5642	0.006956	0.4289	0.1260	0.03028	0.8437	0.4388
0.3635	0.01752	0.6190	0.5724	0.006829	0.4208	0.1112	0.03477	0.8540	0.4620
0.3880	0.01823	0.5938	0.6147	0.006512	0.3788	0.09623	0.03937	0.8644	0.5195
				T = 313.2 K					
0.2961	0.01554	0.6884	0.6162	0.002519	0.3813	0.05335	0.02702	0.9196	0.5634
0.3171	0.01616	0.6667	0.6548	0.002612	0.3425	0.05229	0.03014	0.9176	0.6031
0.3399	0.01682	0.6433	0.6709	0.002674	0.3264	0.04530	0.03301	0.9217	0.6263
0.3636	0.01752	0.6189	0.6804	0.002709	0.3169	0.04030	0.03738	0.9223	0.6410
0.3878	0.01824	0.5939	0.7104	0.002940	0.2866	0.04127	0.03849	0.9202	0.6701

[a] Standard uncertainties u are u(temperature) = 0.1 K, $u(PPG_{PRP})$ =0.0049, $u(PPG_{ERP})$ = 0.00147, $u(electrolyte_{PRP})$ = 0.000358, $u(electrolyte_{ERP})$ = 0.00054, $u(water_{PRP})$= 0.0049, $u(water_{ERP})$= 0.0010 and u(p) = 0.20 kPa.

Table 6. Experimental (liquid + liquid) equilibrium data for the system PEO900 (1) + $(NH_4)_2C_6H_6O_7$ (electrolyte) (2) + water (3) for mole fractions x at the temperature 298.2 K and pressure p = 0.09341 MPa.[a]

overall			polymer-rich phase(PRP)			electrolyte-rich phase(ERP)			
x_1	x_2	x_3	x_1	x_2	x_3	x_1	x_2	x_3	TLL
				T = 298.2 K					
0.1418	0.03764	0.8206	0.2574	0.02326	0.7193	0.002870	0.05776	0.9406	0.2569
0.1514	0.03899	0.8096	0.2805	0.02082	0.6987	0.001720	0.06140	0.9368	0.2817
0.1608	0.04036	0.7989	0.3030	0.01927	0.6778	0.00007100	0.06584	0.9341	0.3065
0.1715	0.04186	0.7866	0.3202	0.01822	0.6615	0.00007357	0.07201	0.9279	0.3246

[a] Standard uncertainties u are u(temperature) = 0.1 K, $u(PEO_{PRP})$ = 0.0034, $u(PEO_{ERP})$ = 0.00113000, $u(electrolyte_{PRP})$ = 0.00018, $u(electrolyte_{ERP})$ = 0.00061, $u(water_{PRP})$= 0.0033, $u(water_{ERP})$= 0.0015 and u(p) = 0.20 kPa.

The tie-lines were obtained by linear regression fitting the values of overall composition and the compositions of the PPG425-rich phase and electrolyte-rich phase. The TLL presented in Tables 2 to 6 express the difference in phase composition between both ATPS phases, and at constant pressure and temperature could be related to the difference in intensive thermodynamic properties between the polymer-rich phase and the concentrated salt phase. The TLL can be calculated by

Eq. (1):

$$\mathbf{TLL} = \left[\left(x_{\mathrm{P}}^{\mathrm{PRP}} - x_{\mathrm{P}}^{\mathrm{ERP}}\right)^2 + \left(x_{\mathrm{E}}^{\mathrm{PRP}} - x_{\mathrm{E}}^{\mathrm{ERP}}\right)^2\right]^{1/2} \quad (1)$$

where $x_{\mathrm{P}}^{\mathrm{PRP}}$ and $x_{\mathrm{P}}^{\mathrm{ERP}}$ are the polymer mole fractions in the polymer- and electrolyte-rich phases, respectively, and $x_{\mathrm{E}}^{\mathrm{PRP}}$ and $x_{\mathrm{E}}^{\mathrm{ERP}}$ are the corresponding electrolyte mole fractions in the polymer- and electrolyte-rich phases, respectively.

As normally observed for other salt-polymer ATPS, an increase in TLL promotes the enrichment of polymer content along with a decrease of water and electrolyte quantity in the PRP, while in the ERP, water and electrolyte concentrations increase along with a decrease in the polymer concentration.

3.2. Effect of the nature of anion on the phase separation process

The minimum composition required for the formation of two phases is represented by the binodal curve. In the present work, was investigated the binodal position for the four electrolytes with different anionic structures ($C_4H_4O_6^{2-}$, $C_6H_6O_7^{2-}$, $C_2H_3O_2^-$, and CHO_2^-) at 298.2 K (Fig. 1). As the phase separation process occurs due to a decrease in the Gibbs free energy of the system, caused by specific molecular interactions between the ATPS components (H_2O-H_2O, H_2O-PPG, H_2O-ion, PPG-PPG, PPG-ions, and ion-ion), it was appropriate to express the phase diagram in mole fraction to facilitate comparison with systems containing the same number of molecules.

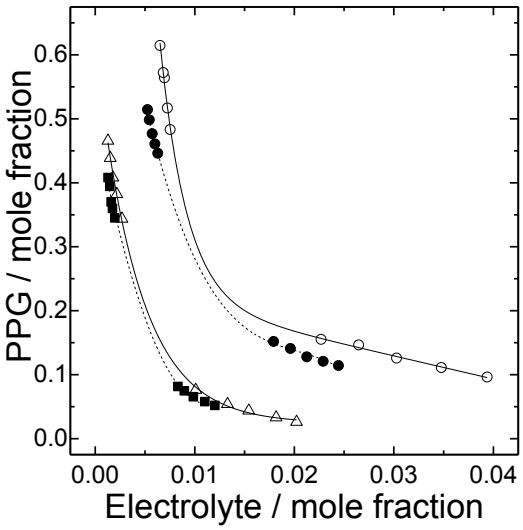

Fig. 1. Influence of the anion on the phase diagram of the PPG425 + ammonium electrolyte + H_2O systems at 298.2 K. (■) $(NH_4)_2C_4H_4O_6$, (Δ) $(NH_4)_2C_6H_6O_7$, (●) $NH_4C_2H_3O_2$ and (○) NH_4CHO_2.

Considering that all four electrolytes shared a common cation (NH_4^+), the difference in the phase diagram could be attributed to the anion effect. The ability of the anions to promote phase splitting decreases in the following order: $C_4H_4O_6^{2-}$ > $C_6H_6O_7^{2-}$ > $C_2H_3O_2^-$ > CHO_2^-.

A microcalorimetric investigation of the driving force for the ATPS formation process, carried out by da Silva and Loh [28], verified that at polymer and salt compositions which produce phase separation, the change in system enthalpy caused by the phase appearance is positive, implying that the phase splitting process is entropically driven. As proposed by these authors, the mechanism of phase separation could be described as follows: while the polymer-electrolyte mixture is homogenous, the electrolyte cations/anions interact with the macromolecule chains, releasing the water molecules that solvated them, increasing the system entropy. This macromolecule-electrolyte interaction continues as more salt is added, until an energetic saturation of the macromolecule chains occurs. At this point, the added ions will organize the water molecules in their solvating layers, increasing the Gibbs free energy ($\Delta_{mix}G$) of mixing of the system due to the decrease in configuration entropy. In order to reduce the $\Delta_{mix}G$, the polymer-electrolyte mixture segregates into two phases. Based on the da Silva and Loh [28] model, our results regarding the anion effect on the phase diagram may be interpreted considering the interactions between each kind of anion with the PPG-cation surface.

In general, as the electrical charge of an anion increases, the intensity of its

interaction with the polymer-cation surface and its capacity to promote phase separation increase, because it is possible to energetically saturate the macromolecule surface with a lower amount of salts. In order to determine the electrical charge of the predominant species in the ATPS, the relative concentrations of the species as a function of the pH, called alpha coefficients (α) [29], were determined. For the PPG425 + $(NH_4)_2C_4H_4O_6$ + H_2O ATPS at TLL = 0.3565, the system pH (pH^{PRP} = 7.06 and pH^{ERP} = 6.21) induces the formation of the $tart^{2-}$ chemical species (α^{PRP} = 99.8 % and α^{ERP} = 98.6 %) in both phases. The pH of the ATPS composed by PPG425 + $(NH_4)_2C_6H_6O_7$ + H_2O at TLL = 0.4399 (pH^{PRP} = 5.67 and pH^{ERP} = 4.86) leads to the formation of the species H_2Cit^- (α^{PRP} = 9.40 % and α^{ERP} = 43.3 %), $HCit^{2-}$ (α^{PRP}= 76.2 % and α^{ERP} = 54.4 %), and Cit^{3-} (α^{PRP} = 14.4 % and α^{ERP} = 1.59 %). As both salts produced predominantly bivalent anions, which interact similarly with the polymer-cation surface, they have almost equal binodal positions with a slightly larger two-phase region for the tartrate ATPS. This proposal is supported by the results of Hamzehzadeh and Zafarani-Moattar [30]. The authors evaluated the effect of pH on the binodal position of the PPG400 + sodium citrate/citric acid + H_2O ATPS. It was verified that the two-phase area expands upon increasing the pH of the aqueous medium, i.e., the increase in pH induced the formation of the more deprotonated species. The species with higher electrical charge strongly interacts with the polymer-cation surface and promotes the phase separation with a lower quantity of the electrolyte. The system pH of PPG425 + $NH_4C_2H_3O_2$ + H_2O at TLL = 0.4006 (pH^{PRP} = 7.45 and pH^{ERP} = 7.32) and PPG425 + NH_4CHO_2 + H_2O at TLL = 0.5195 (pH^{PRP} = 6.89 and pH^{ERP} = 6.82) induces, respectively, the preferential formation of acetate anion (α^{PRP} = 99.80 % and α^{ERP} = 99.73 %) and formate anion (α^{PRP} =99.93 % and α^{ERP} =99.92 %). As the formate and acetate anions have lower valence (-1) than the tartrate and citrate ions, they are less effective in inducing phase separation. Probably, the higher capacity of the acetate compared to formate to induce phase separation is related to the additional methyl group in the acetate structure, which increases the hydrophobic contribution to the interaction of this anion with the polymer chain hydrophobic segments.

3.3. Effect of temperature on ATPS composition

The minimum polymer and electrolyte concentrations at which the ATPS is

produced at two different temperatures are presented in Fig. 2. The temperature effect was investigated in all the PPG-systems at three different temperatures. However, since some systems remained turbid for a long time, which made their quantification unfeasible, we decided to show the effect of two temperatures for each phase diagram. Fig. 2 shows the phase diagrams for the PPG425 + $NH_4C_2H_3O_2$ + H_2O at 283.2 and 298.2 K and PPG425 + NH_4CHO_2 + H_2O system at 283.2 and 313.2 K.

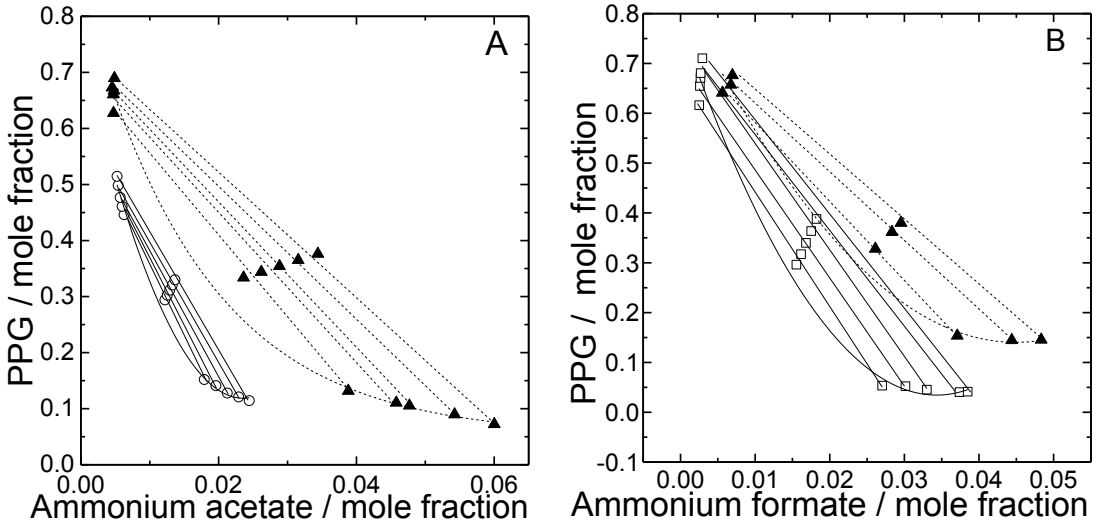

Fig. 2. The effect of temperature on the phase diagram of the PPG425 + electrolyte + H_2O ATPS. a) $NH_4C_2H_3O_2$: (▲) 283.2 K and (○) 298.2 K; b) NH_4CHO_2: (▲) 283.2 K and (□) 313.2 K.

In all investigated systems, the increase in temperature expands the area of the phase diagram where both ATPS phases coexist. The same behavior was observed for the PPG425 + $(NH_4)_2C_4H_4O_6$ + H_2O ATPS, and PPG425 + $(NH_4)_2C_6H_6O_7$ + H_2O ATPS. This is an indication that the phase-separation process is endothermic, i.e., the phase-separation process is entropically driven as proposed by da Silva and Loh [28]. A possible molecular mechanism for this temperature effect on the binodal position could be described as follows: the interactions of PPG segments with water molecules become less intense while the PPG-PPG interactions become stronger at higher temperatures, resulting in a decrease in PPG solubility. This causes the exclusion of PPG by the electrolyte, promoting the formation of the ATPS systems [30, 31].

The effect of temperature on the composition of the phase equilibrium can also be analyzed through the slopes of the tie-line (STL). The STL values (Table 7) can be calculated by Eq. (2):

$$STL = \frac{(x_{PPG\_}^{PRP} x_{PPG}^{ERP})}{(x_{ELT\_}^{PRP} x_{ELT}^{ERP})} \quad (2)$$

where x_{PPG}^{PRP} and x_{PPG}^{ERP} are the PPG425 mole fractions in the polymer- and electrolyte-rich phases, respectively, and x_{ELT}^{PRP} and x_{ELT}^{ERP} are the electrolyte mole fractions in the polymer- and electrolyte-rich phases, respectively.

According to the results (Table 7), for all analyzed systems, the increase in temperature promotes an increase in the module of the STL. By analyzing the numerator of Eq. (2), the term x_{PPG}^{PRP} is always higher than the term x_{PPG}^{ERP}, so this term is always positive. In the denominator, the term x_{ELT}^{ERP} is always higher than x_{ELT}^{PRP} . Thus, the value in the denominator is always negative. Thus, a mathematical analysis of this equation shows that the increase of the module of STL is due to an increase in the polymer mole fraction in the PRP, and a reduction in the electrolyte mole fraction in the ERP. As proposed in other references [15, 17, 18, 21, 30], this can be explained by considering that, at the same global composition, higher temperatures promote the transfer of water molecules from the polymer-rich phase to the electrolyte-rich phase. This causes an increment in x_{PPG}^{PRP} , and a reduction in x_{PPG}^{ERP}.

Table 7. STL systems values at 283.2, 298.2, and 313.2 K.

PPG425 + $NH_4C_2H_3O_2$ + H_2O			
TLL	283.2 K	298.2 K	313.2 K
0.2943	-	-25.27	-
0.3201	-	-23.48	-
0.3493	-	-22.46	-
0.3779	-	-21.58	-
0.4006	-	-20.81	-
0.4969	-14.56	-	-
0.5514	-13.39	-	-
0.5634	-13.08	-	-
0.5854	-11.71	-	-
0.6199	-11.18	-	-
0.5582	-	-	-26.35
0.6296	-	-	-27.55
PPG425 + $(NH_4)_2C_4H_4O_6$ + H_2O			
TLL	283.2 K	298.2 K	313.2 K
0.2638	-	-41.60	-
0.2854	-	-39.60	-
0.3088	-	-37.43	-
0.3366	-	-35.19	-
0.3565	-	-33.09	-
0.5037	-16.74	-	-
0.5372	-16.57	-	-
0.5460	-15.76	-	-
PPG425 + $(NH_4)_2C_6H_6O_7$ + H_2O			
TLL	283.2 K	298.2 K	313.2 K
0.2676	-	-35.79	-
0.3283	-	-28.99	-
0.3647	-	-26.33	-
0.4060	-	-23.93	-
0.4399	-	-22.88	-
0.5006	-	-	-59.86
0.5277	-	-	-54.23
0.5350	-	-	-50.40
0.5716	-	-	-46.13
PPG425 + NH_4CHO_2 + H_2O			
TLL	283.2 K	298.2 K	313.2 K
0.3283	-	-21.67	-
0.3709	-	-19.21	-
0.4388	-	-18.61	-
0.4620	-	-16.33	-
0.5195	-	-15.54	-
0.4884	-15.46	-	-
0.5141	-13.62	-	-
0.5325	-12.84	-	-
0.5634	-	-	-23.01
0.6031	-	-	-21.87
0.6263	-	-	-20.56
0.6410	-	-	-18.34
0.6701	-	-	-18.73

3.4. Effect of the polymer hydrophobicity on the binodal position

We analyzed the efficiency of two polymers (PEG900 and PPG425) in forming the aqueous biphasic system. Fig. 3 shows the phase diagram of PEG900 + $(NH_4)_2C_6H_6O_7$ + H_2O ATPS and PPG425 + $(NH_4)_2C_6H_6O_7$ + H_2O ATPS at 298.2 K.

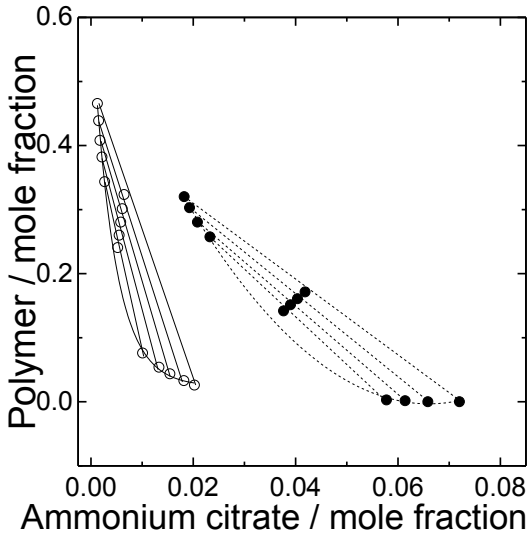

Fig. 3. Influence of the polymer hydrophobicity on the phase diagram of the polymer + $(NH_4)_2C_6H_6O_7$ + H_2O systems at 298.2 K for (○) PPG425 and (●) PEG900.

The ATPS containing PPG425 showed a phase separation process at lower polymer and electrolyte concentrations than that observed in the system formed by PEG900. When comparing the PEG900 + $(NH_4)_2C_6H_6O_7$ + H_2O and PPG425 + $(NH_4)_2C_6H_6O_7$ + H_2O ATPS, the PPG425 concentrations were higher than the PEG content in the macromolecule-rich phase while the water quantity in the PPG425-rich phase was considerably lower (Tables 4 and 6). These results can be explained considering that PPG is more hydrophobic than PEG due to the additional methyl group in the polymer chain. The PPG structure decreases the water-macromolecule and electrolyte-macromolecule interactions, favoring the phase separation process at lower ATPS component concentrations.

3.5. Thermodynamic modeling and Estimation Procedure

The nonrandom two-liquid (NRTL) [27] model was used in this work to correlate the liquid-liquid equilibrium data of the systems. In particular, the NRTL model is dependent of the compound since the energetic parameters are adjusted according to temperature, molar mass and compositions of the systems phases. This model is based on concept of the local composition, being applicable to partially-

miscible systems [32]. The local composition concept, which was introduced by Wilson [33], considers that the composition of the system in the neighborhood of a molecule is not the same that the bulk composition due the intermolecular interactions [34, 35]. This model was not developed for systems involving electrolytes. Nevertheless, the original NRTL model has been empirically extended to consider the electrolyte effect on liquid-liquid equilibrium [36].

The NRTL activity coefficient (γ_i) in multicomponent systems is given by Eq.(3):

$$\ln \gamma_i = \frac{\sum_j \frac{\tau_{ji} G_{ji} w_j}{M_j}}{\sum_j \frac{G_{ji} w_j}{M_j}} + \sum_j \left[\frac{w_j G_{ji}}{M_j \sum_k \frac{G_{kj} w_k}{M_k}} \left(\tau_{ij} - \frac{\sum_k \frac{w_k \tau_{kj} G_{kj}}{M_k}}{\sum_k \frac{G_{kj} w_k}{M_k}} \right) \right] \tag{3}$$

where w_j and M_j are the mass fraction and molar mass, respectively, and the parameters of interaction energy of the molecules i-j (G_{ij}) can be calculated by Eq.(4):

$$G_{ij} = \exp\left(-\alpha_{ij}\tau_{ij}\right) \text{ where } \tau_{ij} = \frac{A_{ij}}{T} \quad \left(\tau_{ij} \neq \tau_{ji}\right) \tag{4}$$

The modified NRTL model has five adjustable parameters for each binary pair (A_{0ij}, A_{0ji}, A_{1ij}, A_{1ji} and α_{ij}), which are determined by mean regression of experimental data for a specific system.

Where α is the non-randomness factor in the mixture ($\alpha_{ij} = \alpha_{ji}$), which is derived from the local composition concept [34, 35], and range from 0.2 to 0.47 [37]. If, $\alpha_{ij} = 0$ means to complete randomness, or ideal solution [38]. This parameter can also be kept fixed. A_{0ij}, A_{0ji}, A_{1ij}, A_{1ji} are interaction parameters which represent the energy of interaction between molecules i and j [32, 34, 35, 39]. These parameters take into account pure-component liquid interactions and mixed-liquid components

interactions [40], and are given by Eq. (5) and Eq. (6):

$$A_{ij} = A_{0ij} + A_{1ij}T \tag{5}$$

$$A_{ji} = A_{0ji} + A_{1ji}T \tag{6}$$

These parameters of interaction energy were estimated using experimental data. For this, the estimation was performed using the Fortran code WTML-LLE, based on the Simplex method [41] and Maximum Likelihood principle [42], by means of minimizing of a concentration-based objective function, S, given by Eq. (7):

$$S = \sum_{k}^{D}\sum_{j}^{Nk}\left\{\left(\frac{T_{jk} - T_{jk}^{m}}{\sigma_{Tjk}}\right)^2 + \sum_{i}^{Ck-1}\left[\left(\frac{w_{ijk}^{\alpha} - w_{ijk}^{\alpha,m}}{\sigma_{wijk\alpha}}\right)^2 + \left(\frac{w_{ijk}^{\beta} - w_{ijk}^{\beta,m}}{\sigma_{wijk\beta}}\right)^2\right]\right\} \tag{7}$$

where D is the number of data sets, Nk and Ck are the number of tie-lines and components in each data set k, respectively. σ_{Tjk}, $\sigma_{wijk\alpha}$ and $\sigma_{wijk\beta}$ are the standard deviations obtained in the independent variables temperature, compositions of phase α and compositions of phase β, respectively. The superscript *m* means measured.

The results of the new interaction energy parameters of all systems in this work, for the modified NRTL model, are shown in Table 8.

Table 8. Estimated NRTL parameters.

i	j	A_{0ij}	A_{0ji}	A_{1ij}	A_{1ji}	α_{ij}
PPG425	ammonium acetate	-337.23	7526.4	-0.57566	-23.682	0.46922
PPG425	ammonium tartrate	-589.97	2045.2	2.2273	16.393	0.46708
PPG425	ammonium citrate	-10310.1	4355.7	-105.12	41.997	0.37578
PPG425	ammonium formate	-251.98	21.585	0.90389	1.6910	0.46999
PPG425	Water	7567.9	-11601.1	500.24	42.627	0.28629
PPG425	PEO	-0.26161	133.12	74.865	56.838	0.21323
ammonium acetate	Water	29745.2	181.22	14.744	1.8461	0.24902
water	ammonium tartrate	3603.9	56058.2	40.970	173.85	0.20442
water	ammonium citrate	-270.34	12.715	9.1537	28.066	0.30610
water	ammonium formate	0.96002	-28.384	0.51585	-3.9746	0.29330
water	PEO	2785.7	765.33	0.12446	19.960	0.26828

With the energy interaction parameters estimated, correlations of equilibrium data were performed. Comparing the experimental and calculated composition of each component of both phases were made through root-mean-square (rms) deviation. The rms deviations are given by Eq. (8):

$$\partial w = 100\sqrt{\frac{\sum_i \left\{\left(w_i^{\alpha} - w_i^{\alpha,m}\right)^2 + \left(w_i^{\beta} - w_i^{\beta,m}\right)^2\right\}}{2NkCk}} \tag{8}$$

The root mean square deviation between experimental and calculated compositions is shown in Table 9.

Table 9. Root mean square deviations in ternary systems.

Systems	NRTL ∂w (%)
PPG425 + ammonium acetate + water at 283.2 K	1.42
PPG425 + ammonium acetate + water at 292.2 K	1.69
PPG425 + ammonium acetate + water at 313.2 K	2.29
PPG425 + ammonium tartrate + water at 283.2 K	1.21
PPG425 + ammonium tartrate + water at 292.2 K	1.37
PPG425 + ammonium citrate + water at 298.2 K	1.29
PPG425 + ammonium citrate + water at 312.2 K	1.92
PPG425 + ammonium formate + water at 283.2 K	1.33
PPG425 + ammonium formate + water at 298.2 K	1.48
PPG425 + ammonium formate + water at 313.2 K	1.85
PEO900 + ammonium acetate + water at 298.2 K	1.22
global (*48 tie-lines*)	1.82

The results of the correlation showed in Table 9 are very satisfactory. The global root mean square deviation, with 48 tie-lines of the modified NRTL model is 1.82 %.

4. Conclusion

Experimental ATPS data were obtained for five new aqueous two-phase systems: PPG425 + $NH_4C_2H_3O_2$ + H_2O, PPG425 + $(NH_4)_2C_4H_4O_6$ + H_2O, PPG425 + $(NH_4)_2C_6H_6O_7$ + H_2O, PPG425 + NH_4CHO_2 + H_2O, and PEG900+ $(NH_4)_2C_6H_6O_7$ + H_2O at different temperatures (283.2, 298.2 and 313.2 K) and tie-line lenght. The influence of temperature, ATPS forming-electrolyte, and the polymer hydrophobicity were investigated, and all these parameters were shown to affect the phase diagram. As the temperature increased, the two-phase area expanded and the slope of tie-line increased. The ability of the anions to promote phase separation in the systems formed by PPG425 was successfully explained by the da Silva and Loh model and followed the order: $C_4H_4O_6^{2-}$ > $C_6H_6O_7^{2-}$ > $C_2H_3O_2^-$ > CHO_2^-. The ATPS containing the hydrophobic PPG425 polymer exhibited a phase separation at lower polymer and electrolyte concentrations than that observed in the system formed by the hydrophilic PEG900 polymer. The activity coefficient value was calculated and the new

interactions parameters for the modified NRTL model were obtained. This model could correlate 11 systems and they are very satisfactory for the liquid-liquid equilibrium data in this work, since the global root mean square deviation is 1.82 %.

The results presented here increase the literature database of liquid-liquid equilibrium data for polymer + electrolyte + water ATPS. The developed PPG425 systems display interesting hydrophobic nature, and are strategic ATPS for the manipulation of hydrophobic solutes.

5. References

[1] P.R. Patrício, R.C. Cunha, S.J. Rodriguez Vargas, Y.L. Coelho, L.H. Mendes da Silva, M.C. Hespanhol da Silva, Chromium speciation using aqueous biphasic systems: Development and mechanistic aspects, Sep. Purif. Technol., 158 (2016) 144-154.

[2] R.C. da Cunha, P.R. Patrício, S.J.R. Vargas, L.H.M.d. Silva, M.C.H. da Silva, Green recovery of mercury from domestic and industrial waste, J. Hazard. Mater., 304 (2016) 417-424.

[3] L. Bulgariu, D. Bulgariu, Selective extraction of Hg(II), Cd(II) and Zn(II) ions from aqueous media by a green chemistry procedure using aqueous two-phase systems, Sep. Purif. Technol., 118 (2013) 209-216.

[4] J.M. de Alvarenga, R.A. Fideles, M.V. da Silva, G.F. Murari, J.G. Taylor, L.R. de Lemos, G.D. Rodrigues, A.B. Mageste, Partition study of textile dye Remazol Yellow Gold RNL in aqueous two-phase systems, Fluid Phase Equilib., 391 (2015) 1-8.

[5] A.B. Mageste, T.D.A. Senra, M.C.H. da Silva, R.C.F. Bonomo, L.H.M. da Silva, Thermodynamics and optimization of norbixin transfer processes in aqueous biphasic systems formed by polymers and organic salts, Sep. Purif. Technol., 98 (2012) 69-77.

[6] S. Chethana, C.A. Nayak, K.S.M.S. Raghavarao, Aqueous two phase extraction for purification and concentration of betalains, J. Food Eng, 81 (2007) 679-687.

[7] L.H. Haraguchi, R.S. Mohamed, W. Loh, P.A.P. Filho, Phase equilibrium and insulin partitioning in aqueous two-phase systems containing block copolymers and potassium phosphate, Fluid Phase Equilib., 215 (2004) 1-15.

[8] G. Reh, B. Nerli, G. Picó, Isolation of alpha-1-antitrypsin from human plasma by partitioning in aqueous biphasic systems of polyethyleneglycol–phosphate, J. Chromatogr. B: Anal. Technol. Biomed. Life Sci, 780 (2002) 389-396.

[9] A.M. Azevedo, A.G. Gomes, P.A.J. Rosa, I.F. Ferreira, A.M.M.O. Pisco, M.R. Aires-Barros, Partitioning of human antibodies in polyethylene glycol-sodium citrate aqueous two-phase systems, Sep. Purif. Technol, 65 (2009) 14-21.

[10] G.D. Rodrigues, L.R. de Lemos, P.D. Patricio, L.H.M. da Silva, M.D.H. da Silva, Aqueous two-phase systems: a new approach for the determination of p-aminophenol, J. Hazard. Mater., 192 (2011) 292.

[11] G.D. Rodrigues, L.R. de Lemos, L.H.M. da Silva, M.C.H. da Silva, L.A. Minim, J.S.R. Coimbra, A green and sensitive method to determine phenols in water and wastewater samples using an aqueous two-phase system, Talanta, 80 (2010) 1139-1144.

[12] J. Persson, H.-O. Johansson, I. Galaev, B. Mattiasson, F. Tjerneld, Aqueous polymer two-phase systems formed by new thermoseparating polymers, Bioseparation, 9 (2000) 105-116.

[13] Z. Zhao, Q. Li, X. Ji, R. Dimova, R. Lipowsky, Y. Liu, Molar mass fractionation in aqueous two-phase polymer solutions of dextran and poly(ethylene glycol), J. Chromatogr. A, 1452 (2016) 107-115.

[14] L.A. Ferreira, N.R. da Silva, S.R. Wlodarczyk, J.A. Loureiro, P.P. Madeira, J.A. Teixeira, V.N. Uversky, B.Y. Zaslavsky, Interrelationship between partition behavior of organic compounds and proteins in aqueous dextran-polyethylene glycol and

polyethylene glycol-sodium sulfate two-phase systems, J. Chromatogr. A, 1443 (2016) 21-25.
[15] Y. Barrueto, K. Muñoz, K. Garnica, I. Villalobos, Y.P. Jimenez, Aqueous two-phase system of poly(ethylene glycol) 4000 and sodium molybdate at different temperatures, Fluid Phase Equilib., 399 (2015) 66-73.

[16] Y.P. Jimenez, H.R. Galleguillos, M. Claros, Liquid-liquid partition of perchlorate ion in the aqueous two-phase system formed by $NaNO_3$ + Poly(ethylene glycol) + H_2O, Fluid Phase Equilib., 421 (2016) 93-103.

[17] G.F. Murari, J.A. Penido, P.A.L. Machado, L.R. de Lemos, N.H.T. Lemes, L.S. Virtuoso, G.D. Rodrigues, A.B. Mageste, Phase diagrams of aqueous two-phase systems formed by polyethylene glycol + ammonium sulfate + water: equilibrium data and thermodynamic modeling, Fluid Phase Equilib., 406 (2015) 61-69.

[18] A.F.C. Rengifo, G.M.D. Ferreira, G.M.D. Ferreira, M.C.H. da Silva, L.H.M. da Silva, Phase diagrams, densities and refractive indexes of poly(ethylene oxide) + organic salts + water aqueous two-phase systems: Effect of temperature, anion and molar mass, Fluid Phase Equilib, 406 (2015) 70-76.

[19] S. Malekghasemi, B. Mokhtarani, S. Hamzehzadeh, H. Hajfarajollah, A. Sharifi, M. Mirzaei, Phase diagrams of aqueous biphasic systems composed of ionic liquids and dipotassium carbonate at different temperatures, Fluid Phase Equilib, 415 (2016) 193-202.

[20] A. Paraj, A. Haghtalab, B. Mokhtarani, [1-Ethyl-2,3-dimethyl-imidazolium][ethylsulfate]-based aqueous two phase systems: New experimental data and modeling, Fluid Phase Equilib., 382 (2014) 212-218.

[21] X. Tang, J. Han, Y. Hu, Y. Wang, Y. Lu, T. Chen, L. Ni, The study of phase behavior of aqueous two-phase system containing [Cnmim]BF_4 (n = 2,3,4) + $(NH_4)_2SO_4$ + H_2O at different temperatures, Fluid Phase Equilib., 383 (2014) 100-107.

[22] L. Bulgariu, D. Bulgariu, Extraction of gold(III) from chloride media in aqueous polyethylene glycol-based two-phase system, Sep. Purif. Technol., 80 (2011) 620-625.

[23] V.G. Lacerda, A.B. Mageste, I.J.B. Santos, L.H.M. da Silva, M.D.H. da Silva, Separation of Cd and Ni from Ni–Cd batteries by an environmentally safe methodology employing aqueous two-phase systems, J. Power Sources, 193 (2009) 908-913.

[24] U. Dorn, S. Enders, Heat of mixing and liquid-liquid equilibrium of water + polypropylene glycol (PPG) with different molecular weights and water + propylene glycol dimethyl ether, Fluid Phase Equilib., 424 (2016) 58-67.

[25] C. Wu, J. Wang, Y. Pei, H. Wang, Z. Li, Salting-Out Effect of Ionic Liquids on Poly(propylene glycol) (PPG): Formation of PPG + Ionic Liquid Aqueous Two-Phase Systems, J. Chem. Eng. Data, 55 (2010) 5004-5008.

[26] L.Y. Garcia-Chavez, M. Shazad, B. Schuur, A.B. de Haan, (Liquid + liquid) equilibrium data for the system (propylene glycol + water + tetraoctyl ammonium 2-methyl-1-naphthoate), J. Chem. Thermodyn., 54 (2012) 238-244.

[27] H. Renon, J.M. Prausnitz, Local compositions in thermodynamic excess functions for liquid mixtures, AIChE J., 14 (1968) 135-144.

[28] L.H.M. da Silva, W. Loh, Calorimetric Investigation of the Formation of Aqueous Two-Phase Systems in Ternary Mixtures of Water, Poly(ethylene oxide) and Electrolytes (Or Dextran), J. Phys. Chem. B, 104 (2000) 10069-10073.

[29] D.A. Skoog, D.M. West, F.J. Holler, Fundamentals of analytical chemistry, Saunders College Pub., 1996.

[30] S. Hamzehzadeh, M.T. Zafarani-Moattar, Phase separation in aqueous solutions of polypropylene glycol and sodium citrate: Effects of temperature and pH, Fluid Phase Equilib., 385 (2015) 37-47.

[31] X. Xie, Y. Yan, J. Han, Y. Wang, G. Yin, W. Guan, Liquid-Liquid Equilibrium of Aqueous Two-Phase Systems of PPG400 and Biodegradable Salts at Temperatures of (298.15, 308.15, and 318.15) K, J. Chem. Eng. Data 55 (2010) 2857-2861.

[32] E. Cunha, M. Aznar, Liquid-Liquid Equilibrium in Aqueous Two-Phase (Water + PEG 8000 + Salt): Experimental Determination and Thermodynamic Modeling, J. Chem. Eng. Data, 54 (2009) 3242.

[33] G.M. Wilson, Vapor-Liquid Equilibrium. XI. A New Expression for the Excess Free Energy of Mixing, J. Am. Chem. Soc., 86 (1964) 127-130.

[34] F.S. Santos, S.G. d'Ávila, M. Aznar, Salt effect on liquid–liquid equilibrium of water+1-butanol+acetone system: experimental determination and thermodynamic modeling, Fluid Phase Equilib., 187-188 (2001) 265-274.

[35] R.A.G. Sé, M. Aznar, Thermodynamic modelling of phase equilibrium for water + poly(Ethylene glycol) + salt aqueous two-phase systems, Braz. J. Chem. Eng., 19 (2002) 255-266.

[36] G.R. Santos, S.G. d'Ávila, M. Aznar, Salt effect of KBr on the liquid-liquid equilibrium of the water/ethanol/1-pentanol system, Braz. J. Chem. Eng., 17 (2000) 721-734.

[37] J.M. Prausnitz, R.N. Lichtenthaler, E.G. de Azevedo, Molecular thermodynamics of fluid-phase equilibria, Pearson Education, 1998.

[38] L.D. Simoni, Y. Lin, J.F. Brennecke, M.A. Stadtherr, Modeling liquid− liquid equilibrium of ionic liquid systems with NRTL, electrolyte-NRTL, and UNIQUAC, Ind. Eng. Chem. Res., 47 (2008) 256-272.

[39] R.M. Maduro, M. Aznar, Liquid-liquid equilibrium of ternary systems containing nicotine, Fluid Phase Equilib., 259 (2007) 83-88.

[40] S. Gebreyohannes, B.J. Neely, K.A.M. Gasem, One-parameter modified nonrandom two-liquid (NRTL) activity coefficient model, Fluid Phase Equilib., 379 (2014) 196-205.

[41] J.A. Nelder, R. Mead, A simplex method for function minimization, Comput. J., 7 (1965) 308-313.

[42] T.F. Anderson, D.S. Abrams, E.A. Grens, Evaluation of parameters for nonlinear thermodynamic models, AIChE J., 24 (1978) 20-29.

CAPÍTULO 3

Chloramphenicol partitioning in ATPS: a driving-force determination approach

Abstract

Aqueous two-phase systems (ATPS) are efficient for extraction of different solutes, featuring low cost and non-toxicity, and being easy to handle. However, understanding the transfer thermodynamic process of solutes in these systems is still a great challenge. Here, the transfer standard Gibbs free energy change ($\Delta_{tr}G^{\theta}$), transfer standard enthalpy change ($\Delta_{tr}H^{\theta}$), and transfer standard entropy change ($\Delta_{tr}S^{\theta}$) for chloramphenicol were determined, enabling the comprehension of the ATPS properties in the transfer thermodynamic process of this antibiotic in polymer + electrolyte + water ATPS. Antibiotic partition from the electrolyte-rich phase to the polymer-rich phase was enthalpically driven, with (-80.88±1.30) kJ mol^{-1} < $\Delta_{tr}H^{\theta}$ < (-8.33±0.04) kJ mol^{-1}, (-64.09±0.85) kJ mol^{-1} < $T\Delta_{tr}S^{\theta}$ < (1.26±0.12) kJ mol^{-1} and (-15.45±0.02) kJ mol^{-1} < $\Delta_{tr}G^{\theta}$ < (-2.64±0.02) kJ mol^{-1}, showing preferential and spontaneous transfer of the solutes to the polymer-rich phase. The nature of cation and polymer molar mass changed the magnitude of the interactions between the antibiotics and ATPS components, influencing the values of partition coefficient and transfer thermodynamic parameters. The ATPS composed by the cation Li^{+} presented k values about six and seven times higher than the ATPS formed by Mg^{2+} and Na^{+} cations, respectively. For molar mass effect, ATPS composed by PEO1500 presented k values about four and eleven times higher than ATPS formed by PEO10000 and 35000, respectively. Chloramphenicol partitioning to the polymer-rich phase depends on the nature of the ATPS, being governed by enthalpic and entropic contributions. This study allows extending the ATPS applications to extraction and pre-concentration of antibiotics in different matrices.

Keywords: Aqueous two-phase systems, chloramphenicol, partition, driving force, thermodynamic

1. Introduction

Aqueous two-phase systems (ATPS) are an attractive alternative for conventional liquid-liquid extraction (LLE) [1]. These systems are composed mostly of water and offer an ideal environment for the partition/extraction of different solutes [2-8], besides presenting low cost, low toxicity and possibility of easy handle [9-11]. ATPS are formed by mixing aqueous solutions of two chemically distinct polymers [12], or a polymer and an electrolyte [13], or two electrolytes [14], or even two surfactants [15], under specific thermodynamic conditions, resulting in two immiscible phases. Despite the large number of work using ATPS for partition/extraction of different classes of analytes [16], studies involving the solute transfer thermodynamics between ATPS phases are scarce, and the major contribution of these studies would be the strategic understanding of the driving forces that govern the partitioning.

Until now, only nine works [5, 6, 17-23] have been carried out to obtain thermodynamic parameters of transfer, such as standard Gibbs free energy change ($\Delta_{tr}G^{\theta}$), standard enthalpy change ($\Delta_{tr}H^{\theta}$) and standard entropy change ($\Delta_{tr}S^{\theta}$). In most of them, these parameters were obtained using the van't Hoff approximation. For example, Zhang et al, using this approach, conducted studies of the chloramphenicol transfer in ATPS composed of 1-hydroxylhexyl-3-methylimidazolium chloride (HO[C6mim][Cl]) and potassium carbonate (K_2CO_3) [6]. These authors observed that the temperature greatly influences the chloramphenicol partition from the K_2CO_3-rich phase to the HO[C6mim][Cl]-rich phase, showing that its increase promotes the solute partition decrease, characterizing an exothermic process $\Delta_{tr}H^{\theta}$= (-183.17) kJ mol^{-1}. The influence of temperature in this study was similar to the previous study [24], however it was contrary to other [25], in which the temperature had no significant influence in the partition of different biomolecules. Da Silva et al, also using the Van't Hoff approximation, studied the partition thermodynamic of pentacyanonitrosylferrate ($[Fe(CN)_5(NO)]^{2-}$) and hexacyanoferrate ($[Fe(CN)_6]^{3-}$) anions in ATPS composed by potassium phosphate electrolytes and polymer or triblock copolymers [19]. For the first time, these researchers performed the comparison between the Van't Hoff enthalpy (ranging from (-41.2 ± 0.4) kJ mol^{-1} to (-53.0 ± 0.9) kJ mol^{-1}) and calorimetric enthalpy (ranging between approximately (-27.0) kJ mol^{-1} and approximately (-30.0) kJ mol^{-1}), which indicated an exothermic transfer process. However, the significant

differences in the enthalpy measurements showed that the Van't Hoff approximation presents some limitations, i.e. the modification of ATPS phase composition due temperature alteration, emphasizing the importance of using calorimetry in these studies. With the Isothermal Titration Calorimetry (ITC) technique, Mageste et al studied the partition thermodynamic of the norbixin dye in ATPS formed by polymer or copolymer and organic electrolytes [17]. In contrary of other partition studies performed with dyes in ATPS [2, 26-28], the goal of this work was to understand the driving force responsible for the transfer of dye in ATPS. The obtained values of $\Delta_{tr}H^{\theta}$ showed that the transfer process was exothermic, ranging from (-2.71) kJ mol^{-1} to (-9.10) kJ mol^{-1}, considering all ATPS studied. The norbixin transfer from the electrolyte-rich phase to the polymer-rich phase was favored by enthalpy and entropy contributions. Rengifo et al, also using ITC, studied the transfer thermodynamics parameters of chymosin in ATPS formed by macromolecules (polymer or copolymer) and electrolytes (organic or inorganic) [5]. The authors observed that the process of chymosin transfer from the electrolyte-rich phase to the polymer-rich phase of the ATPS was exothermic (ranging from (-4.84 kJ) mol^{-1} to (-170.34) kJ mol^{-1}) and enthalpically driven, presenting distinct results from the work performed by Spelzini and coworkers [22], which used the van't Hoff approximation for studying chymosin partition in other ATPS and found endothermic values ranging from (33.8) kJ mol^{-1} to (96.0) kJ mol^{-1}. In addition, the authors concluded that this process was entropically driven.

According with studies later mentioned, different approaches have been used to obtain the $\Delta_{tr}H^{\theta}$parameter. However, some limitations may still be found, e.g. the change of partition coefficient values due to modification of the ATPS phase composition, which occurs with temperature alteration, or even by contribution of solute-solute interactions [6, 17].

Even with these relevant studies performed up to here, there is still a demand for elucidation of the solutes transfer phenomenon in ATPS. The goal of this work is to understand the driving forces involved in the choramphenicol (CAP) antibiotic (Fig. 1) transfer process in ATPS formed by polymer + electrolyte + water, through the transfer thermodynamics parameters $\Delta_{tr}G^{\theta}$, $\Delta_{tr}H^{\theta}$ and $\Delta_{tr}S^{\theta}$, and also their dependence on the properties of these systems.

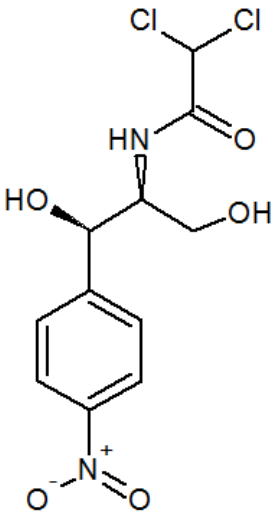

Fig. 1. Chemical structure of chloramphenicol.

2. Experimental section

2.1. Materials

The polymer poly(ethylene oxide) (PEO) of molar mass 1500 was purchased from Synth (São Paulo, Brazil), with purity of 100% and those of molar mass 400, 10000 and 35000 g mol^{-1} were purchased from Aldrich (St. Louis, USA), all also with purity of 100%. The polymer poly(propylene oxide) (PPO), of molar mass 425 g mol^{-1}, was obtained from Aldrich (St. Louis, USA). The electrolytes lithium sulfate ($Li_2SO_4.H_2O$; 99.0%) and magnesium sulfate ($MgSO_4.H_2O$; 98.0%) were obtained from Synth (Diadema, Brazil) and Dinâmica (Diadema, Brazil), respectively. Sodium sulfate (Na_2SO_4; 99.0%), sodium tartrate ($Na_2C_4H_4O_6 \cdot 2H_2O$; 99.5%) and sodium citrate ($Na_3C_6H_5O_7 \cdot 2H_2O$; 99.0%), were obtained from Vetec (Rio de Janeiro, Brazil). All polymers and electrolytes were analytical-grade and used without further purification. Chloramphenicol (≥98.0%) was obtained from Aldrich (St. Louis, USA). Deionized water (Millipore Corp., Molsheim, France) was used for preparing all aqueous solutions.

2.2. ATPS preparation and measurements of the CAP partition coefficient

Solutions with specific concentrations of polymer and electrolyte were prepared and added in tubes of 50 mL according to the desired ATPS overall composition. The ATPS overall compositions were obtained from equilibrium liquid-liquid data as found in the literature [29-33]. The tubes were manually stirred until

reaching turbidity and after that they were left in a controlled bath (MQBTC 99-20, Microquimica, Palhoça, Brazil) with uncertainty of ± 0.1 K at 298.2 K for at least 12 h or until reaching the thermodynamic equilibrium. The equilibrium state was determined by the absence of turbidity in the electrolyte and polymer rich-phases. After achieving the equilibrium state, for each global composition, aliquots of 2.0 g of each phase were collected and mixted with 0.10 g of CAP solution (1.90×10^{-3}) mol kg^{-1} to achieve an adequate concentration in glass tubes. Blanks were prepared under the same conditions by replacing the solute solution with deionized water. The procedure was carried out in duplicate. These systems were stirred in a vortex mixer (Certomat MV, B. Braun Biotech International, Melsungen, Germany) until the turbidity showed, for one minute. They were left in a controlled bath (MQBTC 99-20, Microquimica, Palhoça, Brazil) with uncertainty of ± 0.1 K at 298.2 K for at least 12 h, or until reaching the thermodynamic equilibrium. The equilibrium state was characterized by the absence of turbidity in both phases. Aliquots of the polymer-rich phase and electrolyte-rich phase were collected with a syringe and appropriately diluted with deionized water for spectrophotometric measurements using a UV-Vis spectrophotometer (2550 Shimadzu, Kyoto, Japan).

The partition coefficient (K_{CAP}) of the CAP molecules was calculated using equation 1:

$$K_{CAP} = \frac{(ABS_{276\,nm}^{PRP}).fd^{PRP}}{(ABS_{276\,nm}^{ERP}).fd^{ERP}} \quad (1)$$

where $ABS_{276\,nm}^{PRP}$ and $ABS_{276\,nm}^{ERP}$ are the diluted CAP absorbance values obtained at 276 nm in the polymer-rich phase and in the electrolyte-rich phase, and fd^{PRP} and fd^{ERP} are the dilution factors of the phases, respectively.

2.3. Thermodynamic parameters of CAP transfer

2.3.1. CAP transfer standard Gibbs free energy change ($\Delta_{tr}G^{\theta}$)

The transfer standard Gibbs free energy change ($\Delta_{tr}G^{\theta}$) was obtained from values of the CAP partition coefficient (K_{CAP}) of all studied ATPS, with the following thermodynamic relationship:

$$\Delta_{tr}G^{\theta} = -R\ T\ ln\ K_{CAP} \quad (2)$$

where R is the real gas constant in (kJ mol^{-1} K^{-1}), T is the absolute temperature (K), and K_{CAP} is the CAP partition coefficient.

2.3.2. CAP transfer standard enthalpy change ($\Delta_{tr}H^{\theta}$)

The technique Isothermal Titration Calorimetry (ITC) was used to determine the CAP transfer standard enthalpy change ($\Delta_{tr}H^{\theta}$) from the electrolyte-rich phase to the polymer-rich phase, using a CSC-4200 microcalorimeter (Science Corp. Calorimeter). A gas-tight Hamilton syringe (250 μL) controlled by an instrument was utilized for the injections, and a stirrer helix stirring at 300 rpm was used during the experiment. The experiments were realized by filling the reference and sample cells with 1.80 mL of the electrolyte-rich phase or polymer-rich phase, and titrating the sample solution (contained in the sample cell) with ten consecutive injections of 25 μL of CAP stock solutions at a concentration of ($4.6x10^{-5}$) mol kg^{-1}. The CAP stock solutions were prepared in the electrolyte-rich phase or polymer-rich phase of the ATPS. The same experiment was performed in the CAP absence to discount the energy related with friction effects. The flow of energy registered during all process was recorded as a power versus time curve, being that the area of each peak was integrated to obtain the enthalpy change of each dilution process. The curve of CAP standard dilution enthalpy change ($\Delta_{dil}H^{\theta}_{CAP}$). in the electrolyte- rich phase or polymer-rich phase as function of CAP concentration was plotted and extrapolated to CAP concentration equal zero, obtaining the CAP standard dilution enthalpy change in infinite dilution conditions ($\Delta_{dil}H^{\theta\infty}$), for each phase. Thus, the $\Delta_{tr}H^{\theta\infty}$ values for CAP were obtained through of difference between these measurements in infinite dilution conditions of the polymer-rich phase and electrolyte- rich phase.

$$\Delta_{tr}H^{\theta\infty} = \Delta_{dil}H^{\theta\infty}{}^{PRP}_{CAP} - \Delta_{dil}H^{\theta\infty}{}^{ERP}_{CAP} \quad (3)$$

Equation 3 could then be used to calculate $\Delta_{tr}H^{\theta\infty}$, where $\Delta_{dil}H^{\theta\infty}{}^{PRP}_{CAP}$ and $\Delta_{dil}H^{\theta\infty}{}^{ERP}_{CAP}$ are the CAP standard dilution enthalpy change at infinite dilution conditions in the polymer-rich phase and electrolyte-rich phase, respectively.

2.3.3. CAP transfer standard entropy change ($T\Delta_{tr}S^{\theta}$)

The CAP transfer standard entropy change ($T\Delta_{tr}S^{\theta}$) was determined through the classic thermodynamics relationship:

$$\Delta_{tr}G^{\theta} = \Delta_{tr}H^{\theta} - T\Delta_{tr}S^{\theta} \quad (4)$$

where $\Delta_{tr}G^{\theta}$ and $\Delta_{tr}H^{\theta}$ values are known for a given temperature T.

3. Results and discussion

3.1. Influence of CAP concentration in the partition coefficient

In ATPS partition studies it is of importance to evaluate the influence of solute concentration on it partitioning coefficient. The K values will be independent of solute concentration only if during the transfer processes to occur the partitioning of just one molecular species between the phases of the ATPS systems [34]. In order to determine if only one molecular species is transferred during CAP partitioning experiment, the dependence of K_{CAP} values in relation to antibiotic concentration was measured in the tie-line length (TLL) (≅ 29% m/m) of the system PEO1500 + H_2O + Li_2SO_4, at 298.2 K, as shown in Fig. 2.

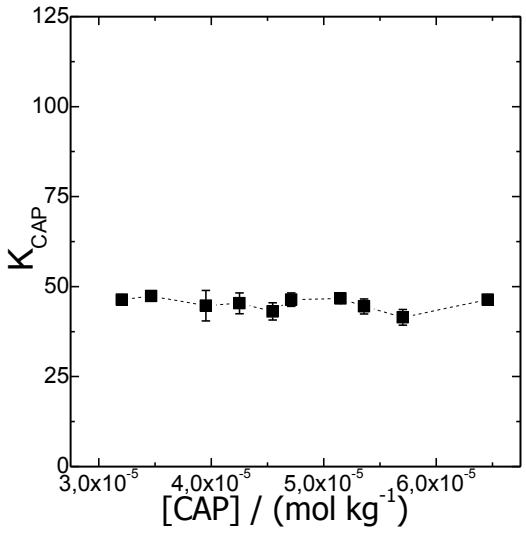

Fig. 2. Partition coefficient values of CAP as a function of its concentration in ATPS formed by PEG1500 + Li_2SO_4 + H_2O in the TLL of (≅ 29 %(m/m)) at 298.2 K.

As can be seen, for all the studied CAP concentration range, the K_{CAP} values were almost independent of antibiotic concentration, ranging from 41.47±2.19 to

47.36±0.06, with a relative standard deviation of approximately 4.0%, presenting a good accuracy. Based on this independent CAP concentration transfer process, we can to conclude that only one chemical species is been partitioned between both ATPS phases.

3.2. The effect of tie-line length of aqueous two-phase systems on the partitioning of CAP

The analytes distribution between ATPS phases can be explained through intermolecular interactions occurring between system components and the partitioned solute [35]. Generally, in works that studies the solute partitioning behavior in ATPS, an important parameter analyzed is the tie-line length (TLL), which expresses the differences between the ATPS component interactions occurring in the polymer-rich phase from that interactions present in the electrolyte-rich phase of the ATPS [36]. The TLL can be calculated with equation 5:

$$\mathbf{TLL} = \left[\left(\boldsymbol{C}_{\mathbf{P}}^{\mathbf{PRP}} - \boldsymbol{C}_{\mathbf{P}}^{\mathbf{ERP}}\right)^{\mathbf{2}} + \left(\boldsymbol{C}_{\mathbf{E}}^{\mathbf{PRP}} - \boldsymbol{C}_{\mathbf{E}}^{\mathbf{ERP}}\right)^{\mathbf{2}}\right]^{\mathbf{1/2}} \quad (5)$$

where $C_{\mathrm{P}}^{\mathrm{PRP}}$ and $C_{\mathrm{P}}^{\mathrm{ERP}}$ are the polymer concentrations in % (m/m) and $C_{\mathrm{E}}^{\mathrm{PRP}}$ and $C_{\mathrm{E}}^{\mathrm{ERP}}$ are the electrolyte concentrations in % (m/m), in the polymer-rich phase and electrolyte-rich phase, respectively.

As long as the TLL values increase, the differences between intensive thermodynamic properties of ATPS phases are enhanced, making the solute molecular interactions with polymer-rich phase component more different from solute molecular interaction with electrolyte-rich phase component, and usually increasing the unequal solute distribution. Fig. 3 shows K_{CAP} measured in ATPS composed by PEG1500 + lithium sulfate + H_2O as a function of TLL, at 298.2 K

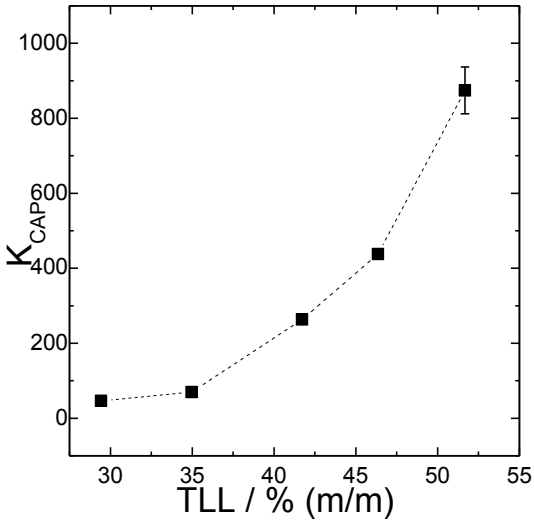

Fig. 3. Partition coefficient of CAP as a function of TLL in ATPS formed by PEG1500 + Li_2SO_4 + H_2O at 298.2 K.

CAP prefers to concentrate in the polymer-rich phase of the ATPS, showing its greater affinity with polymer-rich phase components, since the K_{cap} presented values higher than unity. TLL values increase promotes enhancement in the solute transfer process from the electrolyte-rich phase to the polymer-rich phase of ATPS, with partition coefficients ranging from 46.37±1.88 to 874.33±62.48, when TLL change from 29 to 52% (m/m), almost presenting an exponential behavior.

The solute transfer process from electrolyte-rich phase to polymer rich-phase occur due the rupture of solute interactions with the components of electrolyte-rich phase and formation of interactions between the constituents of this phase, while simultaneously, in the polymer-rich phase, interactions between the components this phase are disrupted to formation of a cavity into which the solute fit to interact with these constituents [21].

The energy resulting from these molecular interactions balance is expressed by standard transfer Gibbs free energy change ($\Delta_{tr}G^{\theta}$)**.** The $\Delta_{tr}G^{\theta}$ value is the free energy change of the system whenever one mole of solute is transferred from the electrolyte-rich phase to the polymer-rich phase (see equation 2).

Fig. 4 shows $\Delta_{tr}G^{\theta}$ values to CAP as a function of TLL, using the system formed by PEO1500 + Li_2SO_4 + H_2O at 298.2 K.

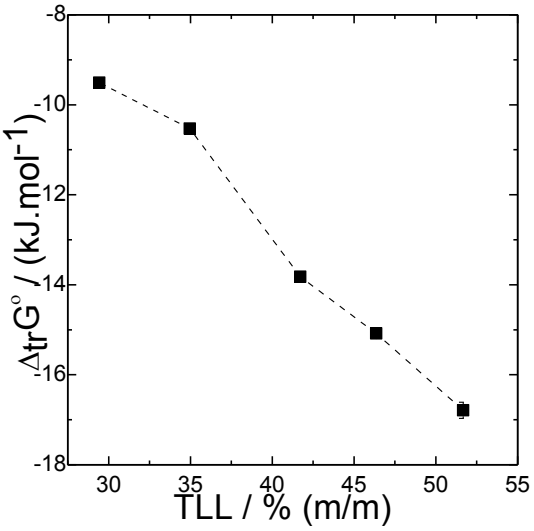

Fig. 4. $\Delta_{tr}G^{\theta}$ of CAP as a function of the TLL for the ATPS composed by PEO1500 + Li_2SO_4 + H_2O at 298.2 K.

The $\Delta_{tr}G^{\theta}$ values decrease almost linearly with the increase in TLL, ranging from (-9.51±0.10) to (-16.79±0.18) kJ mol^{-1}. To the best of our knowledge, the results presented here are the first concerning the CAP partitioning in ATPS composed by polymer + electrolyte + H_2O. According to reported works in the literature, the only used ATPS for CAP partition or extraction has been those formed by ionic liquids + electrolytes [6, 37, 38]. All results of partitioning demonstrated that occurs the preferential transfer of CAP to ionic liquid-rich phase. As our results, for these works, the obtained $\Delta_{tr}G^{\theta}$ values are all negative, ranging from (-4.49) to (-11.92) kJ mol^{-1}. However, the K_{CAP} values shown range from 5 to 160, which are smaller than the those obtained in the present work, using the system formed by PEO1500 + Li_2SO_4 + H_2O.

To better understand the CAP partition process it is necessary to evaluate the energetic and configurational solute transfer contributions to $\Delta_{tr}G^{\theta}$, i.e. the enthalpic ($\Delta_{tr}H^{\theta}$) and entropic ($T\Delta_{tr}S^{\theta}$) components of $\Delta_{tr}G^{\theta}$ (see equation 4).

The $\Delta_{tr}H^{\theta}$ contribution to the ATPS solute transfer process can be determined by using an isothermal titration calorimeter, which detects low levels of system enthalpy change. To obtain the $\Delta_{tr}H^{\theta}$, it is necessary to determine the solute dilution enthalpy change in infinite dilution condition ($\Delta_{dil}H^{\theta,\infty}$), which is the net energy from the interactions of solute with the components of each ATPS phase. $\Delta_{dil}H^{\theta,\infty}$ values were obtained from fitting the experimental data of curves of

$\Delta_{dil}H$ as a function of CAP concentration for both ATPS phases, and extrapolating the analytical functions obtained by the fitting to zero CAP concentration. Fig. 5 shows $\Delta_{dil}H$ as a function of CAP concentration obtained for both ATPS phases, in all TLL of the system PEO1500 + Li_2SO_4 + H_2O at 298.2 K. The results for the others ATPS here studied are showed in the appendix (see figures F1 to F6).

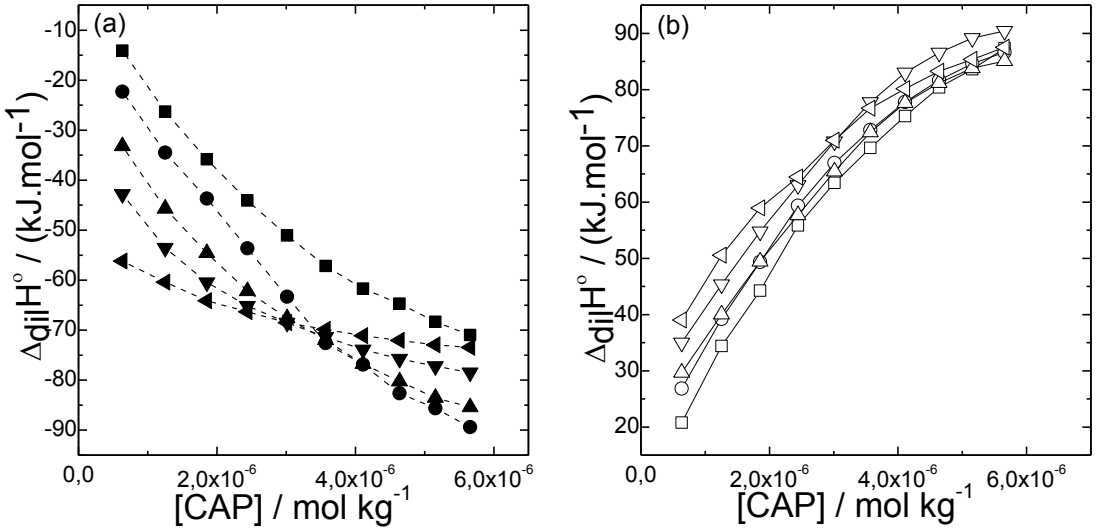

Fig. 5. CAP $\Delta_{dil}H$ value in polymer-rich phase (a) and electrolyte-rich phase (b) for PEO1500 + Li_2SO_4 + H_2O ATPS: (■/□) (≅ 29 %(m/m)) TLL, (●/○) (≅ 35 %(m/m)) TLL, (▲/△) (≅ 42 %(m/m)) TLL, (▼/▽) (≅ 46 %(m/m)) TLL and (◀/◁) (≅ 52 %(m/m)) TLL at 298.15 K.

Despite of TLL values, the CAP dilution process was ever exothermic in the polymer-rich phase while in the electrolyte-rich phase the same process was ever endothermic. In addition, the CAP-CAP interaction is enthalpy favorable on the polymer-rich phase while in the electrolyte-rich phase this kind of interaction is unfavorable. $\Delta_{dil}H^{\theta,\infty}$ magnitude measured in both PEO1500 + Li_2SO_4 + H_2O ATPS phases, at 298.15 K, are showed in the table 1. Some results were also obtained for others ATPS studied in this work (see appendix tables T1 to T6).

Table 1. CAP $\Delta_{dil}H^{\theta,\infty}$ values in polymer-rich phase and electrolyte-rich phase, for different TLL of system PEO1500 + Li_2SO_4 + H_2O at 298.15 K.

TLL / (% m/m)	$\Delta_{dil}H^{\theta,\infty}$ / (kJ.mol^{-1}) polymer-rich phase	$\Delta_{dil}H^{\theta,\infty}$ / (kJ.mol^{-1}) electrolyte-rich phase
29	-1.85±0.62	6.66±0.87
35	-7.55±1.44	12.67±0.37
42	-22.73±1.21	16.04±0.92
46	-35.39±1.53	21.38±0.92
52	-52.21±0.45	28.67±0.90

The $\Delta_{dil}H^{\theta,\infty}$ values measured in the polymer-rich phase were negative and in the electrolyte-rich phase were positive. As long as TLL increase, $\Delta_{dil}H^{\theta,\infty}$ values are more negatives in the polymer-rich phase while in the electrolyte-rich, are more positives. Despite of the great amount of water in both ATPS phases, $\Delta_{dil}H^{\theta,\infty}$ values were very distinct in these phases, indicating that the mains molecular components in CAP solvation shells is not only water but mainly polymer (in the polymer-rich phase) and ions (in the electrolyte- rich phase). For ATPS studied the polymer-CAP interactions were exothermic while electrolyte-CAP were endothermic, except for ATPS formed by PEO1500 + $MgSO_4$ + H_2O, which electrolyte-CAP were exothermic (see appendix tables T1 to T6). The negative values obtained in polymer rich-phase imply enthalpically favorable interaction, while positives values obtained in the electrolyte-rich phase indicate unfavorable interaction.

By means of the $\Delta_{dil}H^{\theta,\infty}$ measured in the polymer-rich phase and electrolyte-rich phase for each TLL, it is possible to determine the $\Delta_{tr}H^{\theta}$of CAP with equation 6:

$$\Delta_{tr}H^{\theta} = \Delta H^{\theta,\infty}_{dil\ CAP-PRP} - \Delta H^{\theta,\infty}_{dil\ CAP-ERP} \quad (6)$$

where $\Delta H^{\theta,\infty}_{dil\ CAP-PRP}$ is the standard dilution enthalpy change at infinite dilution state resulting of the CAP interaction with the components of the polymer-rich phase, and $\Delta H^{\theta,\infty}_{dil\ CAP-ERP}$ is the standard dilution enthalpy change at infinite dilution state resulting of the CAP interaction with the components of electrolyte-rich phase.

The $\Delta_{tr}H^{\theta}$ values express the system enthalpy change whenever one mole of CAP is transferred from the electrolyte-rich phase to the polymer-rich phase, disregarding solute-solute interactions during the transfer process. In Fig. 6 the $\Delta_{tr}H^{\theta}$ of CAP is shown as a function of TLL for the system PEO1500 + Li_2SO_4 + H_2O at 298.2 K.

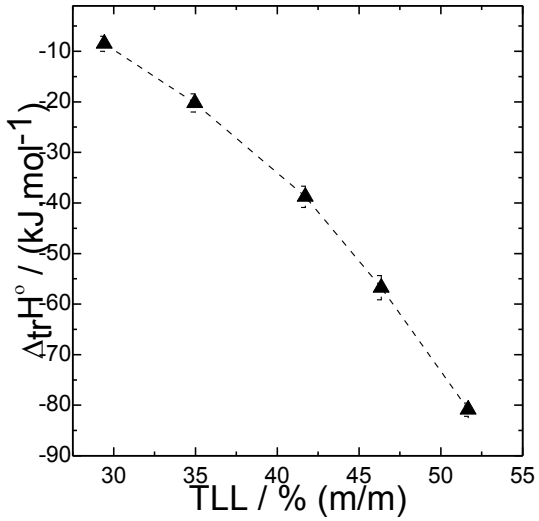

Fig. 6. $\Delta_{tr}H^{\theta}$ of CAP as a function of the TLL for the ATPS composed by PEO1500 + Li_2SO_4 + H_2O at 298.2 K.

The CAP transfer process is exothermic, with $\Delta_{tr}H^{o}$ becoming more negative, ranging from (-8.51±1.49) to (-80.88±1.22) kJ mol^{-1}, with TLL increase. The CAP transfer process occurs from the electrolyte-rich phase to the polymer-rich phase. Thus, in the electrolyte-rich phase occurs the process of disruption of CAP-polymer, CAP-water and CAP-electrolyte interactions, while that polymer-polymer, electrolyte-electrolyte, water-water, water-electrolyte, water-polymer and electrolyte-polymer interactions are formed. In the polymer-rich phase, the main energy involved in the processes is related to the rupture of water-water, polymer-polymer, electrolyte-electrolyte, polymer-water, electrolyte-water and polymer-electrolyte interactions for cavity formation, followed by solvation process of CAP molecules, which are surrounded by polymer, water and electrolyte, establishing new interactions of CAP-polymer, CAP-water and CAP-electrolyte. Forming interactions reduce the enthalpy of the system by means of energy release, while to rupture interactions, causing an increase of energy. This balance shows that more energy is released than absorbed to break interactions.

Another evaluated parameter was the CAP $T\Delta_{tr}S^{\theta}$. This term describes the increase or decrease in the number of different possibilities of components distribution present in the ATPS, due the transfer process of CAP from the electrolyte-rich phase to the polymer-rich phase. Fig. 7 shows the $T\Delta_{tr}S^{\theta}$ values obtained for CAP partitioning as a function of TLL, for system PEO1500 + Li_2SO_4 + H_2O at 298.2 K.

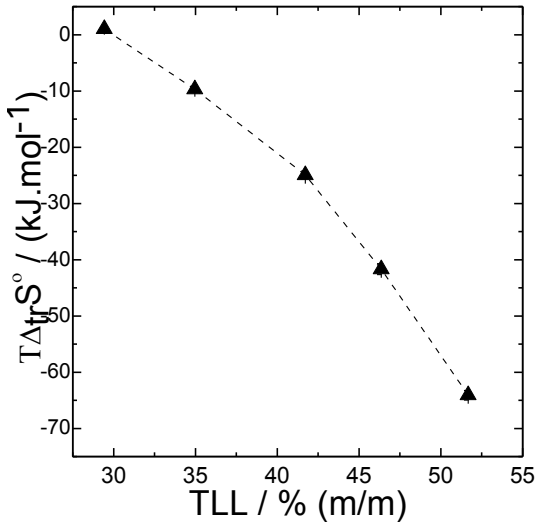

Fig. 7. $T\Delta_{tr}S^{\theta}$ of CAP as a function of the TLL for the ATPS composed by PEO1500 + Li_2SO_4 + H_2O at 298.2 K.

In Fig. 7 it can be observed that $T\Delta_{tr}S^{\theta}$ values are almost all negative, except the first TLL. The values range from (1.00±0.09) to (-64.09±0.85) kJ mol^{-1}. These negative values indicate that the CAP transfer process occurs with enthalpic contributions. According to the model developed by Johansson et al [39], the entropic contribution to the CAP partition can be obtained with equation 7:

$$lnK_{CAP} = \frac{M_{CAP}}{\rho}\left(\frac{n^{PRP}}{V^{PRP}} - \frac{n^{ERP}}{V^{ERP}}\right) \quad (7)$$

where M_{CAP} is the molar mass of the partitioning solute, ρ is the number of lattice sites per unit volume, n^{PRP} and n^{ERP} are the total number of molecules in the polymer-and electrolyte-rich phases, respectively, and V^{PRP} and V^{ERP} are the volumes of the polymer-and electrolyte-rich phases, respectively.

As shown by equation 7, considering only entropic effects, the partition of the solute will occur to the phase with more molecules per volume. The numerical density is higher in the electrolyte-rich phase than the polymer-rich phase, due to its higher content of water. The liquid-liquid equilibrium data of the system PEO 1500 + Li_2SO_4 + H_2O at 298.2 K show that the difference between the amount of water in the electrolyte-rich phase and polymer-rich phase increase with increasing TLL [31]. According to the Johansson et al model [39], the solute should be concentrated in the electrolyte-rich phase, in which it has greater configurational entropic contribution.

Nevertheless, different behavior of CAP partition was observed, presenting partition coefficient values higher than unity, indicating more interaction of this solute with the polymer-rich phase. Thus, the CAP concentration in the polymer-rich phase causes a decrease in the entropy of the system with increasing TLL because there is a lower amount of water in this phase. This behavior confirms that the CAP tranfer process must be enthalpically driven.

3.3. Effect of cation on the CAP partitioning

The change in the electrolytes cations which make up the ATPS can alter the intensity of the intermolecular interactions and, consequently, the partition coefficient [35]. Studies have been performed to evaluate this effect on different-solute partitioning behavior in these systems [5, 26, 40]. Fig. 8 shows the CAP partition coefficient (Fig. 8a) and $\Delta_{tr}G^{\theta}$ (Fig. 8b) as a function of TLL, in different systems composed by the same polymer (PEO1500) and different sulfate electrolytes (Li_2SO_4, Na_2SO_4 and $MgSO_4$), at 298.2 K.

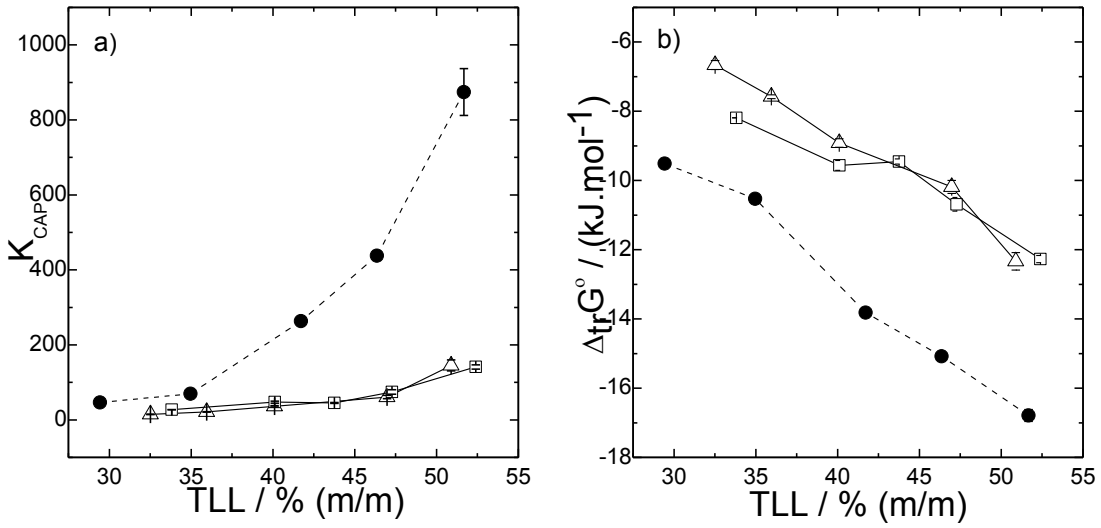

Fig. 8. CAP partition coefficient (a) and $\Delta_{tr}G^{\theta}$ (b) as a function of the tie-line length (TLL), at 298.2 K. ATPS: (●) PEO1500 + Li_2SO_4 + H_2O; (△) PEO1500 + Na_2SO_4 + H_2O; (□) PEO1500 + $MgSO_4$ + H_2O.

It was observed that comparing the partition coefficient in similar TLL (≅ 40% m/m), the ATPS composed by electrolyte Li_2SO_4 (k=263±4) presented higher partition coefficient of CAP than the ATPS composed by Na_2SO_4 (k=36±2) and $MgSO_4$ (k=47±2) electrolytes. Similar cation effect was observed in other previously [40] reported works [2, 5, 26]. This effect can be explained according to the work

realized by da Silva et al [41]. In this work, was realized the partitioning of the anions pentacyanonitrosylferrate-(II), $[Fe(CN)_5NO]^{2-}$, and hexacyanoferrate, $[Fe(CN)_6]^{3-}$, both with the same molar volume, in ATPS formed by PEO 35000, different sulfate electrolytes (Li_2SO_4, Na_2SO_4 and $MgSO_4$) and water. The results showed that hexacyanoferrate anion also transfers to the polymer-rich phase, but this transfer is smaller when compared with the $[Fe(CN)_5NO]^{2-}$ anion. The authors verified that the cost of energy involved in process of cavity formation is not the only force which influences the transfer process of the both anions. It was observed that the presence of the NO groups in the anion structure influenced the partitioning behavior of ions in ATPS. This direct interaction was confirmed by infrared spectroscopy measurements, showing that NO stretching band is very sensitive to PEO concentration in relation to pure water, indicating a site-specific interaction [41]. Based on this, the CAP transfer from the electrolyte-rich phase to the polymer-rich phase occurs due to specific enthalpic interactions between CAP and segments of PEO macromolecules by means of NO groups present in this molecule and electron pairs of oxygen atoms. Moreover it is well known that lithium cations have higher capacity to interact with the PEO segments, which compose the polymeric chain due to stronger interactions [41]. Thus, since the CAP has pka = 5.5 [42-44] and the pH of ATPS probably are near neutrality, the CAP specie are negatively charged favoring also the transfer process due interaction com positively-charged polymer chain (pseudopolycation). The $\Delta_{tr}G^{\theta}$ values were negative ranging from (-16.79±0.18) to (-6.66±0.13) kJ mol^{-1}, and the cation effect was discrete for the $\Delta_{tr}G^{\theta}$ parameter, being in the ATPS composed by electrolytes Li_2SO_4, $\Delta_{tr}G^{\theta}$ = (-13.82±0.04) kJ mol^{-1}, Na_2SO_4, $\Delta_{tr}G^{\theta}$ = (-8.91±0.12) kJ mol^{-1}, and $MgSO_4$, $\Delta_{tr}G^{\theta}$ = (-9.56±0.14) kJ mol^{-1}; however, $\Delta_{tr}G^{\theta}$ value obtained in the ATPS formed Li_2SO_4 electrolyte was more negative, indicating greater interaction with the solute.

To better understand the driving forces that direct the CAP partition in the ATPS, the transfer thermodynamic parameters $\Delta_{tr}H^{\theta}$ and $T\Delta_{tr}S^{\theta}$ were evaluated. In Fig. 9 the transfer thermodynamic parameters $\Delta_{tr}H^{\theta}$ (Fig. 9a) and $T\Delta_{tr}S^{\theta}$ (Fig. 9b) are shown as functions of the tie-line length (TLL), at 298.2 K.

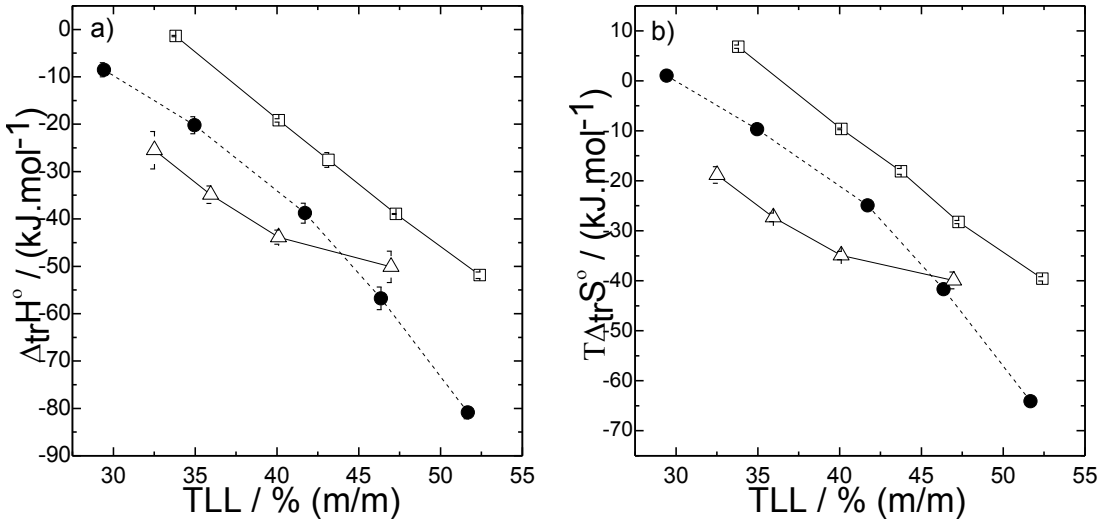

Fig. 9. $\Delta_{tr}\boldsymbol{H^{\theta}}$ (a) and $\boldsymbol{T\Delta_{tr}S^{\theta}}$ (b) as a function of the tie-line length (TLL), at 298.2 K. ATPS: (●) PEO1500 + Li_2SO_4 + H_2O; (△) PEO1500 + Na_2SO_4 + H_2O; (□) PEO1500 + $MgSO_4$ + H_2O.

The $\Delta_{tr}H^{\theta}$ values are negative, ranging from (-80.88±1.30) to (-1.37±0.14) kJ mol^{-1}, while $T\Delta_{tr}S^{\theta}$ values range from (-64.09±0.85) kJ to (6.82±0.35) kJ mol^{-1}, decreasing with TLL increase for all studied systems. This behavior shows that the CAP transfer process is enthalpically driven. The results in similar TLL can be pointed out according table 2:

Table 2. $\Delta_{tr}\boldsymbol{H^{\theta}}$ and $\boldsymbol{T\Delta_{tr}S^{\theta}}$ obtained CAP transfer process in ATPS formed by different cations.

ATPS	TLL / (% m/m)	$\Delta_{tr}H^{\theta}$ / (kJ mol^{-1})	$T\Delta_{tr}S^{\theta}$ / (kJ mol^{-1})
PEO 1500 + Li_2SO_4 + H_2O	42	-38.77±2.10	-24.95±0.71
PEO 1500 + Na_2SO_4 + H_2O	40	-43.86±1.49	-34.95±0.83
PEO 1500 + $MgSO_4$ + H_2O	40	-19.20±0.37	-9.64±0.16

It can be observed that interactions governed by enthalpic nature are stronger in the ATPS composed of Na_2SO_4. Despite this, as already mentioned, $\Delta_{tr}G^{\theta}$ parameter in the ATPS formed Li_2SO_4 electrolyte was more negative. Evaluating theses entropy values according the model proposed by Johansson and coworkers, the liquid-liquid equilibrium data of these systems [31] show that the difference between the water content of the electrolyte-rich phase and polymer-rich phase does not obey a relation with the values of entropy, indicating that besides the configurational entropy, other entropic contributions should be involved.

3.4. Effect of polymer molar mass on the CAP partitioning

Molar mass is also an important variable studied in partitioning processes since the solute distribution in the ATPS can be affected by size of the system-forming polymer [45]. Commonly, an increase of polymer-molar mass, decrease the solute concentration in the polymer-rich phase [17, 26]. This occurs due steric and entropic effects. Based on this, it is of fundamental importance to evaluate the influence of the polymer molar mass in the partition behavior of CAP.

Fig. 10 shows the CAP partition coefficient (Fig. 10a) and $\Delta_{tr}G^{\theta}$ (Fig. 10b) as functions of TLL in ATPS composed by the same electrolyte (Li_2SO_4) and polymers (PEO) with different molar masses (1500, 10000 and 35000 g.mol^{-1}) at 298.2 K.

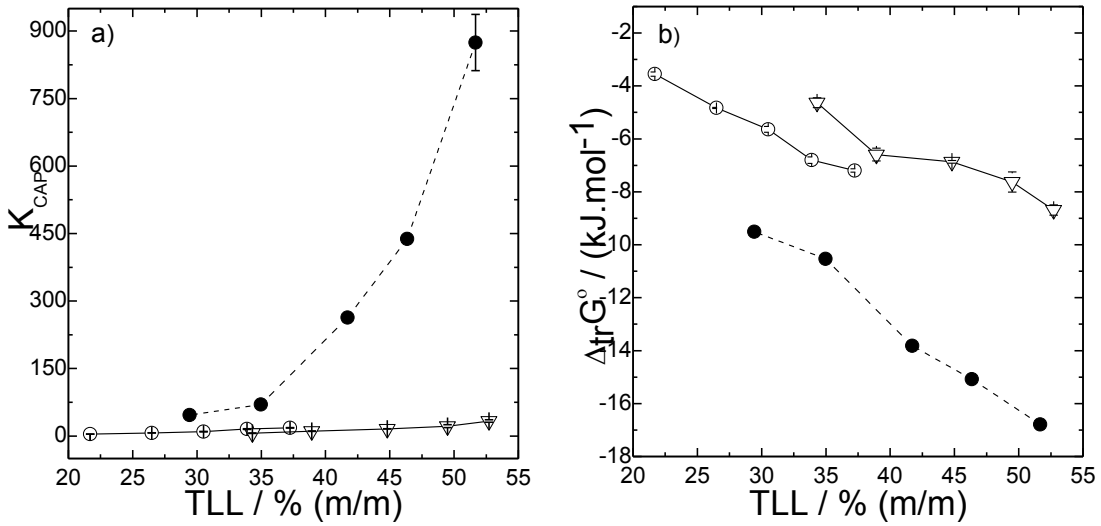

Fig. 10. CAP partition coefficient (a) and $\Delta_{tr}G^{\theta}$ (b) as a function of the tie-line length (TLL), at 298.2 K. ATPS: (●) PEO1500 + Li_2SO_4 + H_2O; (○) PEO10000 + Li_2SO_4 + H_2O; (▽) PEO35000 + Li_2SO_4 + H_2O.

The ATPS composed by polymers PEO 1500, 10000 and 35000, in similar TLL of approximately 34 %(m/m), presented partition coefficient (k = 70±1), (k = 16±1) and (k = 6±0.5), respectively, following the order $K_{PEO\ 1500} > K_{PEO\ 10000} > K_{PEO\ 35000}$. This behavior is explained because, with the increase of polymer molar mass, there occurs a decrease in the contribution of configurational entropy for CAP in the polymer-rich phase, due to spatial unavailability of some segments of PEO [26, 46]. The obtained results agree with some data presented in the literature [26, 47], confirming this partition behavior for certain solutes. The $\Delta_{tr}G^{\theta}$ values range from (-16.79±0.18) kJ mol^{-1} to (-3.55±0.08) kJ mol^{-1}. $\Delta_{tr}G^{\theta}$ obtained were $\Delta_{tr}G^{\theta}$ = (-

10.53±0.01) kJ mol^{-1}, $\Delta_{tr}G^{\theta}$ = (-6.80±0.12) kJ mol^{-1} and $\Delta_{tr}G^{\theta}$= (-4.63±0.19) kJ mol^{-1} for ATPS composed by PEO 1500, 10000 and 35000, respectively. In order to evaluate, the enthalpic and entropic contributions in the solute transfer process the parameters $\Delta_{tr}H^{\theta}$ and $T\Delta_{tr}S^{\theta}$ were studied.

Fig. 11 shows the transfer thermodynamic parameters $\Delta_{tr}H^{\theta}$ (Fig. 11a) and $T\Delta_{tr}S^{\theta}$ (Fig. 11b) as functions of the tie-line length (TLL), at 298.2 K.

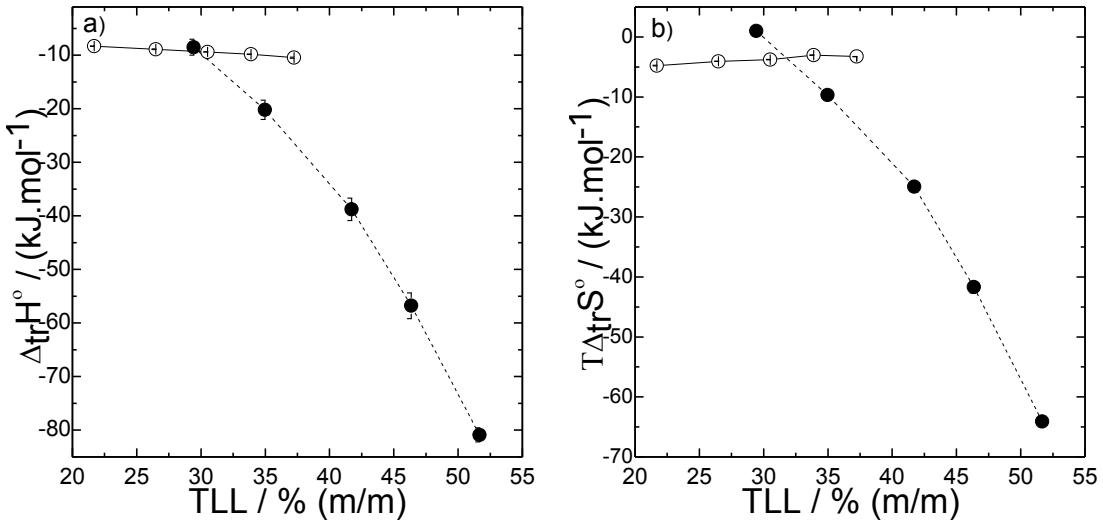

Fig. 11. $\Delta_{tr}\boldsymbol{H^{\theta}}$ (a) and $\boldsymbol{T\Delta_{tr}S^{\theta}}$ (b) as a function of the tie-line length (TLL), at 298.2 K. ATPS: (●) PEO1500 + Li_2SO_4 + H_2O; (○) PEO10000 + Li_2SO_4 + H_2O.

Due to experimental limitations, enthalpy and entropy associated with CAP transfer process were not studied for ATPS formed by PEO35000 + Li_2SO_4 + H_2O. The $\Delta_{tr}H^{\theta}$ values ranging from (-80.88±1.30) to (-8.33±0.04) kJ mol^{-1} decrease with TLL increase for both ATPS and present more negative values for the ATPS composed by PEO1500 than ATPS composed by PEO10000. The $T\Delta_{tr}S^{\theta}$ values range from (-64.09±0.85 kJ mol^{-1}) to (1.00±0.09 kJ mol^{-1}), decreasing with TLL increase for the system formed by PEO1500, and present almost constant behavior with TLL increase for the system composed by PEO10000. The $\Delta_{tr}H^{\theta}$ values were more negative for ATPS composed by PEO1500 $\Delta_{tr}H^{\theta}$ = (-20.22±1.8) kJ mol^{-1} than PEO10000, $\Delta_{tr}H^{\theta}$ = (-9.82±0.05) kJ mol^{-1}, because PEO1500 presents higher number of sites available to interact with CAP molecules, thus interacting directly and more strongly, while $\Delta_{tr}H^{\theta}$ value is less negative for PEO10000 because, in order to CAP interact with this polymer, it has to spend more energy to break the segment-segment interactions of this macromolecule, because of high entanglement.

The obtained $T\Delta_{tr}S^{\theta}$ values were more negative for PEO1500, $T\Delta_{tr}S^{\theta}$ = (-9.69±0.43) kJ mol^{-1}, than for PEO10000, $T\Delta_{tr}S^{\theta}$ = (-3.02±0.04) kJ mol^{-1}, since the difference of water content between the electrolyte-rich phase and polymer-rich phase in the ATPS composed by PEO1500 is higher than the difference of this content in the ATPS composed by PEO10000, thereby causing a greater decrease in entropy for the system composed by macromolecules with lower molar mass [31]. A similar behavior was reported by Rengifo et al in the Chymosin partition ATPS [5].

3.5. Effect of anion on the CAP partitioning

As already mentioned, the change of ATPS components can affect the solute partitioning process [48]. As the cation, anion can also to influence on the process of solute partition in ATPS. Thus, understanding the interactions between these ions, the other ATPS components and the solute, contributes to an advance on separation and extraction process. Based on this, Fig. 12 shows the influence exerted by the ATPS-forming anion on the values of the partition coefficient (Fig. 12a) and $\Delta_{tr}G^{\theta}$ (Fig. 12b), for different TLL, at 298.2 K.

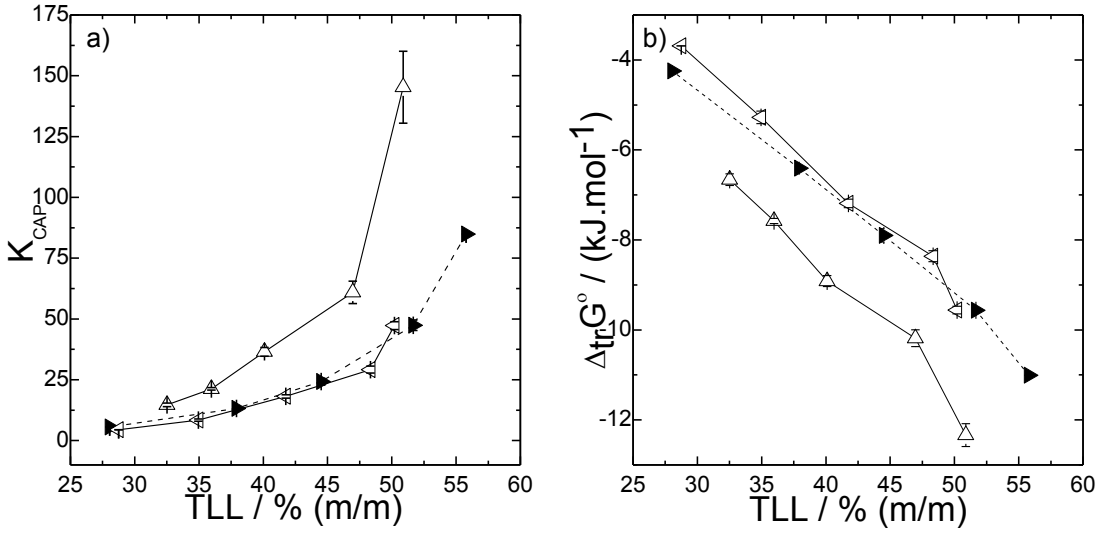

Fig. 12. CAP partition coeficiente (a) and $\Delta_{tr}G^{\theta}$ (b) as a function of the tie-line length (TLL), at 298.2 K. ATPS: (△) PEO1500 + Na_2SO_4 + H_2O; (▶) PEO1500 + $Na_3C_6H_5O_7$ + H_2O; (◁) PEO1500 + $Na_2C_4H_4O_6$ + H_2O.

The anion effect was less pronounced when compared to the cation effect. The ATPS composed by the SO_4^{-2} anion (k = 36±2) presented higher partition coefficient of CAP than the ATPS composed by $C_4H_4O_6^{-2}$ (k = 18.±0.7) and $C_6H_5O_7^{-3}$ (k = 13±0.2) anions, considering TLL of approximately 40% (m/m). For all ATPS

there is an increase in the CAP partition coefficient values with increasing of TLL. It can still be observed that SO_4^{-2} anion presents a greater effect in relation to citrate and tartrate anions. This occurs because the sulfate anions present higher charge density when compared to other anions. As a result, the solute transfer process to the polymer-rich phase occurs more markedly due to repulsion between the CAP molecules (negatively charged) and these anions in the electrolyte-rich phase. As reported by Han and coworkers [37], in a study of pH effect on the extraction efficiency of CAP, using the ATPS composed by [Bmim]BF_4-$Na_3C_6H_5O_7$, CAP was stable in pH ranging from 6 to 10, being that in others conditions of the reaction medium, such as acid or strongly alkaline, CAP was decomposed. The pH this system studied was about 8.0, without adjustment. Thus CAP molecules were negatively charge under the experimental conditions realized. Based on this and also in the pka of CAP, in the present work it was assumed that the reaction medium has a pH close to neutrality and that the CAP is negatively charged. The $\Delta_{tr}G^{\theta}$ values range from (-12.34±0.25) to (-3.68±0.01) kJ mol^{-1}. The anion effect also was not very pronounced for the Δ_{tr}G° parameter, as shown by the following results: ATPS composed by anions SO_4^{-2}, $\Delta_{tr}G^{\theta}$ = (-8.91±0.12) kJ mol^{-1}, $C_4H_4O_6^{-2}$, $\Delta_{tr}G^{\theta}$ = (-7.18±0.09) kJ mol^{-1}, and $C_6H_5O_7^{-3}$, $\Delta_{tr}G^{\theta}$ = (-6.40±0.04) kJ mol^{-1}. However, based on these values, the stronger interaction of CAP with the components of the polymer-rich phase was confirmed for the ATPS formed by the SO_4^{-2} anion.

In the Fig. 13 the transfer thermodynamic parameters $\Delta_{tr}H^{\theta}$ (Fig. 13a) and $T\Delta_{tr}S^{\theta}$ (Fig. 13b) are shown as functions of the tie-line length (TLL) in ATPS formed by PEO1500 + Na_2SO_4 + H_2O and PEO1500 + $Na_3C_6H_5O_7$ + H_2O, at 298.2 K.

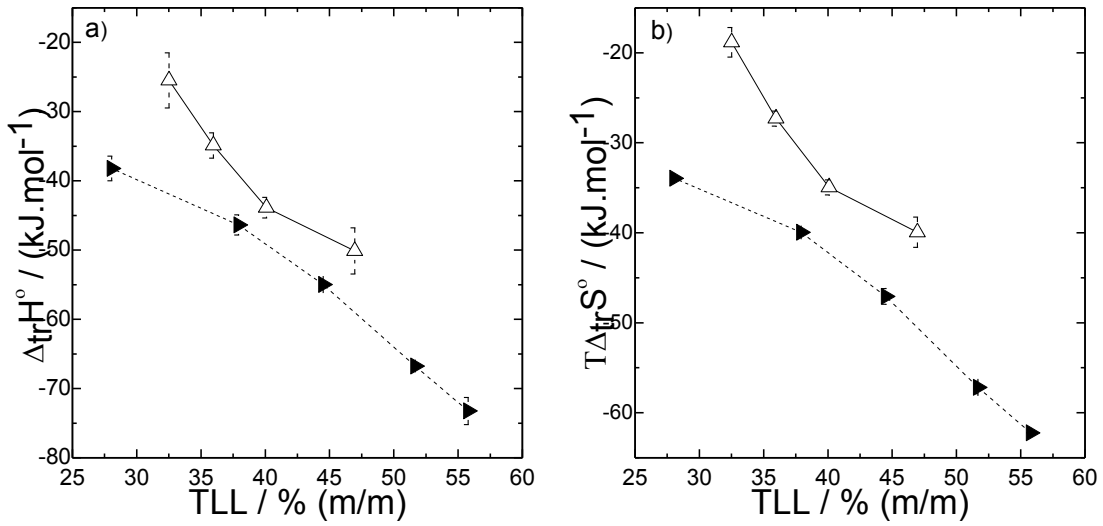

Fig. 13. $\Delta_{tr}\boldsymbol{H^{\theta}}$ (a) and $\boldsymbol{T\Delta_{tr}S^{\theta}}$ (b) as a function of the tie-line length (TLL), at 298.2 K. ATPS: (△) PEO1500 + Na_2SO_4 + H_2O; (▶) PEO1500 + $Na_3C_6H_5O_7$ + H_2O.

The $\Delta_{tr}H^{\theta}$ values range from (-73.23±1.96) to (-25.49±3.97) kJ mol^{-1}, while $T\Delta_{tr}S^{\theta}$ values range from (-62.23±0.01) to (-18.83±1.65) kJ mol^{-1}. As can be seen the $\Delta_{tr}H^{\theta}$ values are all negatives. This can be explained considering some main interactions in the transfer process. In the electrolyte-rich phase, the electrolyte-CAP interactions are broken, while in the polymer-rich phase, are broken polymer-water interactions (endothermic process). Mutually, electrolyte-water interactions are formed in the electrolyte-rich phase and CAP-polymer interactions are formed in the polymer-rich phase (exothermic processes). Thus, the $\Delta_{tr}H^{\theta}$ values are negative because to form interactions more energy is released than the energy expended to break interactions. In TLL closer 40% (m/m), the $\Delta_{tr}H^{\theta}$ values were (-46.36±1.46) and (-43.86±1.49) kJ mol^{-1} for ATPS composed by $C_6H_5O_7^{-3}$ and SO_4^{-2}, respectively. The $\Delta_{tr}H^{\theta}$ value showed that the interaction of CAP with components of the polymer-rich phase in the ATPS composed by the $C_6H_5O_7^{-3}$ anion is more enthalpically favorable, releasing more energy in relation to other system. The $T\Delta_{tr}S^{o}$ values for both anions were $C_6H_5O_7^{-3}$, $T\Delta_{tr}S^{\theta}$ = (-39.96±0.22) kJ mol^{-1}, and SO_4^{-2}, $T\Delta_{tr}S^{\theta}$ = (-34.95±0.83) kJ mol^{-1}. This greater entropic loss for ATPS formed by anions $C_6H_5O_7^{-3}$ can be attributed to chemical species as H_2O and citrate ions, which interact and partition with the CAP, from the electrolyte-rich phase (which present higher-number-density) to polymer-rich phase, thus causing its greatest loss configurational entropy. These entropic contributions of chemical species for partition coefficient are important and should be considered. Thus, both

thermodynamic parameters contribute to the CAP transfer process in these ATPS studied.

3.6. Effect of hydrophobicity on the CAP partitioning

The hydrophobic nature of the propylene oxide segments that compose the polymer/copolymer macromolecule contribute to increase the polymer-rich phase hydrophobicity [17]. Since these segments present weak interactions with water molecules in relation to ethylene oxide segments, in this study the influence of polymer hydrophobicity was investigated in the CAP transfer process. Fig. 14 shows the partition coefficient of CAP (Fig. 14a) and $\Delta_{tr}G^{\theta}$ (Fig. 14b) as functions of TLL for ATPS formed by PEO400 + Na_2SO_4 + H_2O and PPO425 + Na_2SO_4 + H_2O, at 298.2 K.

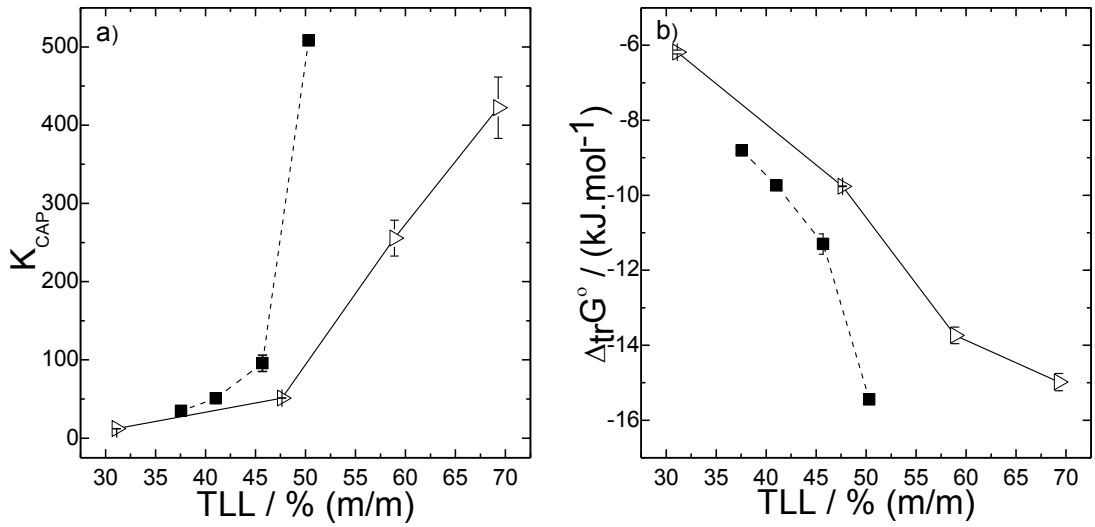

Fig. 14. CAP partition coefficient (a) and $\Delta_{tr}G^{\theta}$ (b) as a function of the tie-line length (TLL), at 298.2 K. ATPS: (■) PEO400 + Na_2SO_4 + H_2O; (▷) PPO425 + Na_2SO_4 + H_2O.

As shown in Fig. 14, the increase in hydrophobicity promotes a small decrease in the CAP partition coefficient to the polymer-rich phase, showing that the hydrophobic interactions present a small effect to the CAP partitioning. The partition coefficients obtained were k = 95±10 and k = 51±0.2 for ATPS PEO400 + Na_2SO_4 + H_2O and PPO425 + Na_2SO_4 + H_2O, respectively, considering TLL of approximately 46% (m/m). The $\Delta_{tr}G^{\theta}$ values were all negative ranging from (-15.45±0.27) to (-6.18±0.05) kJ mol^{-1}. In the ATPS composed by polymers PEO400, $\Delta_{tr}G^{\theta}$ = (-11.30±0.27) kJ mol^{-1}; and PPO425, $\Delta_{tr}G^{\theta}$ = (-9.76±0.01) kJ mol^{-1}. According to this

result, the hydrophobic interactions have a small influence in the CAP partition coefficient. Nevertheless, according to the $\Delta_{tr}G^{\theta}$ values, the CAP interactions with the polymer-rich phase components of the ATPS composed of PEO400 + Na_2SO_4 + H_2O is stronger than interactions with the polymer-rich phase of the components of ATPS formed by PPO425 + Na_2SO_4 + H_2O, confirming the characteristic higher hydrophilicity of these molecules. A less pronounced hydrophobic effect was also reported by Rengifo and coworkers [5] in the study of Chymosin partition. The hydrophobic effect was also analyzed through the transfer thermodynamic parameters $\Delta_{tr}H^{\theta}$ and $T\Delta_{tr}S^{\theta}$. In Fig. 15 $\Delta_{tr}H^{\theta}$ (Fig. 15a) and $T\Delta_{tr}S^{\theta}$ (Fig. 15b) are shown as functions of the TLL in ATPS formed by PEO400 + Na_2SO_4 + H_2O and PPO425 + Na_2SO_4 + H_2O, at 298.2 K.

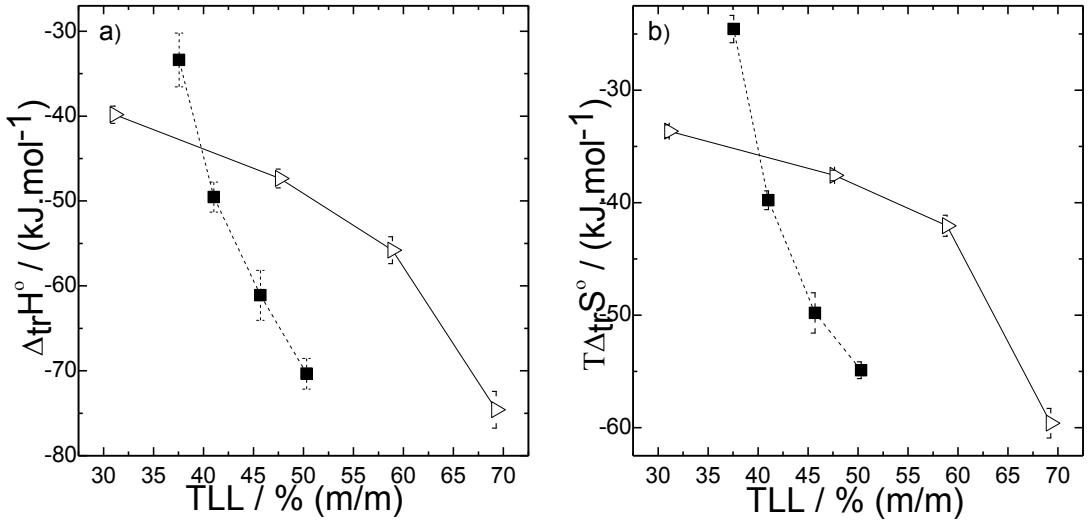

Fig. 15. $\Delta_{tr}H^{\theta}$ (a) and $T\Delta_{tr}S^{\theta}$ (b) as a function of the tie-line length (TLL), at 298.2 K. ATPS: (■) PEO400 + Na_2SO_4 + H_2O; (▷) PPO425 + Na_2SO_4 + H_2O.

The $\Delta_{tr}H^{\theta}$ values range from (-74.59±2.17) to (-33.38±3.17) kJ mol^{-1}, and $T\Delta_{tr}S^{\theta}$ values from (-59.61±1.32) to (-24.58±1.22) kJ mol^{-1}, decreasing with TLL increase for both systems, indicating that the CAP transfer process is enthalpically driven. The $\Delta_{tr}H^{\theta}$ values were more negative for ATPS composed by PEO400, $\Delta_{tr}H^{\theta}$ = (-20.22±1.8) kJ mol^{-1}), than PPO425, $\Delta_{tr}H^{\theta}$ = (-9.82±0.05) kJ mol^{-1}, indicating a higher interaction with the polymer-rich phase of system more hydrophilic. As the electrolyte-rich phase of both ATPS are formed by the same electrolyte, the interactions occurred in this phase are of the same magnitude (electrolyte-water and CAP-electrolyte) being disregarded. Thus, evaluating the

process can be observed that to break PEO-water interactions, more energy is spent than to break PPO-water interactions (endothermic process). Consequently, as the $\Delta_{tr}H^{\theta}$ final balance is negative, the process of CAP-PEO interaction releases more energy than the CAP-PPO exothermic process, showing that CAP-PEO and CAP-PPO are the main interactions associated with the transfer process of CAP in both systems. The $T\Delta_{tr}S^{\theta}$ values follow the same behavior, presenting for PEO400, $T\Delta_{tr}S^{\theta}$ = (-49.80±1.8) kJ mol^{-1} and PPO425, $T\Delta_{tr}S^{\theta}$ = (-37.59±0.46) kJ mol^{-1}. Evaluating theses entropy values and comparing with the liquid-liquid equilibrium data of these systems [29, 30], it was observed that the difference between the water content of the electrolyte-rich phase and polymer-rich phase does not have a relation with the values of entropy. The greater difference in water content is observed in the ATPS formed by PPO425. However this system presented lower entropy decrease, indicating that, besides the configurational entropy, others contributions, such as intermolecular interaction are involved in this process.

4. Conclusion

The study of chloramphenicol partition was realized in different aqueous two-phase systems formed by polymers + electrolytes + water. The transfer thermodynamic parameters ($\Delta_{tr}G^{\theta}$, $\Delta_{tr}H^{\theta}$ and $T\Delta_{tr}S^{\theta}$) were determined and showed the influence of driving forces in chloramphenicol transfer process from the electrolyte-rich phase to the polymer-rich phase. It was observed that solute transfer is exothermic, presenting decrease of system entropy, thus characterizing an enthalpically-driven process, with specific chloramphenicol-polymer interactions. Aqueous two-phase systems parameters such as anion and cation nature, polymer molar mass and polymer hydrophobicity affected the chloramphenicol partition coefficient, showing the viability for the development of advantageous methodologies for the partition/extraction of this antibiotic.

5. References

[1] P.R. Patricio, M.C. Mesquita, L.H.M. da Silva, M.C.H. da Silva, Application of aqueous two-phase systems for the development of a new method of cobalt(II), iron(III) and nickel(II) extraction: A green chemistry approach, J. Hazard. Mater., 193 (2011) 311.

[2] J.M. de Alvarenga, R.A. Fideles, M.V. da Silva, G.F. Murari, J.G. Taylor, L.R. de Lemos, G.D. Rodrigues, A.B. Mageste, Partition study of textile dye Remazol Yellow Gold RNL in aqueous two-phase systems, Fluid Phase Equilib., 391 (2015) 1-8.

[3] Y.P. Jimenez, H.R. Galleguillos, M. Claros, Liquid-liquid partition of perchlorate ion in the aqueous two-phase system formed by $NaNO_3$ + Poly(ethylene glycol) + H_2O, Fluid Phase Equilib., 421 (2016) 93-103.

[4] M. Mirsiaghi, G. Pazuki, M. Vossoughi, I. Alemzadeh, Partitioning of l-Lysine Monohydrochloride in Aqueous Two-Phase Systems of Poly(ethylene glycol) and Dipotassium Hydrogen Phosphate or Trisodium Citrate 5-Hydrate, J. Chem. Eng. Data, 55 (2010) 3005.

[5] A.F.C. Rengifo, G.M.D. Ferreira, G.M.D. Ferreira, M.C.H. da Silva, J.R. de Paula, A.C.S. Pires, L.H.M. da Silva, Driving forces for chymosin partitioning on the macromolecule-salt aqueous two phase system, Food Bioprod. Process., 100 (2016) 361-371.

[6] W. Zhang, G. Zhang, J. Han, Y. Yan, B. Chen, C. Sheng, Y. Liu, Phase equilibrium and chloramphenicol partitioning in aqueous two-phase system composed of 1-hydroxylhexyl-3-methylimidazolium chloride-salt, J. Mol. Liq., 193 (2014) 226-231.

[7] A. Frerix, M. Schönewald, P. Geilenkirchen, M. Müller, M.R. Kula, J. Hubbuch, Exploitation of the Coil-Globule Plasmid DNA Transition Induced by Small Changes in Temperature, pH Salt, and Poly(ethylene glycol) Compositions for Directed Partitioning in Aqueous Two-Phase Systems, Langmuir, 22 (2006) 4282-4290.

[8] R.C. da Cunha, P.R. Patrício, S.J.R. Vargas, L.H.M.d. Silva, M.C.H. da Silva, Green recovery of mercury from domestic and industrial waste, J. Hazard. Mater., 304 (2016) 417-424.

[9] W. Zhang, Y. Hu, Y. Wang, J. Han, L. Ni, Y. Wu, Liquid-liquid equilibrium of aqueous two-phase systems containing poly(ethylene glycol) of different molecular weights and several ammonium salts at 298.15K, Thermochim. Acta, 560 (2013) 47-54.

[10] G.D. Rodrigues, L.R. de Lemos, L.H.M. da Silva, M.C.H. da Silva, Application of hydrophobic extractant in aqueous two-phase systems for selective extraction of cobalt, nickel and cadmium, J. Chromatogr. A, 1279 (2013) 13-19.

[11] R. Iyyaswami, P. Belur, B. Girish, Vishwanatha, V.H. Nagaraj, Development and Evaluation of PEG-Lithium Citrate Salt Based Aqueous Two Phase System and Its Application in Partitioning of Proteins from Fish Industry Effluent, Sep. Sci. Technol., 474 (2012) 591-598.

[12] M.L. Moody, H.D. Willauer, S.T. Griffin, J.G. Huddleston, R.D. Rogers, Solvent Property Characterization of Poly(ethylene glycol)/Dextran Aqueous Biphasic Systems Using the Free Energy of Transfer of a Methylene Group and a Linear Solvation Energy Relationship, Ind. Eng. Chem. Res., 44 (2005) 3749-3760.

[13] J.C. Quintão, P.R. Patrício, A.C.G. Veloso, R.M.M. de Carvalho, L.H.M. da Silva, M.C. Hespanhol, Liquid-liquid equilibrium of the ternary ammonium salt + poly(propylene glycol) + water system, Fluid Phase Equilib., 442 (2017) 96-103.

[14] A. Paraj, A. Haghtalab, B. Mokhtarani, [1-Ethyl-2,3-dimethyl-imidazolium][ethylsulfate]-based aqueous two phase systems: New experimental data and modeling, Fluid Phase Equilib., 382 (2014) 212-218.

[15] J.X. Xiao, U. Sivars, F. Tjerneld, Phase behavior and protein partitioning in aqueous two-phase systems of cationic-anionic surfactant mixtures, J. Chromatogr. B Biomed. sci. appl., 743 (2000) 327-338.

[16] S. Ahmed, Aqueous two-phase system (ATPS): an overview and advances in its applications, Biol. Proced. Online, 18 (2016) 1-18.

[17] A.B. Mageste, T.D.A. Senra, M.C.H. da Silva, R.C.F. Bonomo, L.H.M. da Silva, Thermodynamics and optimization of norbixin transfer processes in aqueous biphasic systems formed by polymers and organic salts, Sep. Purif. Technol., 98 (2012) 69-77.

[18] G. Reh, D. Spelzini, G. Tubío, G. Picó, B. Farruggia, Partition features and renaturation enhancement of chymosin in aqueous two-phase systems, J. Chromatogr. B, 860 (2007) 98-105.

[19] L.H.M. da Silva, M.C.H. da Silva, J.A. Júnior, J.P. Martins, J.S.R. Coimbra, L.A. Minim, Hydrophobic effect on the partitioning of $[Fe(CN)_5(NO)]^{2-}$ and $[Fe(CN)_6]^{3-}$ anions in aqueous two-phase systems formed by triblock copolymers and phosphate salts, Sep. Purif. Technol., 60 (2008) 103-112.

[20] L.H.M. da Silva, M.C.H. da Silva, K.R. Francisco, M.V.C. Cardoso, L.A. Minim, J.S.R. Coimbra, PEO-$[M(CN)(5)NO]^{(x-)}$ (M = Fe, Mn, or Cr) interaction as a driving force in the partitioning of the pentacyanonitrosylmetallate anion in ATPS: Strong effect of the central atom, J. Phys. Chem. B, 112 (2008) 11669.

[21] L.A.P. Alcântara, I.V. Amaral, R.C.F. Bonomo, L.H.M. da Silva, M.C.H. da Silva, V.P.R. Minim, L.A. Minim, Partitioning of α-lactalbumin and β-lactoglobulin from cheese whey in aqueous two-phase systems containing poly (ethylene glycol) and sodium polyacrylate, Food Bioprod. Process., 92 (2014) 409-415.

[22] D. Spelzini, B. Farruggia, G. Picó, Features of the acid protease partition in aqueous two-phase systems of polyethylene glycol-phosphate: Chymosin and pepsin, J. Chromatogr. B, 821 (2005) 60-66.

[23] I.S.B. do Nascimento, J.S.R. Coimbra, J.P. Martins, L.H.M. da Silva, R.C.F. Bonomo, M.R. Pirozzi, A. Cinquini, Partitioning of glutenin flour of special wheat using aqueous two-phase systems, J. Cereal Sci., 52 (2010) 270-274.

[24] Y. Pei, Y. Zhao, C. Lu, C. Qin, W. Xiao, The Development and Application of WACM, in: Advances in Water Resources and Hydraulic Engineering: Proceedings

of 16th IAHR-APD Congress and 3rd Symposium of IAHR-ISHS, Springer Berlin Heidelberg, Berlin, Heidelberg, 2009, pp. 288-295.

[25] C. He, S. Li, H. Liu, K. Li, F. Liu, Extraction of testosterone and epitestosterone in human urine using aqueous two-phase systems of ionic liquid and salt, J. Chromatogr. A, 1082 (2005) 143-149.

[26] A.B. Mageste, L.R. de Lemos, G.M.D. Ferreira, M.C.H. da Silva, L.H.M. da Silva, R.C.F. Bonomo, L.A. Minim, Aqueous two-phase systems: An efficient, environmentally safe and economically viable method for purification of natural dye carmine, J. Chromatogr. A, 1216 (2009) 7623-7629.

[27] A.M. Ferreira, J.A.P. Coutinho, A.M. Fernandes, M.G. Freire, Complete removal of textile dyes from aqueous media using ionic-liquid-based aqueous two-phase systems, Sep. Purif. Technol., 128 (2014) 58-66.

[28] G.A. Borges, L.P. Silva, J.A. Penido, L.R. de Lemos, A.B. Mageste, G.D. Rodrigues, A method for dye extraction using an aqueous two-phase system: Effect of co-occurrence of contaminants in textile industry wastewater, J. Environ. Manage., 183 (2016) 196-203.

[29] J.P. Martins, J.S.R. Coimbra, F.C. de Oliveira, G. Sanaiotti, C.A.S. da Silva, L.H.M. da Silva, M.C.H. da Silva, Liquid-Liquid Equilibrium of Aqueous Two-Phase System Composed of Poly(ethylene glycol) 400 and Sulfate Salts, J. Chem. Eng. Data, 55 (2010) 1247-1251.

[30] M.T. Zafarani-Moattar, R. Sadeghi, Phase Diagram Data for Several PPG + Salt Aqueous Biphasic Systems at 25 °C, J. Chem. Eng. Data, 50 (2005) 947-950.

[31] J.P. Martins, C.P. Carvalho, L.H.M. da Silva, J.S.R. Coimbra, M.C.H. da Silva, G.D. Rodrigues, L.A. Minim, Liquid-Liquid Equilibria of an Aqueous Two-Phase System Containing Poly(ethylene) Glycol 1500 and Sulfate Salts at Different Temperatures, J. Chem. Eng. Data, 53 (2008) 238-241.

[32] R.M. de Oliveira, J.S.R. Coimbra, L.A. Minim, L.H.M. da Silva, M.P.F. Fontes, Liquid-Liquid Equilibria of Biphasic Systems Composed of Sodium Citrate + Polyethylene(glycol) 1500 or 4000 at Different Temperatures, J. Chem. Eng. Data, 53 (2008) 895-899.

[33] P.R. Patrício, A.B. Mageste, L.R. de Lemos, R.M.M. de Carvalho, L.H.M. da Silva, M.C.H. da Silva, Phase diagram and thermodynamic modeling of PEO + organic salts + H_2O and PPO + organic salts + H_2O aqueous two-phase systems, Fluid Phase Equilib., 305 (2011) 1-8.

[34] A. Leo, C. Hansch, D. Elkins, Partition coefficients and their uses, Chem. Rev., 71 (1971) 525-616.

[35] F.C. de Oliveira, J.S.R. Coimbra, L.H.M. da Silva, E.E.G. Rojas, M.C.H. da Silva, Ovomucoid partitioning in aqueous two-phase systems, Biochem. Eng. J., 47 (2009) 55-60.

[36] L.R. de Lemos, I.J.B. Santos, G.D. Rodrigues, G.M.D. Ferreira, L.H.M. da Silva, M.C.H. da Silva, R.M.M. de Carvalho, Phase Compositions of Aqueous Two-Phase Systems Formed by L35 and Salts at Different Temperatures, J. Chem. Eng. Data, 55 (2010) 1193-1199.

[37] J. Han, Y. Wang, C.L. Yu, Y.S. Yan, X.Q. Xie, Extraction and determination of chloramphenicol in feed water, milk, and honey samples using an ionic liquid/sodium citrate aqueous two-phase system coupled with high-performance liquid chromatography, Anal. Bioanal. Chem., 399 (2011) 1295-1304.

[38] J. Han, Y. Wang, C. Chen, W. Kang, Y. Liu, K. Xu, L. Ni, (Liquid+liquid) equilibria and extraction capacity of (imidazolium ionic liquids+potassium tartrate) aqueous two-phase systems, J. Mol. Liq., 193 (2014) 23-28.

[39] H.-O. Johansson, G. Karlström, F. Tjerneld, C.A. Haynes, Driving forces for phase separation and partitioning in aqueous two-phase systems, J. Chromatogr. B: Biomed. Sci. Appl., 711 (1998) 3-17.

[40] G.F. Murari, J.A. Penido, H.M. da Silva, B.E.L. Baêta, S.F. de Aquino, L.R. de Lemos, G.D. Rodrigues, A.B. Mageste, Use of aqueous two-phase PEG-salt systems for the removal of anionic surfactant from effluents, J. Environ. Manage., 198 (2017) 43-49.

[41] L.H.M. da Silva, M.C.H. da Silva, R.A.N. de Aquino, K.R. Francisco, M.V.C. Cardoso, L.A. Minim, J.S.R. Coimbra, Nitroprusside-PEO Enthalpic Interaction as a Driving Force for Partitioning of the $[Fe(CN)_5NO]^{2-}$ Anion in Aqueous Two-Phase Systems Formed by Poly(ethylene oxide) and Sulfate Salts, J. Phys. Chem. B, 110 (2006) 23540-23546.

[42] S.G. Ingebrigtsen, A. Didriksen, M. Johannessen, N. Škalko-Basnet, A.M. Holsæter, Old drug, new wrapping - A possible comeback for chloramphenicol?, Int. J. Pharm., 526 (2017) 538-546.

[43] F. Bottari, K. De Wael, Electrodeposition of gold nanoparticles on boron doped diamond electrodes for the enhanced reduction of small organic molecules, J. Electroanal. Chem., 801 (2017) 521-526.

[44] M.B. Ahmed, J.L. Zhou, H.H. Ngo, W. Guo, M.A.H. Johir, K. Sornalingam, M. Sahedur Rahman, Chloramphenicol interaction with functionalized biochar in water: sorptive mechanism, molecular imprinting effect and repeatable application, Sci.Total Environ., 609 (2017) 885-895.

[45] G. Khayati, S. Alizadeh, Extraction of lipase from Rhodotorula glutinis fermentation culture by aqueous two-phase partitioning, Fluid Phase Equilib., 353 (2013) 132-134.

[46] P.-Å. Albertsson, A. Cajarville, D.E. Brooks, F. Tjerneld, Partition of proteins in aqueous polymer two-phase systems and the effect of molecular weight of the polymer, Biochim. Biophys Acta - General Subjects, 926 (1987) 87-93.

[47] G. Khayati, M. Anvari, N. Shahidi, Partitioning of β-galactosidase in aqueous two-phase systems containing polyethyleneglycol and phosphate salts, Fluid Phase Equilib., 385 (2015) 147-152.

[48] L.H. Haraguchi, R.S. Mohamed, W. Loh, P.A.P. Filho, Phase equilibrium and insulin partitioning in aqueous two-phase systems containing block copolymers and potassium phosphate, Fluid Phase Equilib., 215 (2004) 1-15.

CAPÍTULO 4

In-syringe liquid-liquid microextraction using aqueous two-phase system coupled with UV-Vis spectrophotometry: a simple approach for preconcentration and determination of chloramphenicol in aqueous samples

Abstract

A simple and non-toxic in-syringe method for the extraction, preconcentration and determination of the chloramphenicol antibiotic in water samples, based on aqueous two-phase system coupled with UV-Vis spectrophotometry has been developed. The extraction and preconcentration steps were performed using aqueous two-phase system composed by polymer + electrolyte + water within the 10-mL plastic syringe, which was connected to a syringe pump, for subsequently injection and UV-Vis detection. The proposed method presented satisfactory results with a linear range of 14.1-240 μg kg^{-1} and low limits of detection (4.65 μg kg^{-1}) and quantification (14.1 μg kg^{-1}). The repeatability, expressed as relative standard deviation (RSD), was 10.3% (n=3; 115 μg kg^{-1}). A sampling rate of 12 samples per hour was obtained. The chloramphenicol recovery ranged between 100-114%. The proposed method demonstrated to be simple and environmentally safe, presenting satisfactory results, and has been successfully applied to preconcentration and determination of the chloramphenicol in aqueous samples.

Keywords: In-syringe, preconcentration, aqueous two-phase systems, chloramphenicol, determination

1. Introduction

Water is of essential importance to all living organisms in the performance of their vital activities [1], besides presenting important role in economic and social development of every country. Thus, the preservation of water resources is of great importance. However, several emerging contaminants have been a concern due chemical contamination of surface water and groundwater [1, 2]. Unfortunately, these pollutants can be an increasing threat to our waters resources. Among these contaminants, antibiotics are a concern since they have been widely used in human

medicine and also animal medicine [3, 4], being transported to the environment though municipal, agricultural, and industrial wastewater [5, 6]. Researches have showed that although these compounds present low concentrations in the environment (ng L^{-1} to μg L^{-1}), there are potential ecological risks and also, they can cause adverse effects in human health [7, 8]. An example of pollutant antibiotic is the chloramphenicol (CAP) [9]. CAP (2,2-dichloro-N-((1R,2R)-1,3-dihydroxy-1-(4-nitrophenyl)propan-2-yl)acetamide) is a broad spectrum bacteriostatic antimicrobial isolated from bacterium *Streptomyces venezuelae*, which currently is synthetically produced [10, 11]. It presents effective antibacterial activity in the treatment of diseases, being used since the 1950s as human and veterinary antibiotic [9, 11, 12]. Although efficient, its use is associated with serious harmful side effects on humans, such as, aplastic anemia, hypoplastic anemia, thrombocytopenia, bone marrow depression and gray baby syndrome [10, 11, 13, 14]. Besides that, their residues can cause ecological problems [15, 16] in aquatic environment due its toxicity to determined microorganisms [17]. Nowadays, because of these series of problems presented, its use to human therapeutic is restricted to the treatment of serious infections and ophthalmic infections treatment [9, 10, 18]. However, due to its low cost, effectiveness and easy acquisition, CAP is illegally used in livestock and aquaculture, being able to cause unwanted effects [10, 13, 18]. There are some methods for CAP determination [19-24], including also the chromatographic methods, such as gas [25, 26] and liquid [11, 27-29] chromatography, which are widely used. Pretreatment methods as solid-phase extraction (SPE) [27, 30] and liquid-liquid extraction (LLE) [11, 26] have been used. Though this methods present some limitations such as time consuming desorption step and use of organic solvent, still are steps necessary due complexity of matrix and low concentration of CAP in environment samples [13]. Other pretreatment methods is dispersive liquid-liquid microextraction (DLLME) [31], which also have been used coupled with high performance liquid chromatography (HPLC) to determinate CAP in samples of food.

An attractive alternative to the presented methods are aqueous two-phase system (ATPS) [32]. These systems are formed by mixture of determined compositions of components such as two electrolyte [33], two surfactants [34], two structurally different polymers [35], and polymer and electrolyte [36], with water. ATPS are more environmentally friendly, being mainly composed of water and

present low cost. These systems are a useful technique of pretreatment it has been widely applied to purify, recovery and separate several solutes [37-41].

Despite the advantages, there are only four reported methods for the determination of CAP using ATPS [13, 18, 42, 43]. Jiang et al [13] realized a work with ATPS composed by an ionic liquid 1-butyl-3-methylimidazolium chloride ([C4mim]Cl) and K_2HPO_4, coupled with high-performance liquid chromatography (HPLC) for CAP concentration and determination in meat samples. The obtained detection limit was 0.23 ng g^{-1} and recovery of 94.4 to 107%. Another method was proposed by Yao and Yao [43], which use a magnetic ionic liquid aqueous two-phase system coupled with HPLC to preconcentrate and determine CAP in water environment samples. This method presented detection limit of 0.14 ng mL^{-1}, quantitation limit of 0.42 ng mL^{-1}, and recoveries were range of 94.6 to 99.72%. The method developed by Han et al [18] used ATPS formed by imidazolium ionic liquid and organic salt coupled with HPLC for the determination of CAP in different samples. The proposed method presented broad linear range (2 to 1000 ng mL^{-1}), low limit of detection (0.3 ng mL^{-1}) and limit of quantitation (1.0 ng mL^{-1}), and recoveries between 90.4 and 102.7%. Another study, also proposed by Han et al [42], used an ionic liquid aqueous two-phase system with solvent sublation coupled HPLC for CAP analysis. This method presented a linear range of 0.5 to 500 ng mL^{-1}, limit of detection of 0.1 ng mL^{-1} and limit of quantitation of 0.3 ng mL^{-1}. The CAP recoveries were between 97.1 and 101.9%. Though the reported methods present good merit figures, they also have some shortcomings as high cost of ionic liquid, high instrumental cost and laborious methodologies.

Thus, due to scarcity of methods for CAP pretreatment and determination using ATPS, and also for the shortcomings above mentioned, the development of methodologies for preconcentration, extraction and determination of CAP (trace level) in aqueous media is highly important due to the potential risks this solute for environmental [15, 16] and human health [9]. Moreover, simple methodology using ATPS formed by polymers and electrolytes have benefits such as low cost, environmentally safe and easy handling [44, 45].

Based on that, the goal of this work is to propose an in-syringe method using ATPS formed by polymer + electrolyte + water, coupled with in-flow UV-Vis detection for the extraction, preconcentration and determination of the CAP antibiotic in aqueous media.

2. Experimental

2.1. Reagents

The polymer poly(ethylene oxide) (PEO) of molar mass 1500 mol g^{-1} was purchased from Synth (São Paulo, Brazil), with purity of 100%. The magnesium sulfate ($MgSO_4.H_2O$; 98.0%) electrolyte was obtained from Dinâmica (Diadema, Brazil). The polymer and electrolyte were analytical-grade and used without further purification. Chloramphenicol (≥98.0%) was obtained from Aldrich (St. Louis, USA). Deionized water (Millipore Corp., Molsheim, France) was used for preparing the aqueous solutions.

2.2. Apparatus

A syringe pump (NE-1000, New Era Pump Systems, Inc., Farmingdale, USA) coupled with 10-mL plastic syringe was used as fluid propulsion unit. The software (OOIBASE32 spectrometer operating software version 2.0.6.5, Ocean Optics, Dunedin, USA) was used for data acquisition and processing. A spectrophotometer (USB 2000 CCD, Ocean Optics, Dunedin, USA) was coupled to a Z-type 1 cm optical-path flow cell and a UV-Vis radiation source composed of deuterium and halogen lamps (DH-2000-BAL, Ocean Optics, Dunedin, USA), which was transported to the flow cell by means an optical fiber. The data treatment was realized through Origin Pro 8.0 software. Fig. 1 shows the scheme of experimental apparatus of the proposed method.

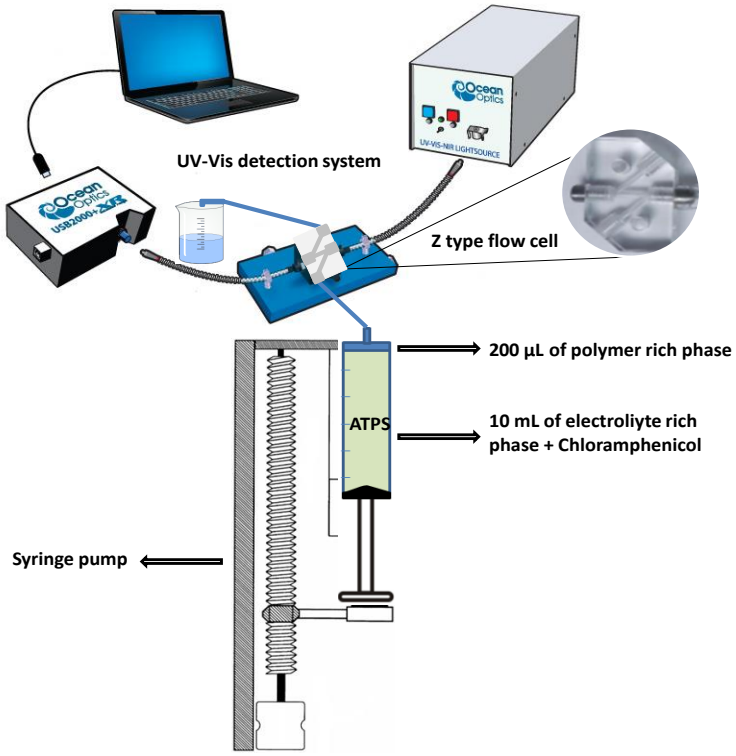

Fig. 1. Experimental scheme of LLME in-syringe using ATPS coupled with in-flow UV-Vis detection.

2.3. ATPS preparation

Solutions with specific concentrations of polymer and electrolyte were prepared and added in tubes of 50 mL according with desired ATPS overall composition. The ATPS overall composition was obtained from equilibrium liquid-liquid data from literature [46]. The ATPS used in this study is composed by PEO1500 + $MgSO_4$ + H_2O. This ATPS was prepared in the tie-line length (TLL) ≅ 52 % (m/m). The tube containing the solutions was manually stirred and left to 25 ^oC, in a temperature-controlled bath (MQBTC 99-20, Microquimica, Palhoça, Brazil) for at least 12 h.

2.4. ATPS preparation in-syringe

It was prepared aqueous solution of CAP in the concentration of 600 mg kg^{-1}. Aliquot of this solution was diluted in certain amount of electrolyte-rich phase in order to obtain the desired stock solution of CAP. Using this stock solution, working solutions were prepared at desired concentrations, being also diluted in electrolyte-rich phase. 10 ml of each solution was sucked in 10-mL plastic syringe (extraction unit), and after that, was injected 200 µL of polymer-rich phase by means of a micropipette into the syringe (which contained electrolyte-rich phase and CAP).

Each syringe was sealed with Teflon and a needle. For extraction, the mixture was vigorously stirred for 3 minutes. After 12 minutes, the separation of the two phases was achieved. The plunger of the syringe was leisurely moved and the polymer-rich phase containing the analyte was fitted onto the tip of the syringe for injection. This procedure was performed for both, the standards and the samples.

2.5. In-syringe flow procedure

The 10-mL plastic syringes containing standard or sample were coupled one at a time to the syringe pump and flow cell. Prior to the injection of the sample zone, the flow cell was always kept filled with polymer-rich phase. Then, the sample zone was injected toward the flow cell, with a flow rate of 70 μL min^{-1} for subsequent spectrophotometric detection at 276 nm. After that, the washing of flow cell was performed with 30 mL of water and dried with air pumping. The residue resultant of injection was directly discharge to waste. The remaining residue of each syringe was dispensed from the syringe to waste. The obtained analytical signals were straight lines, being the average of the signals considered for data treatment.

3. Results and discussion

3.1. Evaluation of In-syringe method performance

Some analytical parameters such as linear range, limit of detection (LOD), limit of quantification (LOQ), repeatability and recovery were studied. As previously mentioned, the ATPS used in this study is composed by PEO1500 + $MgSO_4$ + H_2O in the TLL ≅ 52 % (m/m). Some tests were also performed using PEO1500 + Li_2SO_4 + H_2O ATPS in the TLL ≅ 52 % (m/m), but unsuccessful due to some experimental limitations, such as crystallization of the electrolyte at the tip of the syringe and difficulty in reproducing the results.

Figure 2 shows the in-flow analytical signal obtained for each concentration of standard.

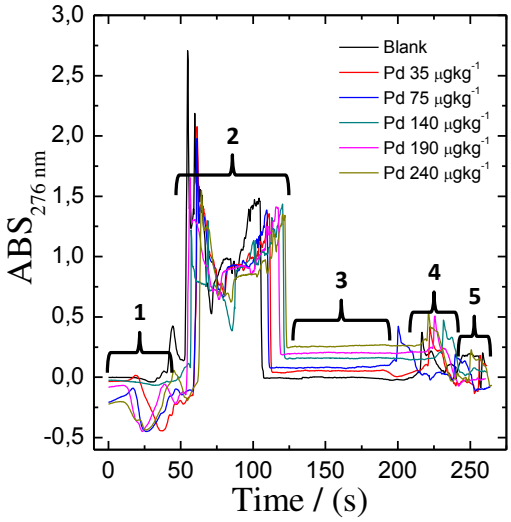

Fig. 2. In-flow analytical signal of standards.

As can be seen, the analytical signal present five distinct parts. The first part (number 1 in figure) corresponds to baseline, the second part (number 2 in figure) corresponds to an air bubble which filled the tip of the syringe to separate the polymer-rich phase which was inside the syringe and contained the analyte, from the polymer-rich phase which was held inside the flow cell to zero the equipment. The third part (number 3 in figure), corresponding to the straight line, is the signal of the chloramphenicol in polymer-rich phase, which is the part of interest, being the mean value this signal, in the same time interval used for quantification. The fourth part (number 4 in figure), characterized by an elevation, occur due to the change of medium, indicating the presence of the electrolyte-rich phase in the flow cell (and detector). Finally the fifth part (number 5 in figure) shows the signal decreases to zero due to the absence of the chloramphenicol at this phase, thus returning to baseline.

Figure 3 shows the spectrum obtained for each concentration of standard with a wavelength (λ) maximum at 276 nm.

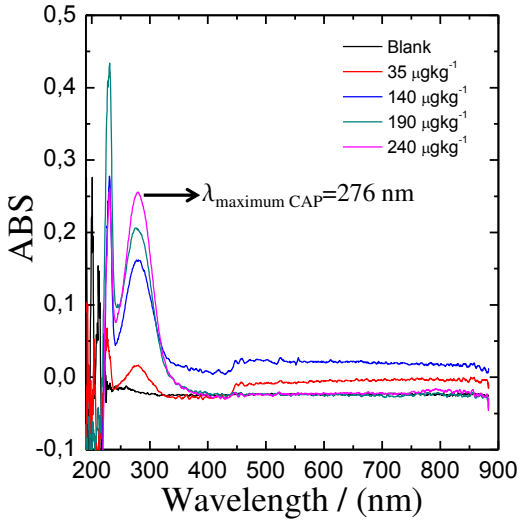

Fig. 3. Spectrum of standards.

The spectra are in agreement with reported data in the literature [47-49], with a small variation in the maximum absorption wavelengths, and can be attributed to the transitions of N=O group ($\pi \rightarrow \pi^*$) and also the transitions of nitrophenil ($\pi \rightarrow \pi^*$) [47].

The analytical curve obtained presented linear range of 35.0-240 μg kg^{-1}. The curve was described by the equation ABS = 0.00105[CAP] + 0.005575, showing a good linearity with a good correlation coefficient of 0.994, where ABS corresponds the CAP absorbance at 276 nm and [CAP] express the chloramphenicol concentration in μg kg^{-1}. The LOD of method presented the value of 4.65 μg kg^{-1} (calculated as 3.3 times the standard deviation of the blank signals divided by the slope of the calibration curve). The LOQ was of 14.1 μg kg^{-1} (calculated as 10 times the standard deviation of the blank signals divided by the slope of the calibration curve). Other methods reported in the literature [42, 43] present LOD and LOQ lower than the proposed method. However these limits are reached due to the use of instruments more sensitive and of higher cost, as also due a higher pre-concentration factor. Nevertheless these results show a good sensitivity of the proposed method. The relative standard deviation (RSD) calculated was acceptable, with value of 10.3%, which was obtained of triplicate analysis of CAP in the concentration of 115 μg kg^{-1}. These results are summarized in the Table 1.

Table 1. Analytical figures of merit of In-syringe method for CAP determination.

Analyte	Linear range / (µg kg^{-1})	R^2	RSD / (%) (n=3)	LOD / (µg kg^{-1})	LOQ / (µg kg^{-1})
CAP	14.1-240	0.994	10.3	4.65	14.1

Figure 4 shows: (4a) the in-flow analytical signal obtained for each concentration of sample; (4b) the spectrum obtained for each concentration of sample with a maximum wavelength at 276 nm.

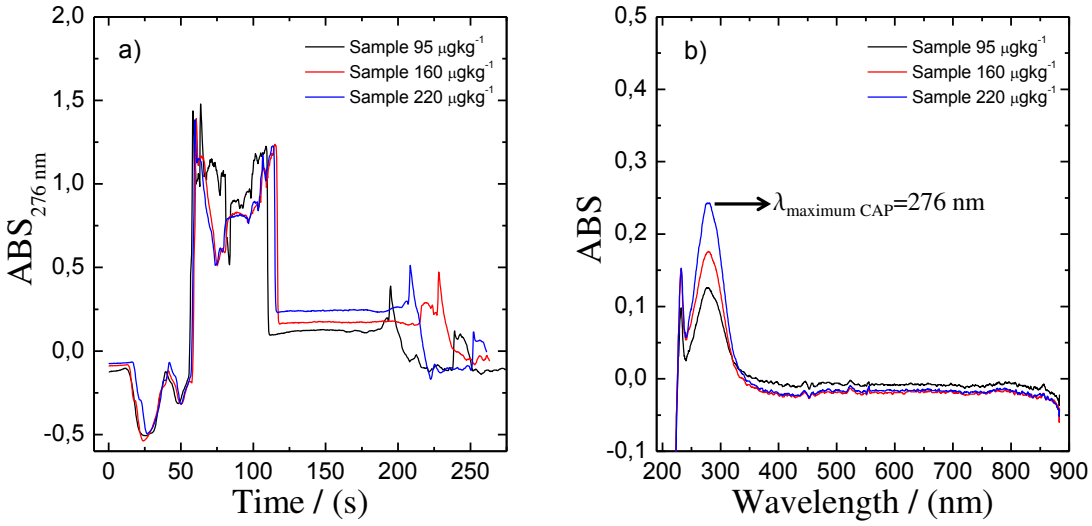

Fig. 4. Determination of CAP: a) In flow analytical signal of samples, b) Spectrum of samples.

The results of chloramphenicol determination in spiked deionized water sample are presented in Table 2.

Table 2. Results of chloramphenicol determination in spiked deionized water sample.

Samples	Concentration added / (µgkg^{-1})	Concentration determined / (µgkg^{-1})	Recovery / (%)	Relative error / (%)
Dz-A	95.9	110	114	14.7
Dz-B	159	159	100	0
Dz-C	220	226	103	2.73

According to Table 2 the chloramphenicol recovery presented values ranging from 100 to 114%, with a relative error ranging from 0 to 14.7%. Besides that, this method presented a short time of analysis (4 minutes per sample), with a sampling rate estimated at 12 determinations per hour. Consume of the sample and reagent was

low, and small residue quantity was generating (about 40 mL per sample) including the washing step.

As previously mentioned, most methods use chromatographic techniques for CAP determination, being HPLC the most used. Due to the complexity of the matrices, in most studies, complicated pretreatments are required involving the use of toxic solvents. Therefore, a simpler, cheaper and environmentally friendly alternative was presented through the present method. In addition, the method uses as UV-Vis spectrophotometry detection system. The table 3 shows some characteristics of the methods reported in the literature and the proposed method.

Table 3. Comparison of some methods for CAP determination.

Detection technique	Organic solvent	Prior procedure / time /s	LOD	LOQ	Linear range	Reference
HPLC - UV-Vis	None	60	0.14 (ng mL^{-1})	0.42 (ng mL^{-1})	12.25-2200 (ng mL^{-1})	[43]
HPLC - ESI-MS/MS	Acetonitrile, ethyl acetate, hexane, methanol	NS[a]	NS[a]	NS[a]	NS[a]	[11]
HPLC - ESI-MS/MS	Ethyl acetate, diethyl ether, methanol, acetone, hexane, toluene	>780	NS[a]	NS[a]	NS[a]	[14]
HPLC - UV-Vis	None	600-900	0.1 (ng mL^{-1})	0.3 (ng mL^{-1})	0.5-500 (ng mL^{-1})	[42]
HPLC - UV-Vis	Trichloroacetic acid	9300	0.23 (ng g^{-1})	0.77 (ng g^{-1})	NS[a]	[13]
HPLC – UV	Trichloroacetic acid	600-900	0.3 (ng mL^{-1})	1.0 (ng mL^{-1})	2-1000 (ng mL^{-1})	[18]
ELISA HPLC-MS/MS	Ethyl acetate, n-hexane, methanol iso-octane/ chloroform,	>1500	NS[a]	NS[a]	NS[a]	[20]
Voltammetry	Methanol	NS[a]	4.3 (µg L^{-1})	NS[a]	9.7-3200 (µg L^{-1})	[23]
GC-MS LC-MS/MS	Ethyl acetate, n-hexane, methanol	>720	NS[a]	NS[a]	NS[a]	[25]
UV-Vis	None	900	4.65 (µg kg^{-1})	14.1 (µg kg^{-1})	14.1-240 (µg kg^{-1})	Propose method

[a]not specified

It can be observed that the proposed method does not use organic solvent as the majority of presented methods, and also uses a cheaper detection technique. Besides, it presents good figures of merit and the time of preparation of the sample is comparable with most reported methods.

Thus, the development of methodologies that encompass simplicity and reliability, associated with low cost and small residue generation is of great importance in relation to environmental, economic and scientific aspects. The

proposed method attained promising and satisfactory results, presenting potential for extraction, preconcentration and determination of chloramphenicol in aqueous samples.

4. Conclusion

An in-syringe liquid-liquid microextraction method using aqueous two-phase system coupled with UV-Vis spectrophotometric detection has been developed for the extraction, preconcentration, and determination of chloramphenicol in water samples. The proposed method used a 10-mL plastic syringe as unit for extraction of chloramphenicol, and it showed some advantages as low instrumental cost and simple operation, besides using ATPS formed by PEO + $MgSO_4$ + H_2O, which presents quick phase separation and is more environmentally safe. Good sampling rate, low reagent consumption and little waste generation were obtained. The method presented satisfactory recovery and repeatability, wide linear range, and low limits of detection and quantification. This study showed that the proposed in-syringe method using ATPS coupled with UV-Vis detection presented a great potential to be used in determination of CAP in aqueous samples.

5. References

[1] M.O. Barbosa, N.F.F. Moreira, A.R. Robeiro, M.F.R. Pereira, A.M.T. Silva, Occurrence and removal of organic micropollutants: An overview of the watch list of EU Decision 2015/495, Water Res., (2016).

[2] Y. Cabeza, L. Candela, D. Ronen, G. Teijon, Monitoring the occurrence of emerging contaminants in treated wastewater and groundwater between 2008 and 2010. The Baix Llobregat (Barcelona, Spain), J. Hazard. Mater., 239-240 (2012) 32-39.

[3] H. Liu, G. Zhang, C.-Q. Liu, L. Li, M. Xiang, The occurrence of chloramphenicol and tetracyclines in municipal sewage and the Nanming River, Guiyang City, China, J. Environ. Monit., 11 (2009) 1199-1205.

[4] F. Tamtam, F. Mercier, B. Le Bot, J. Eurin, Q. Tuc Dinh, M. Clément, M. Chevreuil, Occurrence and fate of antibiotics in the Seine River in various hydrological conditions, Sci. Total Environ., 393 (2008) 84-95.

[5] I.T. Carvalho, L. Santos, Antibiotics in the aquatic environments: A review of the European scenario, Environ. Int., 94 (2016) 736-757.

[6] K. Kummerer, Antibiotics in the aquatic environment-a review-part I, Chemosphere, 75 (2009) 417-434.

[7] M.D. Celiz, J. Tso, D.S. Aga, Pharmaceutical metabolites in the environment: Analytical challenges and ecological risks, Environ. Toxicol. Chem., 28 (2009) 2473-2484.

[8] Z.N. Norvill, A. Shilton, B. Guieysse, Emerging contaminant degradation and removal in algal wastewater treatment ponds: Identifying the research gaps, J. Hazard. Mater., 313 (2016) 291-309.

[9] J.C. Hanekamp, A. Bast, Antibiotics exposure and health risks: Chloramphenicol, Environ. Toxicol. Pharmacol., 39 (2015) 213-220.

[10] L.R. Guidi, P.A.S. Tette, C. Fernandes, L.H.M. Silva, M.B.A. Gloria, Advances on the chromatographic determination of amphenicols in food, Talanta, 162 (2017) 324-338.

[11] H.T. Rønning, K. Einarsen, T.N. Asp, Determination of chloramphenicol residues in meat, seafood, egg, honey, milk, plasma and urine with liquid chromatography-tandem mass spectrometry, and the validation of the method based on 2002/657/EC, J. Chromatogr. A, 1118 (2006) 226-233.

[12] L.R. Guidi, L.H. Silva, C. Fernandes, N.J. Engeseth, M.B.A. Gloria, LC-MS/MS determination of chloramphenicol in food of animal origin in Brazil, Scientia Chromatographica, 7 (2015) 287-295.

[13] L. Wang, Extraction and Determination of Chloramphenicol in Meat Using 1-Butyl-3-methylimidazolium Chloride-K_2HPO_4 Aqueous Two-Phase System Coupled with HPLC, Asian J. Chem., 25 (2013) 8579-8583.

[14] P. Mottier, V. Parisod, E. Gremaud, P.A. Guy, R.H. Stadler, Determination of the antibiotic chloramphenicol in meat and seafood products by liquid chromatography-electrospray ionization tandem mass spectrometry, J. Chromatogr. A, 994 (2003) 75-84.

[15] B.E. Erickson, Analyzing the Ignored Environmental Contaminants, Environ. Sci.Technol., 36 (2002) 140A-145A.

[16] C.G. Daughton, Non-regulated water contaminants: emerging research, Impact Assess. Rev., 24 (2004) 711-732.

[17] L. Wollenberger, B. Halling-Sørensen, K.O. Kusk, Acute and chronic toxicity of veterinary antibiotics to Daphnia magna, Chemosphere, 40 (2000) 723-730.

[18] J. Han, Y. Wang, C.L. Yu, Y.S. Yan, X.Q. Xie, Extraction and determination of chloramphenicol in feed water, milk, and honey samples using an ionic liquid/sodium citrate aqueous two-phase system coupled with high-performance liquid chromatography, Anal. Bioanal. Chem., 399 (2011) 1295-1304.

[19] R.J. Shakila, R. Saravanakumar, S.A.P. Vyla, G. Jeyasekaran, An improved microbial assay for the detection of chloramphenicol residues in shrimp tissues, Innov. Food Sci. Emerg. Technol., 8 (2007) 515-518.

[20] G. Biancotto, L. Contiero, C. Benetti, M. Calligaris, E. Tibaldi, L. Cerni, M. Francese, Depletion of chloramphenicol in trout after a hypothetic therapeutic treatment, Anal. Chim. Acta, 637 (2009) 173-177.

[21] S. Yamato, H. Sugihara, K. Shimada, An Enzymatic Assay of Chloramphenicol Coupled with Fluorescence Reaction, Chem. Pharm. Bull, 38 (1990) 2290-2292.

[22] P. Kowalski, A. Plenis, I. Oledzka, L. Konieczna, Optimization and validation of the micellar electrokinetic capillary chromatographic method for simultaneous determination of sulfonamide and amphenicol-type drugs in poultry tissue, J. Pharm. Biomed. Anal. , 54 (2011) 160-167.

[23] M.L. Mena, L. Agüí, P. Martinez-Ruiz, P. Yáñez-Sedeño, A.J. Reviejo, J.M. Pingarrón, Molecularly imprinted polymers for on-line clean up and preconcentration of chloramphenicol prior to its voltammetric determination, Anal. Bioanal. Chem., 376 (2003) 18-25.

[24] P. Su, N. Liu, M. Zhu, B. Ning, M. Liu, Z. Yang, X. Pan, Z. Gao, Simultaneous detection of five antibiotics in milk by high-throughput suspension array technology, Talanta, 85 (2011) 1160-1165.

[25] L. Santos, J. Barbosa, M.C. Castilho, F. Ramos, C. Ribeiro, M.I.N. da Silveira, Determination of chloramphenicol residues in rainbow trouts by gas chromatography-mass spectometry and liquid chromatography-tandem mass spectometry, Anal. Chim. Acta, 529 (2005) 249-256.

[26] S. Ding, J. Shen, S. Zhang, H. Jiang, Z. Sun, Determination of chloramphenicol residue in fish and shrimp tissues by gas chromatography with a microcell electron capture detector, J. AOAC Int. , 88 (2005) 57-60.

[27] J. Wu, L. Chen, P. Mao, Y. Lu, H. Wang, Determination of chloramphenicol in aquatic products by graphene-based SPE coupled with HPLC-MS/MS, J. Sep. Sci., 35 (2012) 3586-3592.

[28] T. Taka, M. C Baras, Z. F Chaudhry Bet, Validation of a rapid and sensitive routine method for determination of chloramphenicol in honey by LC-MS/MS, Food Addit. Contam. Part A 29 (2011) 596-601.

[29] R.S. Nicolich, E. Werneck-Barroso, M.A.S. Marques, Food safety evaluation: Detection and confirmation of chloramphenicol in milk by high performance liquid chromatography-tandem mass spectrometry, Anal. Chim. Acta, 565 (2006) 97-102.

[30] R. Sheridan, B. Policastro, S. Thomas, D. Rice, Analysis and Occurrence of 14 Sulfonamide Antibacterials and Chloramphenicol in Honey by Solid-Phase Extraction Followed by LC/MS/MS Analysis, J. Agric. Food Chem., 56 (2008) 3509-3516.

[31] H. Chen, H. Chen, J. Ying, J. Huang, L. Liao, Dispersive liquid–liquid microextraction followed by high-performance liquid chromatography as an efficient and sensitive technique for simultaneous determination of chloramphenicol and thiamphenicol in honey, Anal. Chim. Acta, 632 (2009) 80-85.

[32] S. Ahmed, Aqueous two-phase system (ATPS): an overview and advances in its applications, Biol. Proced. Online, 18 (2016) 1-18.

[33] J. Han, Y. Wang, C. Chen, W. Kang, Y. Liu, K. Xu, L. Ni, (Liquid+liquid) equilibria and extraction capacity of (imidazolium ionic liquids+potassium tartrate) aqueous two-phase systems, J. Mol. Liq., 193 (2014) 23-28.

[34] G.-X. Zhao, J.-X. Xiao, Aqueous Two-Phase Systems of the Aqueous Mixtures of Cationic-Anionic Surfactants, J. Colloid Interface Sci. , 177 (1996) 513-518.

[35] S. Sturesson, F. Tjerneld, G. Johansson, Partition of macromolecules and cell particles in aqueous two-phase systems based on hydroxypropyl starch and PEG, Appl. Biochem. Biotechnol., 26 (1991) 281-295.

[36] J.C. Quintão, P.R. Patrício, A.C.G. Veloso, R.M.M. de Carvalho, L.H.M. da Silva, M.C. Hespanhol, Liquid-liquid equilibrium of the ternary ammonium salt + poly(propylene glycol) + water system, Fluid Phase Equilib., 442 (2017) 96-103.

[37] P.R. Patrício, R.C. Cunha, S.J. Rodriguez Vargas, Y.L. Coelho, L.H. Mendes da Silva, M.C. Hespanhol da Silva, Chromium speciation using aqueous biphasic systems: Development and mechanistic aspects, Sep. Purif. Technol., 158 (2016) 144-154.

[38] G.F. Murari, J.A. Penido, H.M. da Silva, B.E.L. Baêta, S.F. de Aquino, L.R. de Lemos, G.D. Rodrigues, A.B. Mageste, Use of aqueous two-phase PEG-salt systems for the removal of anionic surfactant from effluents, J. Environ. Manage., 198 (2017) 43-49.

[39] R.C. da Cunha, P.R. Patrício, S.J.R. Vargas, L.H.M.d. Silva, M.C.H. da Silva, Green recovery of mercury from domestic and industrial waste, J. Hazard. Mater., 304 (2016) 417-424.

[40] J.M. de Alvarenga, R.A. Fideles, M.V. da Silva, G.F. Murari, J.G. Taylor, L.R. de Lemos, G.D. Rodrigues, A.B. Mageste, Partition study of textile dye Remazol Yellow Gold RNL in aqueous two-phase systems, Fluid Phase Equilib., 391 (2015) 1-8.

[41] F.C. de Oliveira, J.S.R. Coimbra, L.H.M. da Silva, E.E.G. Rojas, M.C.H. da Silva, Ovomucoid partitioning in aqueous two-phase systems, Biochem. Eng. J., 47 (2009) 55-60.

[42] J. Han, Y. Wang, C. Yu, C. Li, Y. Yan, Y. Liu, L. Wang, Separation, concentration and determination of chloramphenicol in environment and food using an ionic liquid/salt aqueous two-phase flotation system coupled with high-performance liquid chromatography, Anal. Chim. Acta, 685 (2011) 138-145.

[43] T. Yao, S. Yao, Magnetic ionic liquid aqueous two-phase system coupled with high performance liquid chromatography: A rapid approach for determination of chloramphenicol in water environment, J. Chromatogr. A, 1481 (2017) 12-22.

[44] W. Zhang, Y. Hu, Y. Wang, J. Han, L. Ni, Y. Wu, Liquid-liquid equilibrium of aqueous two-phase systems containing poly(ethylene glycol) of different molecular weights and several ammonium salts at 298.15K, Thermochim. Acta, 560 (2013) 47-54.

[45] G.D. Rodrigues, L.R. de Lemos, L.H.M. da Silva, M.C.H. da Silva, Application of hydrophobic extractant in aqueous two-phase systems for selective extraction of cobalt, nickel and cadmium, J. Chromatogr. A, 1279 (2013) 13-19.

[46] J.P. Martins, C.P. Carvalho, L.H.M. da Silva, J.S.R. Coimbra, M.C.H. da Silva, G.D. Rodrigues, L.A. Minim, Liquid-Liquid Equilibria of an Aqueous Two-Phase System Containing Poly(ethylene) Glycol 1500 and Sulfate Salts at Different Temperatures, J. Chem. Eng. Data, 53 (2008) 238-241.

[47] J.-H. Shi, Y.-f. Zhou, Inclusion interaction of chloramphenicol and heptakis (2,6-di-O-methyl)-β-cyclodextrin: Phase solubility and spectroscopic methods, Spectrochim. Acta A Mol. Biomol. Spectrosc., 83 (2011) 570-574.

[48] M. Shamim Ahmed, S. Rajia, M. Rahman, M.A.U. Islam, Potency and Antibacterial Efficacy of Degraded Chloramphenicol in Marketed Eye Drop Preparations, Bangladesh Pharmaceutical Journal, 16 (2013) 165-169.

[49] A. Zuorro, M. Fidaleo, M. Fidaleo, R. Lavecchia, Degradation and antibiotic activity reduction of chloramphenicol in aqueous solution by UV/H_2O_2 process, J. Environ. Manage, 133 (2014) 302-308.

CONSIDERAÇÕES FINAIS

A realização deste trabalho permitiu a obtenção de novos sistemas aquosos bifásicos (SAB), formados por poli(óxido de propileno) + eletrólito orgânico + água ou por poli(óxido de etileno) + eletrólito orgânico + água, contribuindo para o aumento dos dados de equilíbrio líquido-líquido, principalmente para sistemas formados por poli(óxido de propileno), que são escassos na literatura. Um estudo da termodinâmica de partição do antibiótico cloranfenicol em diferentes SAB formados por polímero + eletrólito + água foi realizado. Através da obtenção dos parâmetros termodinâmicos $\Delta_{tr}G^{\theta}$, $\Delta_{tr}H^{\theta}$ e $T\Delta_{tr}S^{\theta}$ foi possível uma melhor compreensão a respeito das forças motrizes envolvidas neste processo de transferência, contribuindo para o desenvolvimento futuro de metodologias de extração e quantificação deste soluto. Por último foi apresentada uma proposta de análise em fluxo para pré-concentração, extração e quantificação de cloranfenicol utilizando SAB.

O desenvolvimento de todo este trabalho reforça a importância e a vasta aplicabilidade do SAB no desenvolvimento de métodos para extração, purificação e determinação de analitos de interesse alimentício e ambiental, além de possibilitar um conhecimento maior a respeito dos complexos processos envolvidos na formação e partição de soluto nestes sistemas, contribuindo para um avanço em ciências de separação.

APÊNDICE

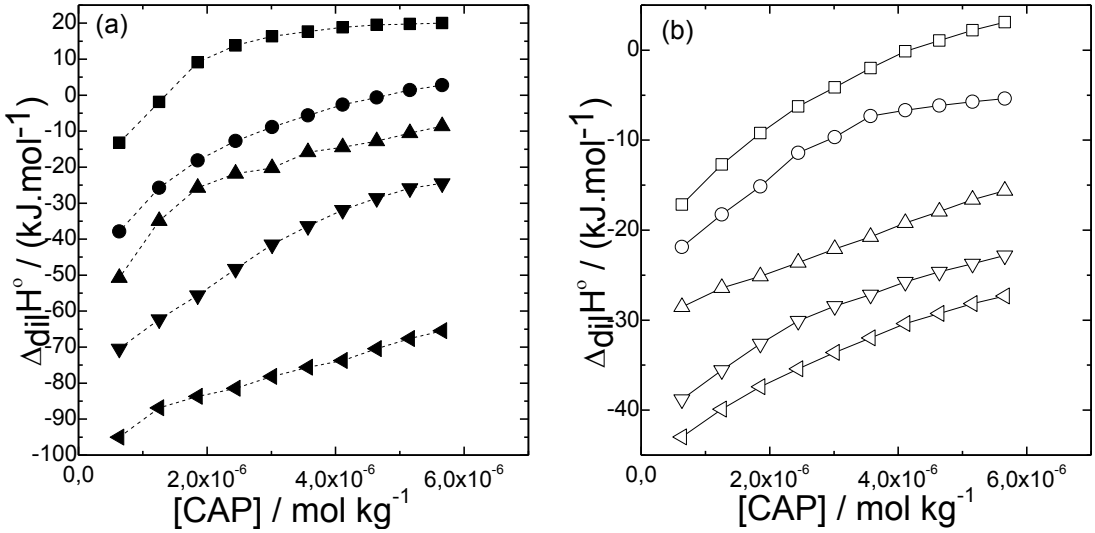

Fig. F1. CAP $\Delta_{dil}H$ value in polymer-rich phase (a) and electrolyte-rich phase (b) for PEO1500 + $MgSO_4$ + H_2O ATPS: (■/□) (≅ 34 %(m/m)) TLL, (●/○) (≅ 40 %(m/m)) TLL, (▲/△) (≅ 44 %(m/m)) TLL, (▼/▽) (≅ 47 %(m/m)) TLL and (◀/◁) (≅ 52 %(m/m)) TLL at 298.15 K.

Table T1. CAP $\Delta_{dil}H^{\theta,\infty}$ values in polymer-rich phase and electrolyte-rich phase, for different TLL of system PEO1500 + $MgSO_4$ + H_2O at 298.15 K.

TLL / (% m/m)	$\Delta_{dil}H^{\theta,\infty}$ / (kJ.mol^{-1}) polymer-rich phase	$\Delta_{dil}H^{\theta,\infty}$ / (kJ.mol^{-1}) electrolyte-rich phase
34	-22,79	-21,42
40	-46,14	-26,94
44	-57,73	-30,16
47	-81,08	-42,14
52	-97,76	-45,88

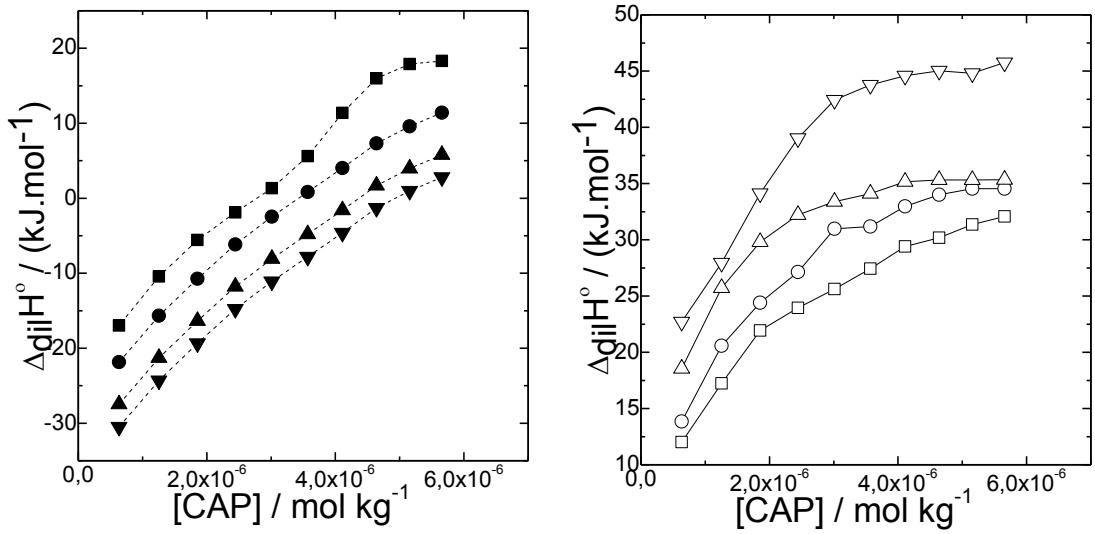

Fig. F2. CAP $\Delta_{dil}H$ value in polymer-rich phase (a) and electrolyte-rich phase (b) for PEO1500 + Na_2SO_4 + H_2O ATPS: (■/□) (≅ 33 %(m/m)) TLL, (●/○) (≅ 36 %(m/m)) TLL, (▲/△) (≅ 40 %(m/m)) TLL, and (▼/▽) (≅ 47 %(m/m)) TLL at 298.15 K.

Table T2. CAP $\Delta_{dil}H^{\theta,\infty}$ values in polymer-rich phase and electrolyte-rich phase, for different TLL of system PEO1500 + Na_2SO_4 + H_2O at 298.15 K.

TLL / (% m/m)	$\Delta_{dil}H^{\theta,\infty}$ / (kJ.mol^{-1}) polymer-rich phase	$\Delta_{dil}H^{\theta,\infty}$ / (kJ.mol^{-1}) electrolyte-rich phase
33	-20,22±2,98	5,27±0,99
36	-28,41±0,58	6,48±1,26
40	-34,04±0,58	9,82±0,91
47	-37,04±1,61	13,08±1,71

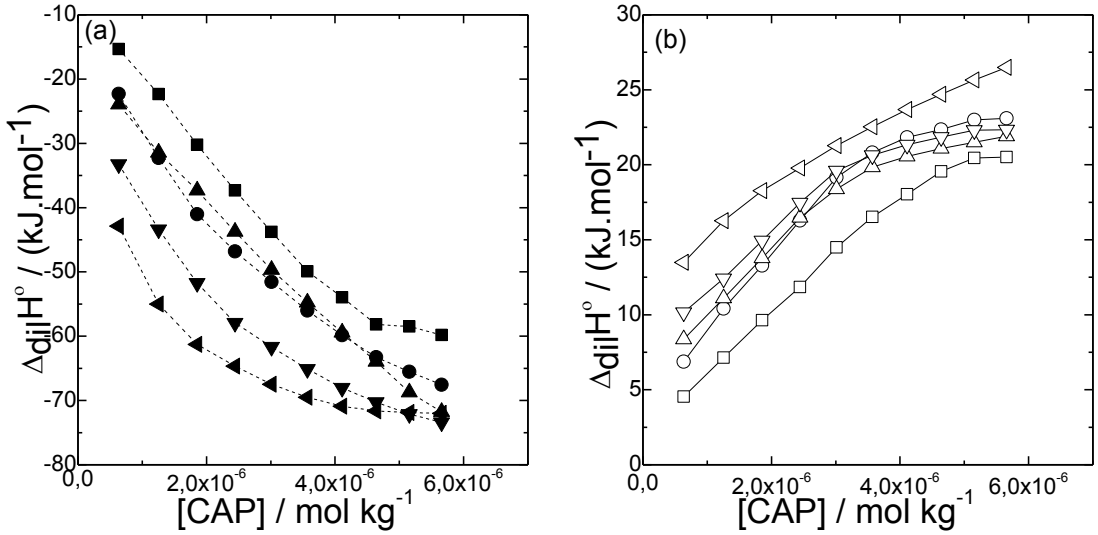

Fig. F3. CAP $\Delta_{dil}H$ value in polymer-rich phase (a) and electrolyte-rich phase (b) for PEO10000 + Li_2SO_4 + H_2O ATPS: (■/□) (≅ 22 %(m/m)) TLL, (●/○) (≅ 26 %(m/m)) TLL, (▲/△) (≅ 31 %(m/m)) TLL, (▼/▽) (≅ 34 %(m/m)) TLL and (◀/◁) (≅ 37 %(m/m)) TLL at 298.15 K.

Table T3. CAP $\Delta_{dil}H^{\theta,\infty}$ values in polymer-rich phase and electrolyte-rich phase, for different TLL of system PEO10000 + Li_2SO_4 + H_2O at 298.15 K.

TLL / (% m/m)	$\Delta_{dil}H^{\theta,\infty}$ / (kJ.mol^{-1}) polymer-rich phase	$\Delta_{dil}H^{\theta,\infty}$ / (kJ.mol^{-1}) electrolyte-rich phase
22	-3,35,±0,02	4,98,±0,02
26	-3,65,±0,02	5,25±0,04
31	-3,82,±0,01	5,58,±0,01
34	-3,94,±0,02	5,88±0,03
37	-4,12,±0,06	6,34,±0,09

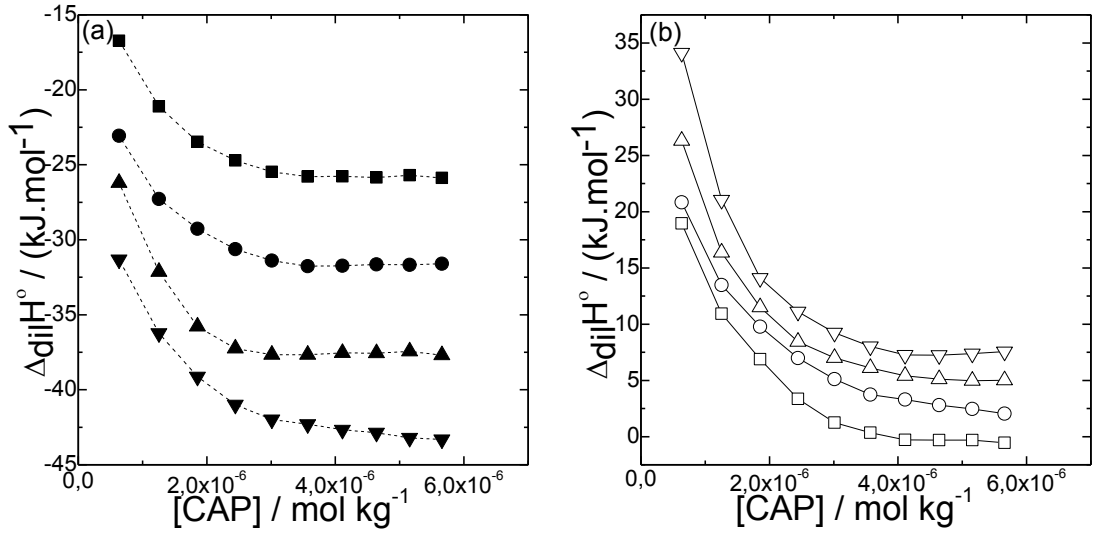

Fig. F4. CAP $\Delta_{dil}H$ value in polymer-rich phase (a) and electrolyte-rich phase (b) for PPO425 + Na_2SO_4 + H_2O ATPS: (■/□) (≅ 31 %(m/m)) TLL, (●/○) (≅ 48 %(m/m)) TLL, (▲/△) (≅ 59 %(m/m)) TLL, and (▼/▽) (≅ 69 %(m/m)) TLL at 298.15 K.

Table T4. CAP $\Delta_{dil}H^{\theta,\infty}$ values in polymer-rich phase and electrolyte-rich phase, for different TLL of system PPO425 + Na_2SO_4 + H_2O at 298.15 K.

TLL / (% m/m)	$\Delta_{dil}H^{\theta,\infty}$ / (kJ.mol^{-1}) polymer-rich phase	$\Delta_{dil}H^{\theta,\infty}$ / (kJ.mol^{-1}) electrolyte-rich phase
31	-11,07±0,36	28,77±0,65
48	-17,91±0,40	29,44±0,71
59	-17,68±0,34	38,12±1,24
69	-24,78±0,35	49,81±1,82

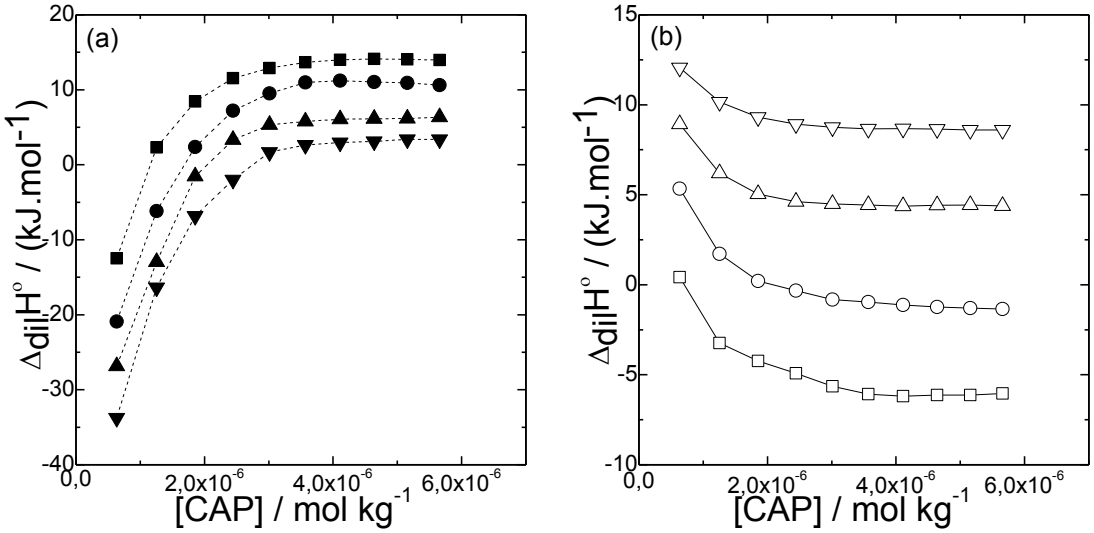

Fig. F5. CAP $\Delta_{dil}H$ value in polymer-rich phase (a) and electrolyte-rich phase (b) for PEO400 + Na_2SO_4 + H_2O ATPS: (■/□) (≅ 38 %(m/m)) TLL, (●/○) (≅ 41 %(m/m)) TLL, (▲/△) (≅ 46 %(m/m)) TLL, and (▼/▽) (≅ 51 %(m/m)) TLL at 298.15 K.

Table T5. CAP $\Delta_{dil}H^{\theta,\infty}$ values in polymer-rich phase and electrolyte-rich phase, for different TLL of system PEO400 + Na_2SO_4 + H_2O at 298.15 K.

TLL / (% m/m)	$\Delta_{dil}H^{\theta,\infty}$ / (kJ.mol^{-1}) polymer-rich phase	$\Delta_{dil}H^{\theta,\infty}$ / (kJ.mol^{-1}) electrolyte-rich phase
38	-29,52±2,37	3,86±0,80
41	-40,14±1,11	9,39±0,66
46	-48,94±1,48	12,17±0,46
51	-55,98±1,53	14,37±0,27

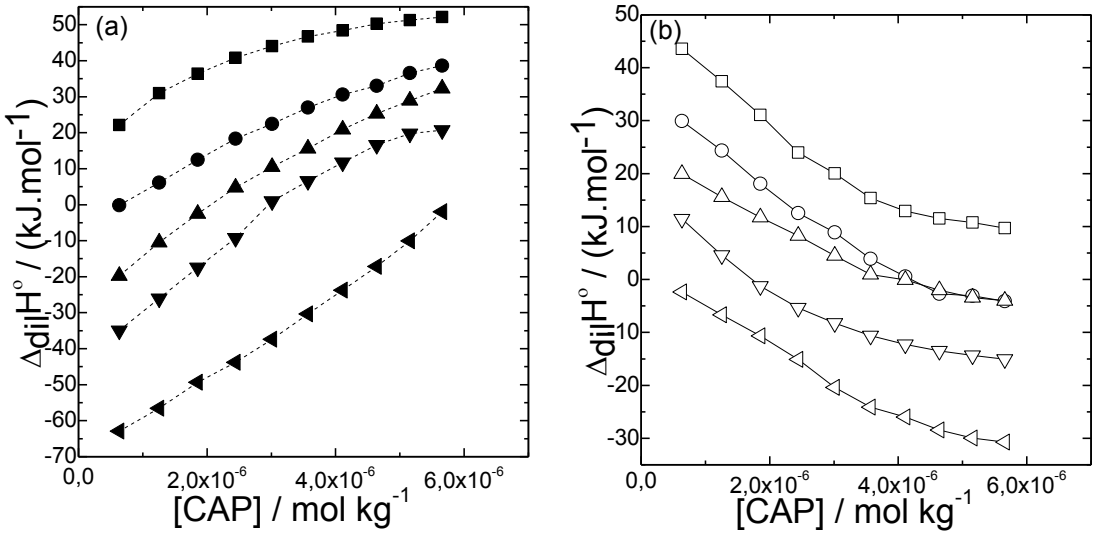

Fig. F6. CAP $\Delta_{dil}H$ value in polymer-rich phase (a) and electrolyte-rich phase (b) for PEO1500 + $Na_3C_6H_5O_7$ + H_2O ATPS: (■/□) (≅ 28 %(m/m)) TLL, (●/○) (≅ 38 %(m/m)) TLL, (▲/△) (≅ 45 %(m/m)) TLL, (▼/▽) (≅ 52 %(m/m)) TLL and (◀/◁) (≅ 56 %(m/m)) TLL at 298.15 K.

Table T6. CAP $\Delta_{dil}H^{\theta,\infty}$ values in polymer-rich phase and electrolyte-rich phase, for different TLL of system PEO1500 + $Na_3C_6H_5O_7$ + H_2O at 298.15 K.

TLL / (% m/m)	$\Delta_{dil}H^{\theta,\infty}$ / (kJ.mol^{-1}) polymer-rich phase	$\Delta_{dil}H^{\theta,\infty}$ / (kJ.mol^{-1}) electrolyte-rich phase
28	15,41±0,45	53.62±0.46
38	-7,76±0.44	38.59±0.21
45	-29,12±0.41	25.84±0.63
52	-48,59±0.26	18.15±0.48
56	-68,38±0.32	4,85±0.30